# Microfluidic Applications in Forensic Science

Charles Philip Clark
Roanoke, Virginia

B.S. Chemistry, The College of William and Mary, 2014

A Dissertation presented to the Graduate Faculty of the University of Virginia in Candidacy for the Degree of Doctor of Philosophy

Department of Chemistry

University of Virginia
**December 2019**

**Abstract**

The separation and detection of cells, biomolecules, and other compounds of interest are essential throughout the biochemical and forensic sciences. These separations are employed in human identification, clinical diagnostics, explosive detection, and narcotic identification, among other applications. The conventional methods and instrumentation for these purposes are labor-intensive, time-consuming, non-integrated, and have not evolved in a significant manner for decades. Microfluidic platforms can alleviate these limitations, providing rapid, cost-efficient, and automated methods for bioanalytical and forensic separations. This dissertation presents microfluidic approaches for two specific applications: sperm cell capture from sexual assault evidence, and explosive compound identification from environmental samples.

The work presented in **Chapter 2** details the design, optimization, and evaluation of a microfluidic platform for acoustic trapping. This approach leverages acoustic forces to capture and purify sperm cells from sexual assault samples, eliminating non-sperm particles and free DNA in order to conclusively identifier a perpetrator. Buccal swabs, vaginal swabs, and post-coital samples were analyzed with this approach, which showed the ability to capture sperm cells effectively from samples with an excess of female epithelial cells. **Chapter 3** describes the validation of this prototype instrument and microchip, during testing performed at two government forensic laboratories in Palm Beach County, Florida, and Mesa, Arizona. The acoustic trapping approach was demonstrated for authentic sexual assault samples, and compared to conventional separation methods. Following prototype evaluation at forensic laboratories, the effect of fluidic properties on acoustic trapping was investigated at a fundamental level, as presented in **Chapter 4**. Sample-to-sample variations in viscosity, density, and compressibility were shown to manifest in changing acoustic conditions, which can be detected through real-time electronic measurements.

That real-time feedback can be used to adapt to the variable liquid properties of each sample, maintaining optimal acoustic trapping under all conditions. Finally, **Chapter 5** describes an electrokinetic separation of explosive compounds, performed on a native polymeric substrate. This work shows that an underivatized polymer microchip can be used to identify multiple explosives in a rapid separation, implementing portable components that may be amenable for field use.

**Acknowledgements**

The journey that has culminated in this dissertation would not have been possible without the support, motivation, and opportunities provided by my research advisor, Professor James Landers. When I first heard you speak about your research, I was instantly drawn to the application-driven nature of your group. I am incredibly grateful for the opportunity to work on such meaningful projects, with access to the best scientific minds and resources, all of it due to your dedication and drive to do something impactful in science. The work ethic you demonstrate (and demand from your students) has made me an exponentially better scientist, and I'll always be proud to tell peers and colleagues what research group I came from. Your expectations for graduate students are high, but as you told me when I joined the group, everything you demand is truly for the student's own benefit. I can't imagine any other situation where I would have had the chance to attend multiple international conferences, travel with you to forensic labs around the country, give a seminar at my alma mater, have dinner and beers with some of the titans of our field, and be made to feel like I belong for all of it. Thank you for teaching me to be a better scientist, and making the last five years some of the most rewarding of my life.

I have had the privilege of working with dozens of exceptional scientists and engineers throughout my PhD research, both at UVA and through collaborations. To each member of the Landers lab, past and present, thank you for your support and knowledge. For their specific contributions to the research in this thesis (in no particular order), I need to highlight Dr. Orion Scott, Dr. Kerui Xu, Vahid Farmehini, Jeff Hickey, An-Chi Tsuei, Prof. Nathan Swami, Liam Spiers, Isabella Mighell, Shane Woolf, Dr. Kimberly Jackson, Daniel Mills, Dr. Daniel Nelson, Dr. Braden Giordano, and Dr. Brian Root.

Mom, Dad, Jenny, and Annie. You have all had plenty of challenges and upheavals of your own in the last 5 years, but have always made sure that I knew I was loved and supported. Being able to share UVA's campus (or grounds, whatever) with both of my sisters was the icing on the cake to my time as a graduate student. I'm forever grateful for the weekly lunches and dinners we shared, which kept us closer than I'd imagined as we all figured out what we want to do in life.

Finally, to Claire. You are the single biggest source of motivation in my life, and I'm always proud to be your husband. From the moment we got married, life became more fulfilling, problems seemed to fade away, I grew tremendously as a person. Aside from the "Fronks incident" of 2014, its been a pretty smooth ride, and I'm so happy that we've made the most of our time in Charlottesville. I love you so much, and without your support, love, and example of what everyone should aspire to be, I wouldn't be where I am today.

**Table of Contents**

**List of Figures**

**Chapter 1: Introduction**



**Chapter 2: Acoustic differential extraction for processing sexual assault samples**

**Chapter 4: Real-time electronic feedback for improved acoustic trapping**

**Chapter 5: Microchip separation of explosive compounds on native polymeric substrate**

**Chapter 6: Final remarks**

**List of tables**

**List of original publications**

The research described in this thesis resulted in the following publications:

1. Clark, C.P.; Farmehini, V.; Spiers, L.; Swami, N.S.; Landers, J.P. Real time electronic feedback for improved acoustic trapping of micron-scale particles. *Micromachines* (2019) 10, 489

2. Clark, C.P.; Xu, K.; Scott, O.; Hickey, J.; Jackson, K.; Tsuei, A.; Landers, J.P. Acoustic trapping of sperm cells from mock sexual assault samples. *FSI: Genetics* (2019) 41, 42-49

3. Xu, K. & Clark, C.P.; Poe, B.L.; Lounsbury, J.A.; Nilsson, J.; Laurell, T.; Landers, J.P. Isolation of a Low Number of Sperm Cells from Female DNA in a Glass-PDMS-Glass Microchip via Bead-Assisted Acoustic Differential Extraction. *Analytical Chemistry* (2019) 91, 2186-2191
   *KX and CPC contributed equally to this work

4. Clark, C.P.; Xu, K.; Scott, O.; Hickey, J.; Woolf, M.; Plean, B.; Edwards, C.; Sikorsky, J.; Crouse, C.; Landers, J.P. External evaluation of an acoustic differential extraction prototype in forensic laboratories. *FSI: Genetics*, In Prep

5. Clark, C.P., Landers, J.P. Modern approaches to differential extraction for sexual assault evidence: A review. *Analytical Chimica Acta*, in prep.

**Abbreviations**

DNA – deoxyribonucleic acid

PCR – polymerase chain reaction

STR – short tandem repeat

ILS – internal lane standard

CODIS – combined DNA index system

SAK – sexual assault kit

DE – differential extraction

DTT - dithiothreitol

LCM – laser capture microdissection

ADE – acoustic differential extraction

PRF – primary radiation force

EPA – environmental protection agency

LC – liquid chromatography

TNT - trinitrotoluene

DNT - dinitrotoluene

RDX – royal demolition explosive

TNB - trinitrobenzene

MEKC – micellar electrokinetic chromatography

EOF – electroosmotic flow

HPLC – high performance liquid chromatography

PMMA – poly (methyl methacrylate)

PDMS - polydimethylsiloxane

GPG – glass-PDMS-glass

EFPI – extrinsic Fabry-Perot interferometry

PLA – polylactic acid

GUI – graphical user interface

HSR – human subjects research

SOB – super optimal broth

RFU – relative fluorescence units

PBSO – Palm Beach County Sheriff's Office

qPCR – quantitative polymerase chain reaction

IPC – internal positive control

AC – alternating current

DC – direct current

PCB – printed circuit board

BNC – bayonet Neill-Concelman

ILIF – indirect laser-induced fluorescence

COC – cyclic olefin copolymer

BGE – background electrolyte

SM – sample matrix

SDS – sodium dodecyl sulfate

PEO – polyethylene oxide

EOF – electroosmotic flow

# Chapter 1: Introduction

## 1.1 Overview

Microfluidics is a rapidly growing field of research and development, specifically in the field of forensic science [1-3]. Microfluidic platforms have many advantages over conventional analytical methods, including reduction in reagent and sample volume, faster analysis, automated processes, and the potential for portable or on-site usage [4]. These benefits can result in rapid, low-cost systems that can improve portability and automation of chemical procedures. This dissertation describes the application of microfluidics to two distinct problems in forensic science: capturing sperm cells from sexual assault samples for suspect identification, and detection of unknown explosive compounds. Isolating and purifying sperm cells is crucial to obtain DNA evidence in sexual assault investigations, but is currently reliant on precise manual cell capture. This specialized procedure is not amenable for robotic automation, but does contain several steps that can be supplemented or replaced through microfluidics [5]. Filling this technology gap for processing sexual assault samples would have a drastic impact on forensic investigations, and ultimately reduce backlogs of DNA evidence. The second project described in this dissertation is the detection of explosive compounds, where the greatest unmet need is a lack of portable techniques for field use. Current methods for identifying mixtures of explosives rely on costly analytical instrumentation, which is effective, but cannot be deployed in the field for on-site use. Developing an approach with the necessary sensitivity to detect trace amounts of explosive compounds, without compromising portability and ease of use, would significantly enhance forensic capabilities for environmental and forensic testing.

## 1.2 Perpetrator identification from sexual assault samples

### *1.2.1 DNA for human identification*

Identifying a person through their DNA is a valuable tool for genealogy, medical research, and criminal investigations. To perform DNA profiling, multiple target sequences are amplified using the well-established polymerase chain reaction (PCR) [6, 7]. PCR generates rapid and exponential amplification of the target DNA by cycling through denaturation, annealing, and elongation thermocycling steps. The resulting DNA amplicons can then be separated based on fragment size, using capillary electrophoresis. This generates an electropherogram, called a short tandem repeat (STR) profile, which can be used for human identification [8]. STRs are variations in a person's DNA sequence, comprised of 2-4 base pair repeated sequences abundant throughout the human genome [9]. These polymorphisms have no obvious phenotypic effect, but are unique to each individual, and thus have great forensic value in conclusively identifying a person [10]. By examining the number of repeated base pairs at nine different genetic loci, the discriminatory power of STR profiling is $1.05 \text{ X } 10^{-10}$, [11] meaning that there is a one in 10 billion chance of two non-related people sharing the same STR pattern at all nine loci. The United States recently expanded their DNA requirements to 20 core loci, further increasing the power of discrimination for criminal investigations [12]. When analyzing an STR profile, such as the electropherogram shown in **Figure 1-1**, it is important to note the number of peaks at each locus, their relative positions, as well as their peak heights. The goal is to generate a 'single source' STR profile, that is, an electropherogram representing the DNA from a single individual. The simplest way to determine this is by observing how many peaks appear in each locus, designated by the gray box at the top of each panel (labelled Amelogenin, D18S51, etc.). In the profile from a single person, each locus may contain one

peak (homozygous), or two peaks (heterozygous), but any additional observed peaks indicate the presence of DNA from multiple people. For more detailed information, the sex of an unknown suspect can be determined by analyzing the Amelogenin locus. This locus will contain either one or two peaks; a single X peak for female DNA, or one X and one Y peak for male DNA.

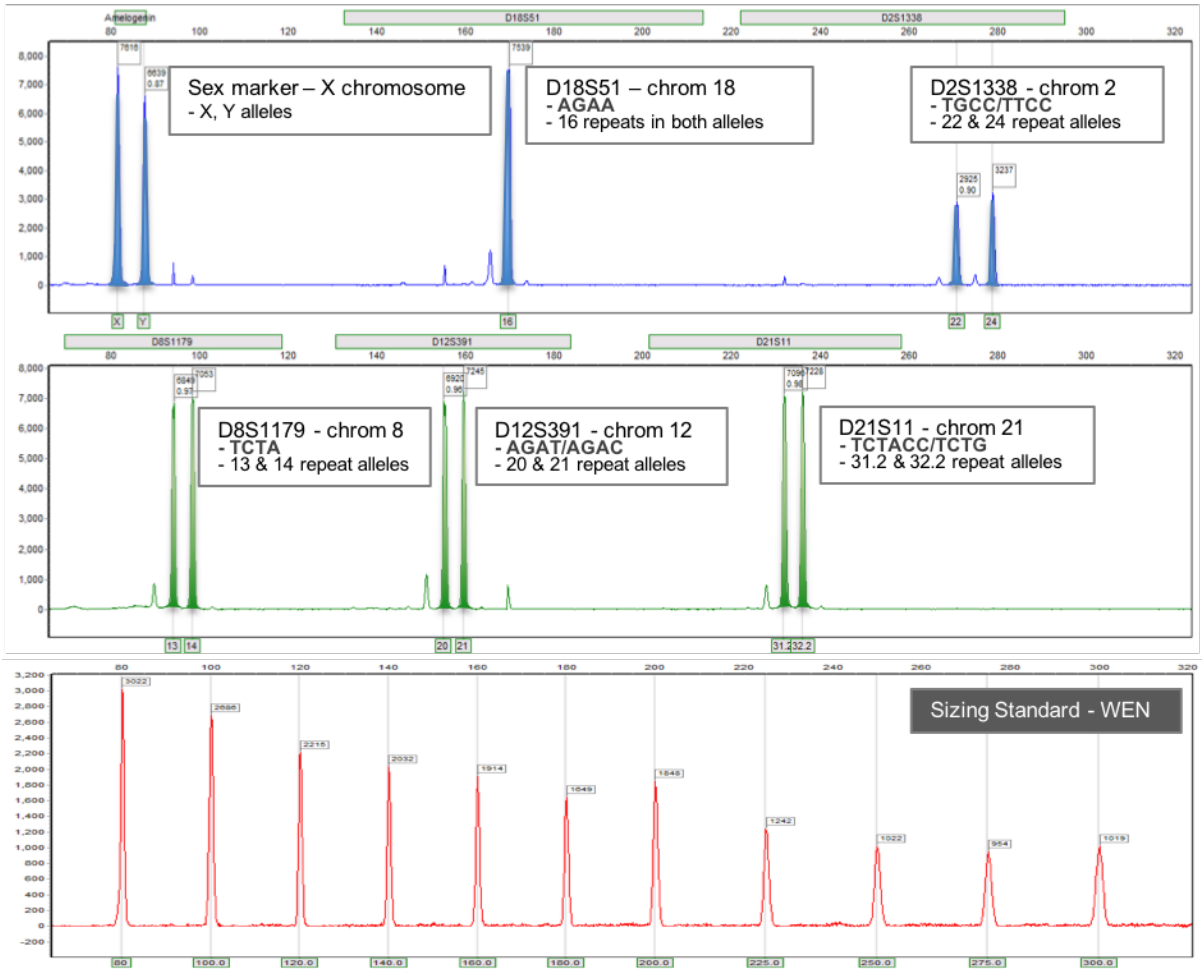


*Figure 1-1. STR profile from male cell donor. A 6-plex amplification kit used with extracted male DNA from sperm cells shows the number of short tandem repeats (STRs) for each allele. Strong peak heights (>1000 RFU) and clear resolution indicate successful separation of DNA. The red trace is the internal lane standard (ILS) which allows for automatic sizing of PCR product.*

The presence of an X and Y peak at significantly disparate peak heights could indicate the presence of both male and female DNA; such mixtures are commonly found in sexual assault evidentiary materials. Examining the other loci in **Figure 1-1**, there are either one or two peaks present, confirming that this is a single source profile. Finally, an internal lane standard (ILS) is

run with every STR profile, in order to provide accurate size determination of the DNA fragments. A profile like this could then be compared to the Combined DNA Index System (CODIS) database, referencing the allele patterns against known individuals, in order to identify a suspect.

### *1.2.2 Sexual assault in the United States and worldwide*

Conclusive identification of an unknown person is paramount for sexual assault investigations, which rely on DNA evidence to corroborate victims' claims. These crimes in the United States are disturbingly common, as one in five women have been a victim of rape [13]. On average, there are over 300,000 victims of rape and sexual assault in the United States each year [14], and worldwide, an estimated 35% of all women experience sexual violence at some point in their life [15]. Non-heterosexual women are victims at an even higher rate [16, 17], and the majority of all rapes go unreported [18]. When sexual assaults and rapes do get reported to the police, a sexual assault kit (SAK) is generated. This consists of cotton swabs collected from the victim, along with any other clothing or belongings that may have been in contact with the attacker. The most common way of identifying the attacker is to recover sperm cells from evidence collected in the SAK, which can unequivocally link a suspect to the crime.

### *1.2.3 Analysis and backlog of sexual assault evidence*

Forensic laboratories across the United States are tasked with processing hundreds of thousands of pieces of biological evidence from crimes each year, and approximately three quarters of these samples require DNA analysis for investigation [19]. Of those samples, a significant portion are comprised of sexual assault evidence, which require more complex processing in order to isolate genomic DNA from the perpetrator, and subsequently identify a suspect [20-23]. The very nature of SAKs make them more difficult to process, as they may

contain many distinct cell types (sperm, epithelial, blood, bacterial) from different people, vary drastically in their composition on a case-to-case basis, and cannot be directly analyzed via DNA profiling (like blood, saliva, or other biological samples). Due in part to the time-consuming, manual protocols required to process SAKs, there is a significant backlog of samples awaiting DNA analysis that have not been tested [24, 25]. This backlog exceeded 150,000 samples across the country in 2006 [26, 27], and has only grown over the last decade. Increased staffing of forensic laboratories has not been sufficient to overcome this backlog, and in fact, the throughput of labs has increased steadily each year since 2009 [28]. However, the demand for forensic DNA casework has increased at an even higher rate, compounding the problem, and leading to an even larger backlog of SAKs [28]. The societal impact of this backlog is profound, as victims of sexual assault crimes may be forced to wait months, or even years before DNA evidence from an investigation can be used to identify and convict their attacker. To address this issue, there have been several initiatives from the federal government level, funding and prioritizing the rapid processing of sexual assault samples [29]. As recently as 2017, the National Institute of Justice committed $117 million for a 'DNA analysis and capacity enhancement program,' which was tasked with addressing the critical forensic DNA backlog [30]. One of these initiatives, a Department of Justice proposal in forensic science for criminal justice purposes, funded the research presented herein. Programs like this, as well as legislation at the state and national level, have caused major strides in how sexual assault cases are reported [31], how the evidence is collected [32, 33], but not how the sample itself is processed.

### *1.2.4 Conventional approaches for processing sexual assault samples*

The most common method for processing DNA evidence from a sexual assault crime is to perform a differential extraction (DE), which isolates sperm cells from the rest of the genetic

material. The foundational paper on conventional DE was published in 1985 by Gill et al., and describes their approach for separating sperm nuclei from vaginal cellular debris, leading to a 'DNA fingerprint' that can identify a suspect [34]. Since this groundbreaking publication, the DE process has been tweaked and optimized, but remains largely the same as it was 40 years ago: sexual assault samples, typically a cotton swab or article of clothing, are subjected to a preferential lysis that breaks open all non-sperm cells and releases their genetic material, leaving sperm cells intact. The lysate is repeatedly centrifuged, washed, and purified by a trained forensic analyst, who manually removes the eluent containing non-sperm DNA, and collects the pellet of sperm with a pipet. Those sperm cells can then be lysed, typically using a surfactant, proteinase K, and dithiothreitol (DTT) [35], resulting in a purified sperm fraction which contains only DNA from the suspected attacker. This is illustrated in **Figure 1-2** (adapted from Butler [35]), showing the steps required to isolate sperm cells via centrifugation. Once male DNA is isolated in the male fraction, the forensic analyst can continue to amplification and separation of the DNA, via PCR and capillary electrophoresis, respectively. Forensic laboratories typically generate high quality

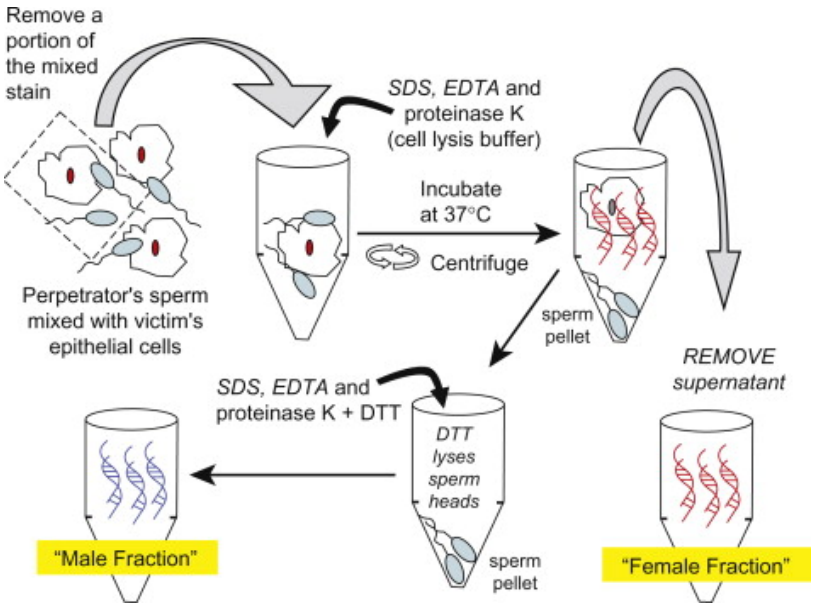


*Figure 1-2. Stepwise schematic of a differential extraction protocol. Preferential lysis of epithelial cells followed by centrifugation isolates sperm cells from the sexual assault sample. Adapted from [35]*

DNA profiles from the conventional DE approach, provided there are ample sperm cells present, and can provide valuable evidence for criminal investigations.

*1.2.5 Shortcomings of current approaches to DE*

It is important to note that for conventional DE, the centrifugation and washing steps each require 5 minutes or longer, and are repeated up to 5 times before a clean male fraction can be obtained [36]. This process is effective at isolating sperm cells and providing DNA from only the attacker, but it is time-consuming (several hours per sample), requires a skilled forensic analyst, and the quality of the separation can vary drastically between labs [37]. There are various commercial options for DE kits and reagents, including Promega, Qiagen, Millipore, and Bio-Rad. However, none of these companies have developed methods that eliminate the manual washing steps of DE, and some require additional DNA concentration after collection of the male fraction (**Table 1-1**, adapted from Vuichard et al. [37]) Some of the time constraints are unavoidable, as cellular lysis, DNA amplification, and DNA separation will remain constant regardless of the technique used to capture sperm cells. However, the hands-on steps of

| Laboratories | First cell lysis | No. of washes | Second cell lysis | DNA Purification | Concentration devices (laboratory number) |
|---|---|---|---|---|---|
| 1, 3 | Differex[a]; proteinase K | 2 | ATL[b] buffer[c]; DTT[d]; proteinase K | QIAamp DNA mini kit[c] | Microcon[e] |
| 2, 4, 7, 9 | Lysis buffer[f]; proteinase K | 1, 3, 4, 3 | Lysis buffer[f]; DTT[d]; proteinase K | Organic | Precipitation (2,4,7); Centricon[e] (9) |
| 5 | Chelex[g]; proteinase K | 3 | Chelex[g]; DTT[d]; proteinase K | Chelex[g] | Centricon[e] |
| 6 | Lysis buffer[f]; proteinase K | 3 | DTT[d]; proteinase K | QIAamp DNA mini kit[c] | Centricon[e] |
| 8 | ATL[b] buffer[c]; proteinase K | 3 | ATL[b] buffer[c]; DTT[d]; proteinase K | QIAamp DNA micro kit[c] | - |

*Table 1-1. Differential DNA extraction protocols. A Promega AG, Dubendorf, Switzerland. B Animal Tissue Lysis. C Qiagen AG, Hombrechtikon, Switzerland. D Dithiothreitol. E Millipore AG, Zug, Switzerland. F Home-made solution. G Bio-Rad Laboratories AG, Reinach BL, Switzerland. Adapted from [37].*

washing, centrifugation, and pellet capture are most problematic, as they are difficult to automate and expose the sample to potential contamination with each successive treatment. For this reason, the most promising research to improve SAK processing is exploring alternative methods

to more effectively capture sperm cells, reducing the analyst time and contamination potential for each sample.

### *1.2.6 Alternative approaches to DE*

The current approach for DE can summarized as functional, but imperfect. Several academic research groups and companies have tackled the issue of improving DE, leading to excellent developments and new technologies. There are a handful of commercialized systems for improved DE, some of which may soon be adopted by forensic laboratories. One such system is the DEPArray™, which uses dielectrophoresis to manipulate and capture individual sperm cells, providing incredible sensitivity and selectivity. This is possible by exposing polarized particles (in this application, cells) to a nonuniform electric field, which exerts force on the cells and generates movement. Precise manipulation of the electric field cages allows for individual cell capture, as demonstrated by Williamson et al. [38]. Subsequent imaging of the captured cells employs a sperm-specific stain and a nucleus-specific stain, showing single cell retention (**Figure 1-3**, adapted from Williamson et al. [38]). The major drawbacks of DEPArray™ are that it requires more time and operator steps than most other methods, and

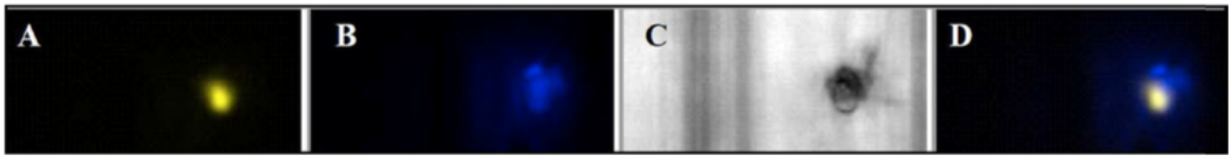


*Figure 1-3. DEPArray™ image gallery showing the sperm cell identified in the 96 h post-coital sample. (A) sperm-specific APC channel, (B) nucleic acid/nucleus-specific DAP1 channel, (C) bright field and (D) sperm/nucleus channel overlay. Adapted from [38]*

includes cell staining/fixation and lengthy incubations [38]. However, this approach is incredibly exciting for its application to trace evidence samples with low numbers of sperm, or instances where there are sperm cells from multiple attackers in a single sample. In either of those example cases, traditional DE would fail to produce a single-source male STR profile that could be used to identify a suspect, but DEPArray™ may succeed due to its ability to capture

individual sperm. Another commercially available DE alternative is the Erase Sperm Isolation Kit (Paternity Testing Corporation). This kit eliminates the washing steps of conventional DE, instead using selective degradation of residual female DNA to produce a clean sperm fraction. Erase has been evaluated directly against conventional DE, with mixed results. Klein et al. demonstrated that, when testing mock sexual assault samples with both methods, the Erase kit produced sperm fractions with a higher ratio of male:female DNA (i.e., more purified), but a 6-fold lower concentration of total male DNA [39]. These results, combined with the fact that Erase still requires centrifugation and manual sperm pellet capture, make it unlikely that this system will replace conventional DE.

While no commercial alternative to DE has supplanted the current method, there are many technologies in the research and development stage. One of the most intriguing approaches has been developed by Inci et al. at Stanford University, in collaboration with Harvard Medical School and the Broward County Sheriff's Office. Their unique method uses an oligosaccharide molecule that has been shown to be crucial for sperm-egg binding during fertilization, and anchors it to a microfluidic chip. When a sample containing sperm cells and

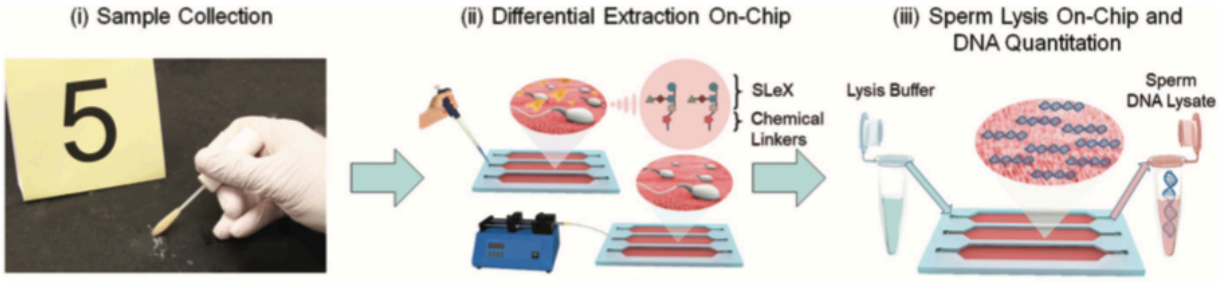


*Figure 1-4. Workflow of on-chip differential extraction. i) In practice, samples are collected using a swab or cotton gauze in a forensic scene, where a mixture of semen and epithelial cells are majorly present on the victim's body and/or garments at the crime scene. ii) After collection, samples are simply introduced into the device using single-step pipetting and incubated for an hour at room temperature. The channels are then washed and sperm cells are specifically captured, while epithelial cells are removed due to their larger size and lack of an adhesion molecule on the channel surface. iii) The captured sperm are treated with a lysis buffer on-chip, and sperm DNA is collected into a tube for potential forensic downstream genomic analyses. Adapted from [40].*

epithelial cells is incubated on-chip, sperm bind the carbohydrate ligand, and are retained under flow when epithelial cells are washed away (**Figure 1-4**, adapted from Inci et al. [40]). This method is being developed with mock sexual assault samples, and has the distinct advantage of performing subsequent sperm cell lysis on-chip. This technique is currently limited to small sample volumes (5-15 μL) and a relatively lengthy incubation to facilitate sperm capture (60 minutes), but has the potential to supplant conventional DE.

A radically different 'nuclease-only' approach does not physically separate sperm cells from the epithelial cells and non-sperm DNA, but instead, relies on a protease and DNase 1 enzyme to completely remove all female DNA from the sample before lysing the sperm cells [41]. Garvin et al. showed that this nuclease-only method can generate male STR profiles of equal or higher quality than traditional DE methods (**Figure 1-5**, adapted from Garvin et al. [41]), but, as all non-sperm DNA is destroyed, there is no STR profile generated for the victim. This method shows promise for its simplicity and effectiveness, but has yet to gain acceptance in many forensic crime laboratories. Another alternative to conventional DE uses pressure cycling

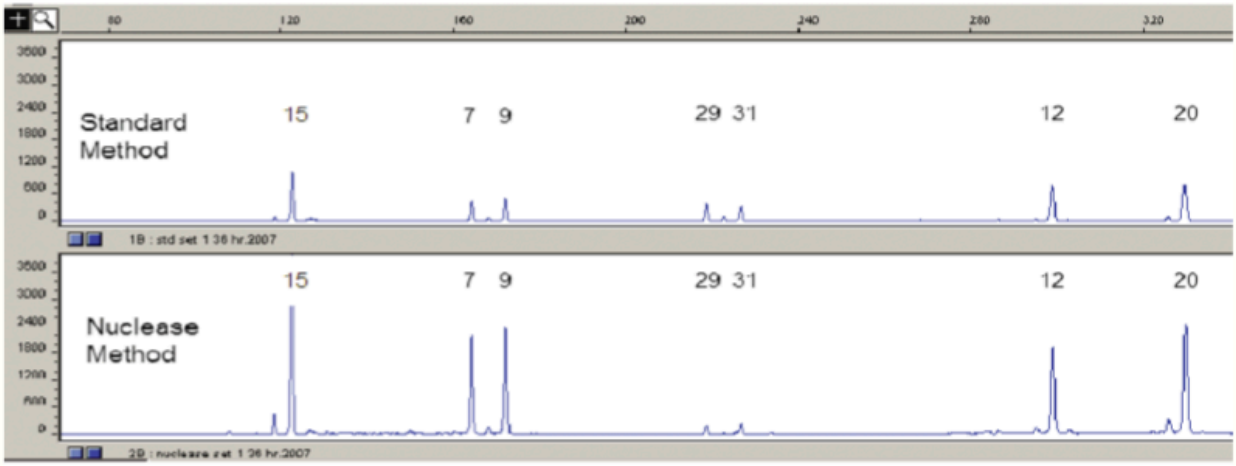


*Figure 1-5. Four STR loci (D3S1358, THO1, D21S11, and D18S51) from the PowerPlex16 kit for buccal swabs and male fractions from postcoital vaginal swabs. Male fractions obtained from a 36 h postcoital swab give a correct male profile with both the standard selective lysis protocol and the nuclease protocol. Adapted from [41]*

to selectively lyse epithelial cells without rupturing the sperm, followed by an alkaline lysis to break open sperm cells, which can improve DNA recovery [42]. This significantly reduces the handling time per sample; however, it still requires repeated manual centrifugation steps by an analyst, and fails to produce clean separations of male and female DNA at cellular ratios of higher than 5:1 epithelial-to-sperm cells [43]. Laser capture microdissection (LCM), one of the most precise capture techniques, harvests sperm cells by individually cutting them out of the substrate. As shown in **Figure 1-6** (adapted from Vandewoestyne et al. [44]), individual cells of interest can be identified and removed into a microfuge tube for DNA processing. LCM can effectively separate sperm cells from mixed samples, but routinely provides sperm fractions with a low number of cells, and like other systems, struggles with laborious and time-consuming steps [44]. In addition, the highly manual nature of LCM makes it unlikely that this technique can be automated in the future [45]. One of the simpler, non-commercialized alternatives to conventional DE uses filtration to sift out sperm cells from the larger epithelial cells. However, as would be expected, this approach is subject to clogging of the membrane with high number of cells, as well as failure to filter out free DNA from the sample that could influence the downstream STR profile [46, 47].

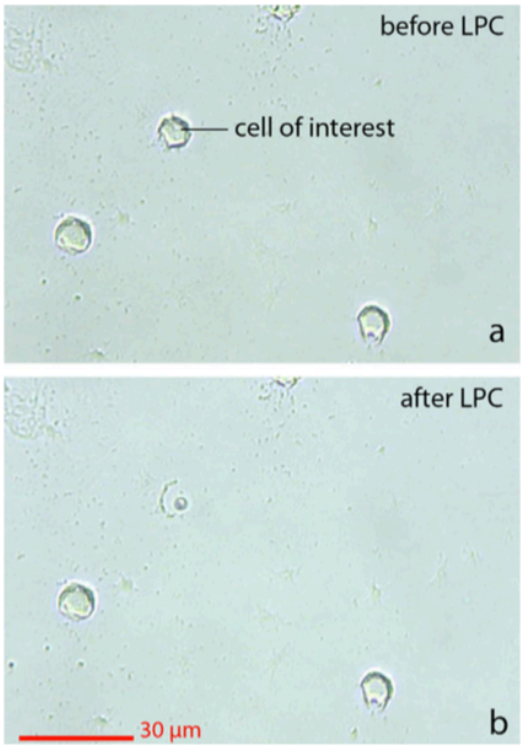


*Figure 1-6. Laser pressure catapulting. (a) Image before LPC (63x magnification); (b) image after LPC of the cell of interest (63x magnification). Adapted from [44].*

Performing sperm cell capture via affinity assays, rather than size-based or manual separation, also shows promise in this field. Zhao et al. have demonstrated that, after a preferential lysis of epithelial cells, sperm cells can be immobilized using antibodies tagged to magnetic beads, which can then be removed from the sample lysate. They used optical and scanning electron microscopy to show binding of intact and damaged sperm to the antibody-tagged beads (**Figure 1-7**, adapted from Zhao et al. [48]). This was the first reported covalently-linked sperm antibody capture technique, and provided clean separations, even in extreme cases of overwhelming amounts of epithelial cells [48]. However, this procedure suffers from complex handling and preparation steps, and can fail to capture significant amounts of sperm from samples more dilute than $10^3$ cells/mL [48].

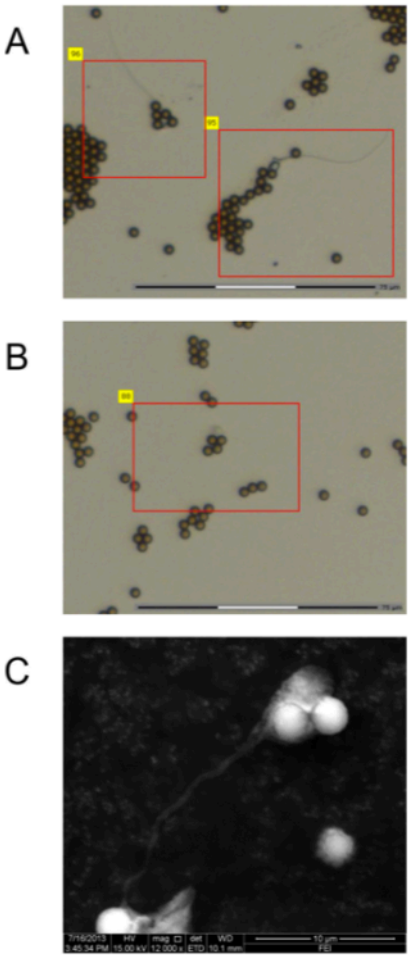


*Figure 1-7. Sperm cells captured by anti-PH-20 IMB. (A) Optical microscopy image for IMB bound to the head of intact sperm cells. (B) Optical microscopy image for IMB bound to the sperm without midpiece and tail. (C) Scanning electron microscopy image for IMB bound to the head of an intact sperm cell. Adapted from [48].*

Each of these novel approaches offer advantages over conventional DE, but none can fully address the issues with current protocols, namely the need for *faster*, more *automated*, and *robust* capture of sperm cells from any type of sexual assault sample. Some methods are more automated and integrated than DE, like the oocyte capture ligand approach from Inci et al. Others, like the Erase Sperm Isolation Kit, have fewer manual steps than conventional DE, while approaches like LCM or the DEPArray™ can salvage sperm cells from samples with low total number of cells. However, none of the commercially available or currently developing

systems for alternative DE can combine all of these aspects to replace the established method.

### *1.2.7 Development of an acoustic differential extraction method*

Confronted with the inability of conventional DE to process all SAKs in a timely manner, and the absence of a universally accepted alternative for capturing sperm cells from these samples, a novel, microfluidic, acoustic approach was created to address this need. The research presented herein describes the development, evaluation, and future of a new technology that may someday replace conventional DE. This approach, deemed acoustic differential extraction (ADE), seeks to completely remove the manual centrifugation, washing, and purification steps associated with conventional DE, and instead, apply acoustic separation principles on a microfluidic platform to capture sperm cells from sexual assault samples. Acoustic forces have been successfully leveraged for particle separations throughout microfluidics and biomedical research, and thus, applying acoustics makes perfect sense for separating sperm cells from other particles in SAKs. ADE was first described at a conference in 2006 [49], and later in the literature by Norris et al. in 2009, where proof-of-principle work was conducted to show that intact sperm cells could be captured using ultrasonic standing waves in a glass microchip [50]. By flowing a solution containing sperm cells and female DNA through a standing acoustic wave, they were able to retain sperm cells and divert them to a male reservoir on the microchip for collection (**Figure 1-8**, adapted from Norris et al. [50]). Their work demonstrated a 16-fold enrichment of sperm concentration, and obtained purified male fractions from mock samples of epithelial cell lysate [49, 50]. At that time, ADE was limited by extremely low flow rates (1 μL/min or slower), relatively large sample volumes (500 μL), and a dangerous and labor-intensive chip fabrication that required glass etching with hydrofluoric acid. In addition, mock samples were formulated with pre-purified genomic DNA or epithelial cell lysate, avoiding the

crucial preferential lysis step required in samples with intact epithelial cells. Nevertheless, this important research laid the groundwork for the current ADE approach.

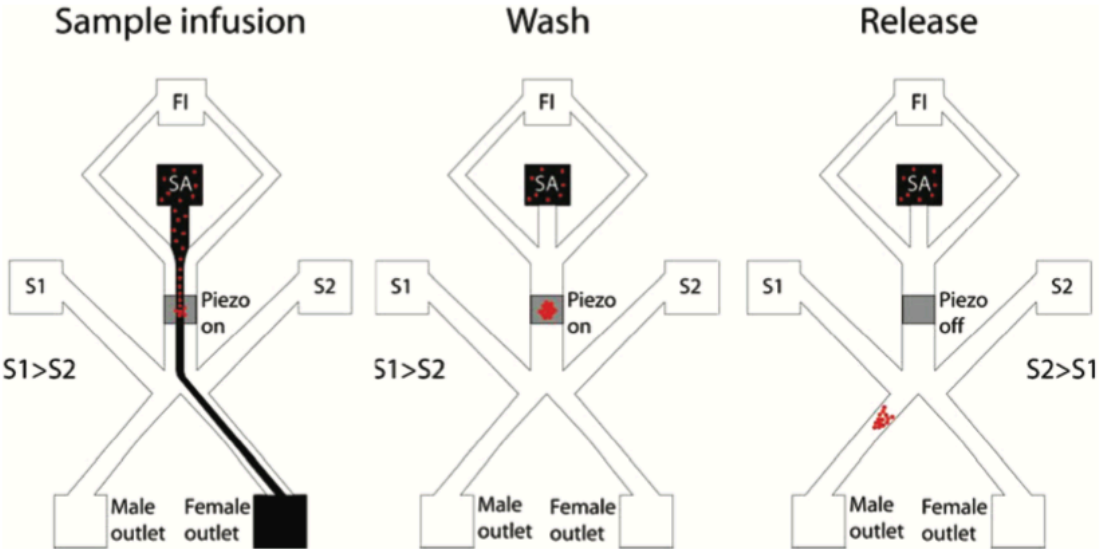


*Figure 1-8. Fluidic design of the ADE chip. Sample infusion: sample is infused through the sample inlet (S) and hydrodynamically focused by the focusing buffer inlet (FI). Cells (red) are trapped above the transducer upon activation of the transducer, while lysate (black) is unretained. Wash: each sample infusion is terminated, and focusing buffer perfuses the trapped cells and removes the residual lysate from the microchannel. Release: Upon termination of the standing wave, cells are released and diverted to the male outlet. The flow ratio of inlets S1 and S2 determines if the sample will be directed to the male or female outlet. Adapted from [50].*

### *1.2.8 Understanding acoustics as it applies to controlling particle motion*

ADE separates particles based on their size, density, and compressibility using forces generated by acoustic waves. Acoustic forces have been described as early as 1866, in Kundt's famous tube experiment, which observed cork dust moving in a standing wave [51]. His findings, and others, have shown that when particles in air or a liquid are subjected to a sound field, the particles experience forces which alter their absolute and relative positions. These 'acoustic radiation forces' have been leveraged for a wide range of applications [52-57], including molecular diagnostics, material science, and the strategy for capturing sperm cells described herein. This is accomplished by balancing many different forces, creating a 'cutoff size' at which only larger particles are trapped. Due to the relatively uniform size, shape, and

density of sperm cells [58], reproducible trapping is possible by tuning the flow rate, and importantly, the applied acoustic forces. The most significant force involved is the primary radiation force (PRF), which causes particles to migrate either to the nodes or antinodes of a standing wave, where they are packed together and held in place [59]. The PRF (**Equation 1**) for a microfluidic system depends on a number of factors, including the acoustic pressure amplitude ($\rho_0$), the volume of the particle ($V_c$), the compressibility of the medium ($\beta_w$), the wavelength of the standing wave ($\lambda$), the acoustic contrast factor ($\phi$), the wave number ($k$) and the distance from a pressure node ($x$).

(1) $$F_r = -\left(\frac{\pi \rho_0^2 V_c \beta_w}{2\lambda}\right) \cdot \phi(\beta, \rho) \sin(2kx)$$

Keeping in mind that many applications of acoustophoresis are in the microfluidic realm, the applied wavelength ($\lambda$) must be such that it 'fits' in the sub-millimeter scale resonant chambers [60], with channel height corresponding to a half wavelength of the transducer frequency. This requires acoustic frequencies on the order of 1.5 MHz or greater, proportional to the chamber height of the microdevice. An important component of the PRF is the acoustic contrast factor, $\phi$ (**Equation 2**), which defines the relationship between particle density ($\rho_c$) and compressibility ($\beta_c$) compared to the medium density ($\rho_w$) and compressibility ($\beta_w$).

(2) $$\phi(\beta, \rho) = \frac{5\rho_c - 2\rho_w}{2\rho_c + \rho_w} - \frac{\beta_c}{\beta_w}$$

This acoustic contrast factor determines where in the microchannel particles will aggregate, and the sign of $\phi$ indicates if particles will migrate towards either a node, or antinode,

in the standing wave. In practical terms, if a particle is denser and less compressible than the surrounding liquid, it migrates towards a pressure node; if the particle is less dense and more compressible, it is drawn to the antinode. For ADE, with samples composed of sperm cells surrounded by lysed non-sperm cells, the acoustic contrast factor is positive, and thus, the cells migrate to the nodes of the standing wave. This effect is illustrated in **Figure 1-9** (adapted from Laurell et al. [59]), which shows the migration of red blood cells and lipids when subjected to a standing wave. All particles experience the PRF, but due to differences in their acoustic contrast factors, the red blood cells (positive $\phi$) aggregate at the pressure node, while lipid particles (negative $\phi$) move to the pressure antinodes.

*Figure 1-9. Cross-section of a separation channel showing negative ϕ-factor particles (lipid particles) collected in the pressure antinodes by the side walls, and positive ϕ-factor particles (red blood cells) in the pressure node in the middle of the chamber. Adapted from [59].*

The other forces involved in acoustic trapping are secondary radiation forces. While the PRF is experienced by single particles, drawing them towards or away from pressure nodes, secondary radiation forces generate particle-particle interactions, causing them to attract or repel one another [61]. Also referred to as 'König forces' [62], secondary forces between solid particles are much weaker than the PRF, but have important effects on particle coagulation and packing at the acoustic nodes [63]. Those forces are dependent upon the particle radius,

resonance frequency, and distance between particles. Minor attraction caused by secondary radiation forces can result in tighter aggregation at the standing wave node or antinode [64]. The combination of primary and secondary radiation forces is illustrated in **Figure 1-10** (adapted from Evander et al. [65]), which shows three stages of acoustic trapping. Prior to applying the standing wave, particles are dispersed throughout the fluid (panel A). When an acoustic wave is applied at the appropriate resonant frequency, the PRF causes particles to aggregate at the

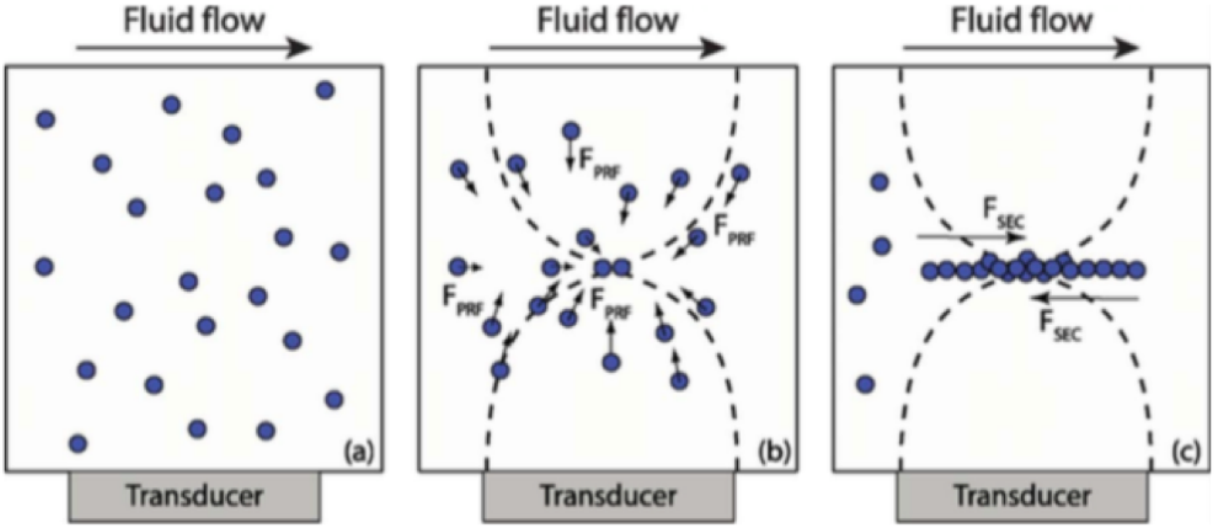


*Figure 1-10. (a) Cross-section of a separation channel where the transducer emits sound perpendicular to the flow. (b) When the transducer is active, a standing wave will form in the fluidic channel, and the primary radiation forces will cause objects to aggregate in the pressure node. (c) Once an aggregate is formed, secondary forces will keep particles together and counteract the Stokes' drag force. Adapted from [65]*

pressure node (panel B). Once particles are brought into closer proximity, the secondary radiation force attracts them together, forming a cluster at the center of the node (panel C). In terms of this ADE application, sperm cells will compress and expand slightly when exposed to a high frequency sound wave, which generates minor forces in addition to the PRF. These smaller, secondary forces impact other particles in solution, causing similarly sized particles (i.e., other sperm cells) to aggregate.

### *1.2.9 ADE for sperm cell capture*

With an understanding of these acoustic radiation forces, a microfluidic system can be designed to capture specific particles under the appropriate conditions. This ADE approach balances primary and secondary radiation forces, as they act against the drag force experience by sperm cells in a laminar flow system. Stokes Law (**Equation 3**) defines the drag force ($F_d$) as a function of the dynamic viscosity (μ), particle radius ($R$), and flow velocity (ν) [66].

(3) $$F_d = 6\pi\mu R\upsilon$$

As long as the combined acoustic radiation forces are stronger than the drag force acting on the sperm cells, they will remain trapped in the acoustic nodes. For smaller particles that should be excluded from acoustic trapping (free DNA, cellular debris), the drag force must exceed the acoustic radiation forces. This can be achieved in part by adjusting flow rate of the system, increasing the drag force on all particles. Importantly, the drag force scales with particle radius, while the PRF scales with the particle volume (i.e., radius *cubed*). This implies that as particle radius decreases, the PRF will diminish much faster than the drag force. At a certain point, the drag force will exceed the PRF for small particles (<1 μm), but the PRF will be stronger than the drag force for large particles. This creates a a threshold where only larger particles (sperm cells) will be trapped, while smaller particles (DNA from lysed e cells, debris) will be washed away. **Figure 1-11** illustrates this selective trapping, as larger particles can be retained under a constant flow rate and application of a standing acoustic wave. A microfluidic platform has been developed for implementing these acoustic forces, and through careful design

and optimization, sperm cells are isolated and purified from samples containing multiple cell types from multiple different people.

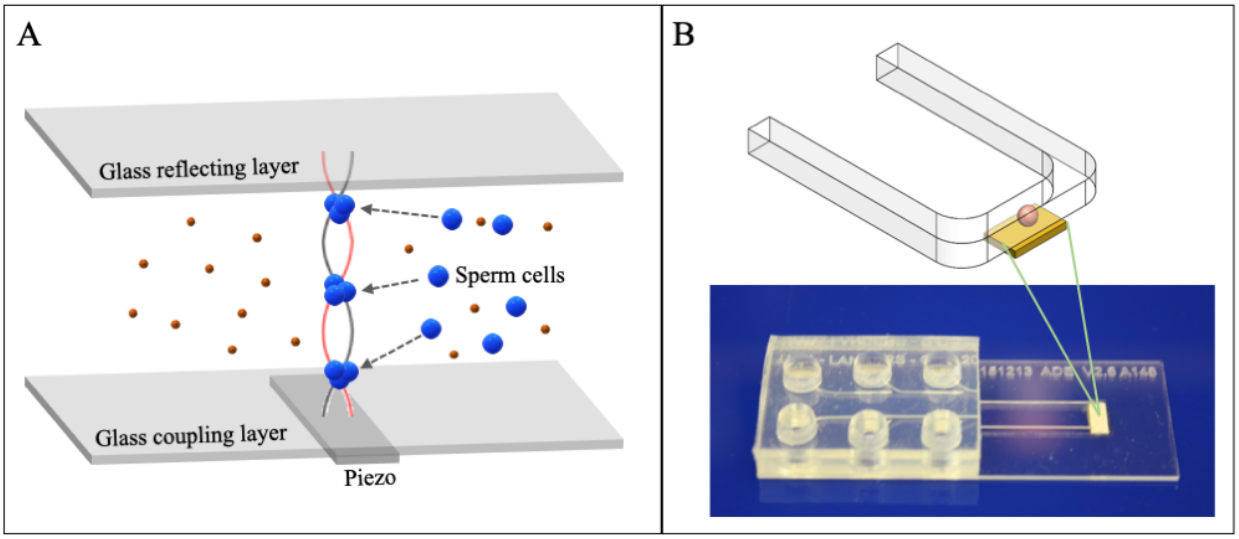


*Figure 1-11. Acoustic trapping of particles. (A) Side view of trapping chamber, fluid flow is right-to-left. A piezoelectric transducer (piezo) vibrates and produces a sound wave at the resonant frequency of the chamber. When subjected to the standing acoustic wave, particles in solution experience acoustic radiation forces which draw them to the pressure node. Larger particles experience a stronger force, allowing for selective trapping based on particle size. (B) The glass-PDMS-glass microchip contains a trapping channel that is 1.1 mm wide, 0.285 mm tall, and 3 mm long. This allows for particle trapping throughout the channel, preventing overpopulation of the trap site.*

## 1.3 Microfluidic platforms for explosive detection

### *1.3.1 Forensic and environmental explosive compound identification*

Identifying explosive compounds and their degradation products remains a priority for military, environmental, and forensic researchers worldwide [67, 68]. In particular, soil and groundwater in close proximity to military installations are at high risk for contamination with explosive compounds, which can be toxic to plant and animal life [69]. Multiple studies have shown that environmental samples collected near munitions sites can contain nitrated explosive compounds at toxic levels [70, 71], yet regular monitoring for these substances is difficult to perform. The primary issue is the necessity to collect samples in remote locations, combined with a lack of portable detection devices. Many areas of interest are difficult to access, and often require sampling dozens of locations in order to ascertain the potential spread of toxic

explosives. Furthermore, the only Environmental Protection Agency (EPA) approved detection technique for environmental explosives is EPA 8330, which is not field-portable [72]. This method requires an acetonitrile extraction, preconcentration, and reverse-phase liquid chromatography (LC) with UV-vis detection, followed by a confirmatory LC-CN (cyanopropylsilane) column. The combination of remote sampling sites with laboratory based detection results in high-effort, time consuming studies to monitor these compounds. As an example, a recent Naval Research Laboratories study measured the levels of 13 nitroaromatic compounds in surface water collected from a Hawaiian estuary [68]. Their protocol required sample collection at more than 30 sites, after which the water samples were stored on ice, shipped overnight to a laboratory, and analyzed for the presence of explosive compounds. Only once the results were relayed back to the researchers, could new sampling locations be determined, requiring return trips to the site in an iterative ordeal. This arduous process would be avoided if the investigators could detect explosives at the areas of interest, in a reasonable time frame, allowing for immediate detection that would inform decisions regarding further collection of new samples. To meet this goal, a fully portable technology with the sensitivity and selectivity to provide the unambiguous detection of a wide panel of analytes is required.

### *1.3.2 On-site detection of explosive compounds*

Portable analytical techniques not only provide actionable information to the researcher much more quickly, but also reduce cost, as expedited shipping, specialized storage, and complex instrumentation are not required. Instead, a point-of-need instrument allows for a user to collect a sample, test it in the field, and receive actionable information right away. Historically, on-site explosive detection has relied on either colorimetric or immunoassay-based approaches. Colorimetric techniques are perhaps the easiest to implement in the field, as rapid,

visually apparent reactions will occur when the compound of interest is present, making instrument-free detection possible. Popular tests have been developed for TNT, DNT, and RDX [73], as well as many other compounds. However, colorimetric approaches struggle to integrate detection of a large panel of explosives, often requiring multiple test kits and many replicate samples from the same unknown compound. Furthermore, colorimetric tests may settle for simple class assignments rather than specific chemical identification, due to similar chromogenic reactions from different explosive molecules. [74]. These colorimetric kits also rely on subjective user interpretation of hue after a reaction, which can lead to erroneous results [75]. The simplest immunoassay technique relies on TNT-specific antibodies, immobilized on latex particles, which will capture TNT and be collected on a membrane. A color-developing solution is added to the membrane, and a visual color change can be used to identify TNT. A similar technique uses a competitive immunoassay, where fluorescently labelled TNB is exposed to an antibody-labelled optical fiber prior to sample introduction [76, 77]. These portable tests have not been widely implemented, however, due to their lack of EPA accreditation and narrow scope of detectable explosives.

More recently, there have been a number of commercialized systems for portable explosive detection, predominantly targeting point-of-interdiction testing such as airport screening and police investigations. One such instrument, GreyScan, uses capillary electrophoresis to identify inorganic explosives in solution, providing results in less than 60 seconds. While currently unable to analyze organic explosive compounds, this technology may represent the future for on-site explosives detection.

### *1.3.3 Micellar electrokinetic chromatography*

To address this forensic and environmental issue, micellar electrokinetic chromatography (MEKC) was chosen as an analytical method. Initially developed by Terabe et al., MEKC is an efficient analytical technique capable of separating neutral compounds, unlike traditional capillary electrophoresis [78]. MEKC has previously been implemented for explosive compound identification [67, 79], with at least two groups exploring portable MEKC for other target analytes [80, 81]. A detailed discussion is provided in **Chapter 5**, but previous work has been limited to laboratory (i.e., non-portable) explosive detection, and on-site MEKC for this application has not yet been realized. MEKC functions by inducing electroosmotic flow (EOF) in a capillary or microchip, moving the bulk fluid past a detector. As the neutral analytes have no inherent electrophoretic mobility, they will migrate with EOF, unless a micelle-forming compound is added. Micelles contain a hydrophobic core protected from the liquid environment by a charged exterior, imparting electrophoretic mobility *against* the bulk EOF. In an aqueous solution, compounds with high hydrophobic character will be drawn to the hydrophobic core of the micelles. When these neutral analytes partition in to and out of micelles during a separation, their overall migration speed is reduced, as they spend some amount of time moving with the bulk solution, and some time moving slower within the micelle. This is illustrated in **Figure 1-12**, adapted from the Handbook of Capillary and Microchip Electrophoresis and Associated Microtechniques [82].

As it relates to this specific project, MEKC is an ideal technique for several reasons. Most importantly, all major classes of military explosives are neutral compounds [72, 83], which can be difficult to separate with other approaches. Additionally, MEKC does not require the packed column or high pressure source that are required for HPLC separations [84].

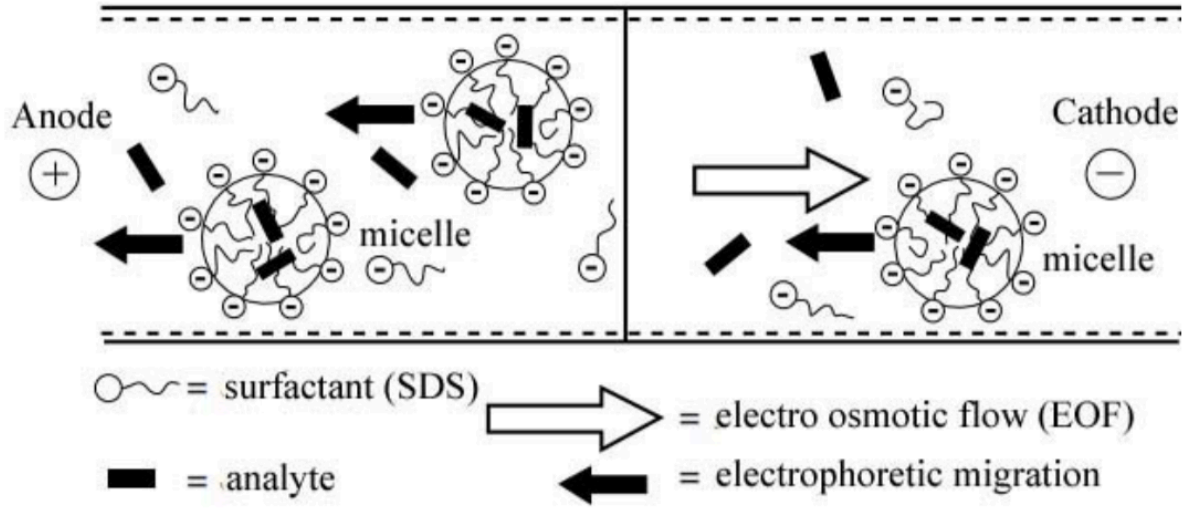


*Figure 1-12. Schematic of MEKC. Analytes partition between the bulk solution and micelle interior, resulting in different migration speed based on micelle permeability. Adapted from [82]*

Eliminating these components reduces potential errors due to irreproducibility in packing, and minimizes flow rate constraints due to back pressure. Electrophoretic separations are also amenable for portable platforms, as they can be performed on various durable substrates, and the hardware requirements are minimal [85, 86]. The first step towards achieving an on-site, MEKC technique for explosives detection, is to optimize the separation parameters on a microchip, taking into account all necessary factors for size and portability. This is the focus of the work presented here, using benchtop experiments to find optimal separation parameters for identifying and resolving mixtures of explosive compounds.

## 1.4 Description of research goals and concluding remarks

This thesis focuses on the development of two distinct separation techniques, seeking to address unique unmet needs in the forensic and environmental sciences. The accomplishments in acoustic capture of sperm cells for sexual assault investigations, as well as explosive compound identification, demonstrate significant breakthroughs and progress towards paradigm-shifting change in the respective fields. Despite increased funding and national efforts towards

reducing the backlog of sexual assault samples, the need for forensic DNA analysis continues to grow. Given that the frequency of sexual assault is unlikely to decline, a technological breakthrough is required to address the staggering backlog of SAKs, and provide rapid resolution of criminal investigations. The work presented herein may provide this solution, as ADE seeks to quickly and efficiently capture sperm cells from sexual assault samples. By tuning acoustic radiation forces and fluidic manipulation, low concentrations of sperm can be separated from female epithelial cells, even at extreme cellular ratios. This method and the results are presented in **Chapter 2**.

This dissertation also details an external evaluation of the ADE approach, comparing results obtained from the prototype instrument to those acquired via conventional DE in a crime laboratory. Those findings are presented in **Chapter 3**. The results from that external evaluation, along with feedback from forensic analysts, prompted significant advancement in optimizing the ADE process. The most impactful change was the development of a feedback system for the ADE prototype, which can account for unforeseen shifts in the optimal trapping frequency. Incorporation of real time feedback for improved sperm cell trapping is described in **Chapter 4**. This 'cruise control' addition to ADE provides the bandwidth to process any sample type, a shortcoming observed with early versions of the technology. In **Chapter 5**, I present the first reported free solution MEKC separations on a native cyclic olefin copolymer device, using indirect laser induced fluorescence to detect a panel of 11 explosive compounds.

In summary, the following chapters focus on the development, validation, and improvement of a novel cell separation technique for processing sexual assault samples. A separate project details an electrokinetic separation of neutral analytes, with direct application in

environmental and forensic research. **Chapter 6** includes a discussion on the impact of these projects, and outlines future directions for this work.

## 1.5 References


1. B. Bruijns, A. Asten, R. Tiggelaar, H. Gardeniers, *Biosensors*, 2016, **6**, 41.
2. C. Lee, S. Scott, and Z. Alie, *Measurement and Control*, 2012, **45**, 306-310.
3. L. Oliveira, D. Rocha, W. Araujo, R. Munoz, T Paixao, M. Salles, *Analytical Methods*, 2018, **10**, 5135-5163.
4. G. Whitesides, *Nature*, 2006, **442**, 368-373.
5. M. Timken, S. Klein, S. Kubala, G. Scharnhorst, M. Buoncristiani, K. Miller, *FSI: Genetics*, 2019, **40**, 96-104.
6. M. Innis, K. Myambo, D. Gelfand, M. Brow, *Proceedings of the National Academy of Sciences U.S.A.*, 1988, **85**, 9436-9440.
7. G. Slater, M. Kenward, I. McCormick, M. Gauthier, *Current Opinion in Biotechnology*, 2003, **14**, 58-64.
8. B. Karger, A. Guttman, *Electrophoresis*, 2009, **30**, 196-202
9. C. Dib, S. Faure, C. Fizames, D. Samson, N. Drouot, A. Vignal, P. Millasseau, S. Marc, J. Hazan, E. Seboun, M. Lathrop, G. Gyapay, J. Morissette, J. Weissenbach, 1996, **380**, 152-154.
10. C. Ruitberg, D. Reeder, J. Butler, *Nucleic Acids Research*, 2001, **29**, 320-322.
11. S. Li, C. Yan, Y. Deng, R. Wang, J. Wang, H. Yang, S. Li, *Genomics Proteomics & Bioinformatics*, 2003, **1**, 166-170.
12. D. Hares, *FSI: Genetics*, 2015, **17**, 33-34.

13. M. Black, K. Basile, M. Breiding, S. Smith, M Walters, M. Merrick, M. Stevens. *Centers for Disease Control and Prevention*, 2011.

14. U.S. Department of Justice, *Office of Justice Programs*, 2018, 1-29.

15. Department of Reproductive Health and Research, *World Health Organization*, 2013.

16. M. Walters, J. Chen, M. Breiding. *Centers for Disease Control and Prevention*, 2013.

17. European Union Agency for Fundamental Rights, *Publications Office of the European Union*, 2014, 184-8.

18. C. Rennison, *U.S. Department of Justice*, 2002, NCJ 194530.

19. U.S. Department of Justice, *Office of Justice Programs*, 2012, 1-104.

20. J. Wen, L. Legendre, J. Bienvenue, J. Landers. *Analytical Chemistry*, 2008, **80(17)**, 6472-9.

21. J. Norris, M. Evander, K. Horsman-Hall, J. Nilsson, T. Laurell, J. Landers, 2009, **81(15)**, 6089-95.

22. K. Strom, J. Ropero-Miller, S. Jones, N. Sikes, M. Pope, N. Horstmann. Final report to the NIJ from grant 2007F_07165, 2009.

23. N. Ritter, *National Institute of Justice Special Report*, 2011.

24. C. Reedy, J. Bienvenue, L. Coletta, B. Strachan, N. Bhatri, S. Greenspoon, J. Landers, *FSI: Genetics*, 2010, **4(3)**, 206-12.

25. M. Nelson, *National Institute of Justice Special Report,* 2011.

26. Y. Chung, M. Jan, Y. Lin, W. Cheng, C. Fan, *Lab Chip*, 2004, **4(2)**, 141-7.

27. L. Hurst, K. Lothridge. Final report to the NIJ from grant 2006-MU-BX-K002, 2010.

28. M. Nelson, R. Chase, L. DePalma, *National Institute of Justice Special Report*, 2013, 1-20.

29. OPS White House, Investments to reduce the national rape kit backlog and combat violence against women, 2015.

30. G. LaPorte, H. Waltke, C. Heurich, R. Chase, *U.S. Department of Justice*, 2018, 1-20.

31. The Sexual Assault Forensic Evidence Reporting Act (SAFER), 2013.

32. National Adults/Adolescents Protocol, *U.S. Department of Justice*, 2013.

33. National best practices for sexual assault kits, *U.S. Department of Justice*, 2017.

34. P. Gill, A. Jefferys, D. Werrett, *Nature*, 1985, **318**, 577-9.

35. J. Butler. Advanced topics in forensic DNA typing: Methodology. 2011.

36. Forensic biology procedures manual, *Virginia Department of Forensic Science*, 2017**.**

37. S. Vuichard, U. Borer, M. Bottinelli, C. Cossu, N. Malik, V. Meier, C. Gehrig, A. Sulzer, M. Morerod, V. Castella, *Investigative Genetics*, 2011, **2**, 11.

38. V. Williamson, T. Laris, R. Romano, M. Marciano, *FSI: Genetics*, 2018, **34**, 265-76.

39. S. Klein, M. Buoncristiani, *FSI: Genetics*, 2017, **29**, 109-17.

40. F. Inci, M. Ozen, Y. Saylan, M. Miansari, D. Cimen, R. Dhara, T. Chinnasamy, M. Yuksekkaya, C. Filippini, D. Kumar, S. Calamak, Y. Yesil, N. Durmus, G. Duncan, L. Klevan, U. Demirci, *Advanced Science*, 2018, **5**, 1800121.

41. S. Garvin, M. Bottinelli, M. Gola, A. Conti, G. Soldati, *Journal of Forensic Science*, 2009, **54**, 1297-1303.

42. D. Nori, B. McCord, *Analytical and Bioanalytical Chemistry*, 2015, **407**, 6975-84.

43. V. Martinez, D. Nori, P. Dimsoski, B. McCord, *Electrophoresis*, 2017, **38**, 2777-85.

44. M. Vandewoestyne, F. Nieuwerburgh, D. Hoofstat, D. Deforce, *FSI: Genetics*, 2012, **6**, 258-62.

45. Z. Budimlija, M Lechpammer, D. Popiolek, F. Fogt, M. Prinz, F. Bieber, *Croatian Medical Journal*, 2005, **46**, 549-55.

46. J. Chen, I. Kobilinsky, D. Wolosin, R. Shaler, H. Baum, *Journal of Forensic Science*, 1998, **43**, 114-118.

47. C. Ladd, E. Carita, E. Pagliaro, A Garvin, A Crumbie, H. Lee, *U.S. Department of Justice*, 2006, 215339.

48. X. Zhao, L. Wang, J. Sun, B. Jiang, E. Zhange, J. Ye, *PLoS One*, 2016, **11**, 1-9.

49. M. Evander, K. Horsman, C. Easley, J. Nilsson, T. Laurell, *Proceedings of uTAS 2006 Conference*, 2006, 1055-57.

50. J. Norris, M. Evander, K. Horsman-Hall, J. Nilsson, T. Laurell, J. Landers, *Analytical Chemistry*, 2009, **81**, 6089-95.

51. A. Kundt, *Annalen der Physick und Chemie*, 1866, **4**, 498-523.

52. E. Trinh, *Review of Scientific Instruments*, 1985, **56**, 2059.

53. C. Lee, A. Anilkumar, T. Wang, *Physics of Fluids*, 1991, **3**, 2497.

54. X. Chen, R. Apfel, *Journal of the Acoustical Society of America*, 1996, **99**, 713.

55. E. Mednikov, *Acoustic Coagulation and Precipitation of Aerosols, Consultants Bureau New York*, 1965.

56. L. Rozenberg, *Physical Principles of Ultrasonic Technology, Plenum New York*, 1973.

57. C. Hill, *Physical Principles of Medical Ultrasonics, Ellis Horwood New York*, 1986.

58. G. Bellastella, T. Cooper, M. Battaglia, A. Strose, I. Torres, B. Hellenkemper, C. Soler, A. Sinisi, *Asian Journal of Andrology*, 2010, **12**, 871-879.

59. T. Laurell, F. Petersson, A. Nilsson, *Chemical Society Review*, 2006, **36**, 492-506.

60. H. Bruus, *Lecture notes for the advanced CISM school, Technical University of Denmark*, 2010.

61. A. Doinikov, *Recent Research Developments in Acoustics,* 2003, **1**, 39-67.

62. W. Konig, *Annals of Physics*, 1891, **42**, 353.

63. S. Woodside, B. Bowen, J. Piret, *American Institute of Chemical Engineers Journal*, 1997, **43**, 1727-36.

64. P. Dayton, K. Morgan, A. Klibanov, G. Brandenburger, K. Nightingale, K. Ferrara, *IEEE Transactions on Ultrasonics, Ferroelectrics, and Frequency Control*, 1997, **44**, 1264-77.

65. M. Evander, J. Nilsson, *Lab on a Chip*, 2012, **12**, 4667-76.

66. G. Stokes, *Transactions of the Cambridge Philosophical Society*, 1851, **9**, 8-106.

67. U. Ahmad, S. Rajendran, L. Ling, Y. Hooi, *Malaysian Journal of Analytical Sciences*, 2008, **12**, 367-74.

68. B. Giordano, M. Montgomery, C. Osburn, C. Lindsay, *Naval Research Laboratory*, 2014, 1-16.

69. K. Panz, K. Miksch, T. Sojka, *Bulletin of Environmental Contamination and Toxicology*, 2013, **91**, 555-9.

70. R. Garg, D. Grasso, G. Hoag, *Hazardous Waste Hazardous Materials*, 1991, **8**, 319-40.

71. J. Goodpaster, V. McGuffin, *Analytical Chemistry*, 2001, **73**, 2004-11.

72. Environmental Protection Agency, *Method 8330a*, 2007.

73. T. Jenkins, M. Walsh, *Talenta*, 1992, **39**, 419-28.

74. S. Giannoukos, B. Brkic, S. Taylor, A. Marshall, G. Verbeck, *Chemical Review*, 2016, **116**, 8146-72.

75. Lake Ontario Ordnance Works, *Final Remedial Investigation Report*, 2011.

76. L. Shriver-Lake, K. Breslin, P. Charles, D. Conrad, J. Golden, F. Ligler, *Analytical Chemistry*, 1995, **67**, 2431-35.

77. L. Shriver-Lake, B. Donner, F. Ligler, *Environmental Science and Technology*, 1997, **31**, 837-41.

78. S. Terabe, K. Otsuka, K. Ichikawa, A. Tsuchiya, T. Ando, *Analytical Chemistry*, 1984, **56**, 113-6.

79. S. Oehrle, *Electrophoresis,* 1997, **18**, 300-2.

80. L. Jang, M. Razu, E. Jensen, H. Jiao, J. Kim, *Lab on a Chip*, 2016, **16**, 3558.

81. S. Wallenborg, C. Bailey, *Analytical Chemistry*, 2000, **72**, 1872-8.

82. J. Landers, *Handbook of Capillary and Microchip Electrophoresis and Associated Microtechniques*, 2008.

83. J. Pichtel, *Applied and Environmental Soil Science*, 2012, 1-33.

84. H. Whatley, *Clinical and Forensic Applications of Capillary Electrophoresis*, 2001, **454**, 21-58.

85. M. Rashid, Y. Dou, V. Auger, Z. Ali, *Micro and Nanosystems*, 2010, **2**, 1-29.

86. C. Gartner, W. Hoffmann, H. Demattio, T. Clemens, M. Klotz, R. Klemm, H. Becker, *Proceedings of SPIE*, 2009.

# Chapter 2: Acoustic differential extraction for processing sexual assault samples

## 2.1 Introduction

Acoustic differential extraction (ADE) is an approach for automated capture of sperm cells from sexual assault samples. ADE offers several advantages over current differential extraction (DE) approaches, most notably for its ease of automation, reduction in the number of pipetting and transfer steps, and faster processing time per sample. Each of these benefits will increase the throughput of forensic laboratories, while also freeing up analyst time to draw conclusions from each short tandem repeat (STR) profile. By completing the sperm cell capture within a sealed microfluidic chip, we also reduce the potential for contamination of the sample due to environmental exposure.

As described in recent publications [1, 2] ADE uses a standing acoustic wave to capture and purify sperm cells from a liquid sample. This is achieved by inducing a high frequency vibration in a piezoelectric transducer (piezo), which transmits that acoustic energy through a glass coupling layer into the fluidic chamber. When the microchannel height is matched to a half-wavelength of the actuation frequency, a standing wave is formed with low-pressure nodes at each intersecting point. As detailed in **Chapter 1**, all particles exposed to the acoustic wave experience a primary radiation force, drawing them either to the pressure nodes or antinodes, with larger particles experiencing a stronger force [3]. This principle has been previously applied to separate blood cells from plasma [4], as well as capturing yeast cells from water [5]. In the context of sexual assault samples, the goal is to capture sperm cells while removing all other cellular and genetic material (i.e. non-sperm particles) from the sample. In ADE, when the sperm cells are

trapped in the standing wave, non-sperm particles will experience a weaker primary radiation force, and thus can be washed away by applying a sufficiently high liquid flow rate (45 μL/min). This results in purified aggregates of sperm cells, held in place with an acoustic standing wave, while all non-sperm particles and extracellular DNA are removed. This step of holding the aggregate in place and 'washing' is crucial, as the majority of sexual assault samples contain far more epithelial cells than sperm cells, and female DNA will be present at much higher concentrations than male DNA.

The work described here also incorporates 'seeding' of the acoustic trapping site, which is the introduction of additional particles to initiate trapping. Seeding is necessary for samples where a low number of sperm may be present, and the secondary radiation forces would be too weak to form a sufficient aggregate. Hammarström et. al [6] demonstrated that when particles are too dilute to be trapped acoustically, the addition of similarly sized beads at a high concentration will initiate the aggregation, after which the target particles (*E. coli* cells in this example) can be efficiently trapped. We use this same approach by adding 6 μm diameter polystyrene particles to each sample, ensuring that if total sperm cell concentration is low, there will still be aggregation in the trapping site [1, 2].

The ADE approach does not seek to replace every aspect of a conventional differential extraction; rather the goal is to improve upon the physical sperm cell capture. The initial differential lysis step to break open all non-sperm cells remains the same, as does the sperm cell extraction and DNA amplification after acoustic trapping. The overall workflow is shown in **Figure 2-1**, where ADE replaces the traditional centrifugation, washing, and pipetting steps of a differential extraction. This results in PCR-ready, male DNA in less than 50 minutes, substantially faster than current forensic capabilities, which require 2-14 hours for a full differential extraction.

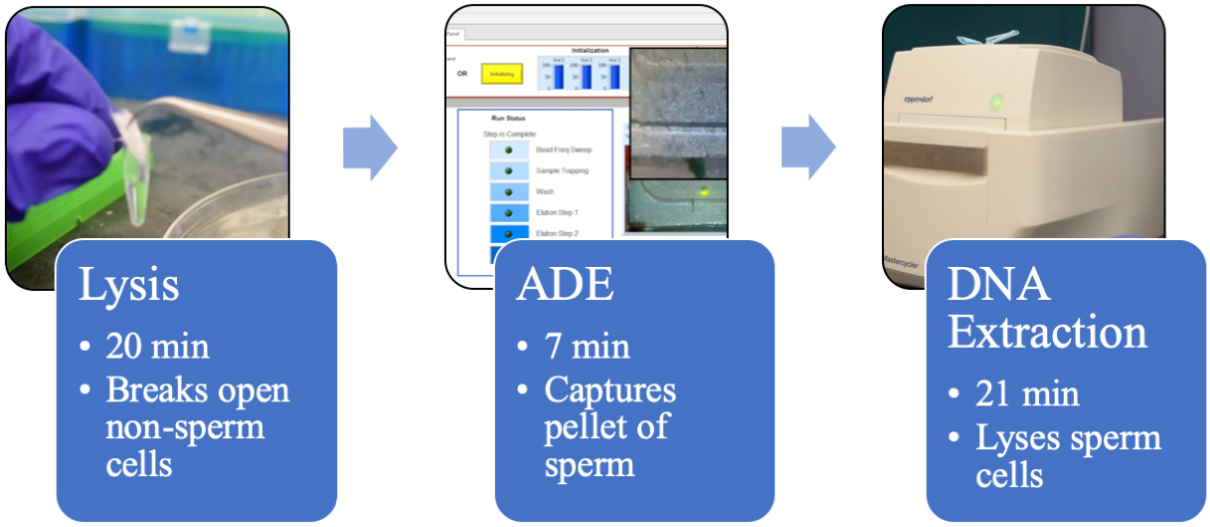


*Figure 2-1. ADE workflow. Traditional differential lysis and DNA extraction are used, but when combined with ADE, the entire process is faster and more automated than a conventional differential extraction. During ADE, there are no pipetting or centrifugation steps, and the scanning, trapping, washing, and eluting steps are performed automatically.*

The primary goal of this research was to develop a technique that fits seamlessly into an existing chemical workflow, while still significantly improving the quality and efficiency of differential extraction for sexual assault samples.

The origins of ADE date to 2006, and a collaboration with Lund University, Sweden. Pioneering acoustic work from the Laurell and Nilsson groups, and others, laid the foundation for applying acoustic separation principles to sexual assault samples. Early ADE research focused on retaining the maximum number of sperm cells from a diluted semen sample, successfully enriching sperm concentration via acoustic trapping [7, 8]. However, those studies were limited by low flow rates (1 µL/min) and relatively high sample volumes (500 µL), hindering applicability to realistic scenarios. Limited studies were conducted with samples containing both male and female DNA, and the project had not progressed past the 'proof-of-concept' stage. After 8 years of research, ADE was shown to be a novel approach for capturing sperm cells, and applied to a limited range of mock sample formulations. It had not, however, reduced the manual requirements of sample manipulation, nor been demonstrated for samples containing intact epithelial cells (a component

of virtually every authentic sexual assault sample), and still relied on a glass-etched, reusable microfluidic chip. Furthermore, the previous ADE research instituted a complex, sprawling apparatus that required advanced engineering capabilities to operate, and was not remotely applicable for a forensic laboratory setting. The following chapter describes significant overhaul of the ADE project, beginning with microchip design and validation, progressing through integration of engineering components into a compact, user-friendly instrument, and culminating with exhaustive testing of realistic mock samples, spanning a wide range of forensically relevant cellular ratios.

## 2.2 Materials and methods

### *2.2.1 Microchip design and fabrication*

The composition of the resonant chamber for acoustic trapping is crucial, requiring a substrate such as glass, that will minimize energy loss compared to the stored energy of the resonator [9]. Other materials, including poly(methyl methacrylate) (PMMA) and SU-8 polymers are feasible for acoustic trapping, but high acoustic attenuation restricts their applicability to only systems with multiple transducers [10]. For this reason, acoustic trapping was performed in a glass-polydimethylsiloxane (PDMS)-glass (GPG) sandwiched microchip, and minimal energy was lost to heat during vibration.

The microchip contained 6 fluidic reservoirs capable of holding 120 μL each, connected by channels with dimensions ranging from 0.5 mm to 1.0 mm diameter, and 283 μm in height (**Figure 2-2**). The fluidic reservoirs were designed to contain yellow fluorescent beads (R1), the sexual assault sample (R2), wash buffer (R3), and to collect the downstream sperm fraction (R4), non-sperm fraction (R5), and waste (R6). The microfluidic ADE chip, shown in **Figure 2-2,** was composed of PDMS: 283 μm (lower) and 1.5 mm (upper), 175 μm glass, 3.2 mm PMMA, and

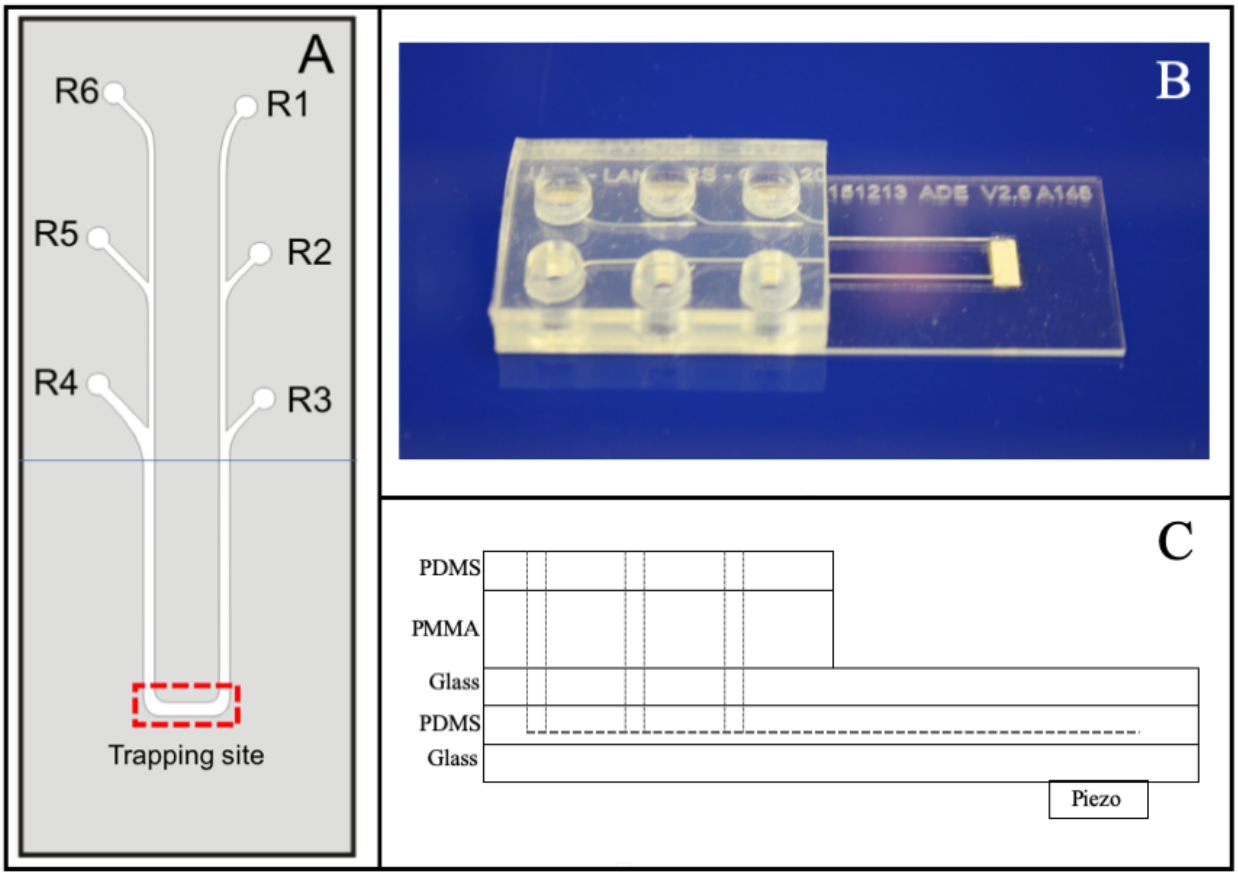


*Figure 2-2. Microfluidic chip design. (A) Top-down view of chip design. 6 reservoirs are included that can each hold up to 110 µL of liquid, and contain fluorescent bead solution (R1), sample (R2), wash buffer (R3), sperm fraction (R4), non-sperm fraction (R5), and waste (R6). (B) Image of the complete microchip. (C) Side-view of chip design. The fluidic reservoirs are cut through the upper PDMS, PMMA, and glass layers, before intersecting the channel cut into the middle PDMS layer.*

pressure-sensitive adhesive. The fluidic architecture was designed in computer assisted design software (CorelDraw, AutoCAD), and cut from each PDMS layer using $CO_2$ laser ablation. Access holes were cut into the upper glass layer using $CO_2$ laser ablation, with 40 repetitions at low power to avoid cracking of the glass. Sample reservoirs were cut from the upper, thicker PDMS layer using an Acu-Punch® 5 mm biopsy punch. To adhere the lower glass and PDMS layers, solvent bonding with methanol was performed. The PDMS layer and glass reflecting layer were irreversibly bonded through plasma oxidation, sealing the resonant chamber for acoustic trapping. The upper PMMA and PDMS layers were adhered using pressure-sensitive adhesive. After assembly, each microchip underwent quality control testing via extrinsic Fabry-Perot

interferometry (EFPI) to precisely determine the channel height of the acoustic trapping region. Due to minor variations in material thickness, each chip will have slightly different channel heights (± 10 μm), thus impacting the optimal trapping frequency. To generate the ultrasonic standing wave, a piezoelectric transducer was adhered to the bottom of each microfluidic chip. Piezos display a linear response in oscillation to an input voltage [11], and will vibrate with the same frequency as the input voltage frequency. Based on the microchannel height (283 μm) and the desire to generate 3 trapping nodes, applied frequencies were on the order of 7-9 MHz.

*2.2.2 Acoustic trapping of particles*

A frequency of sound was chosen such that a standing wave was formed with three nodes, and thus three regions of low pressure where particles would be drawn due to their acoustic radiation force. The resonance frequency of the standing wave was predicted using the 1D resonance approximation (**Equation 1**), which is dependent on the height of the channel (h), ultrasonic wavelength (λ), and the number of acoustic nodes (n).

$$(1) \qquad h = n\lambda/2 = nv/2f \; (n = 1,2,3...)$$

The microchips were fabricated with 283 μm thick PDMS as the fluidic layer, and thus, the necessary wavelength to generate three nodes was calculated to be 188 μm, or a frequency of 7.71 MHz. Due to variability in material thickness, the necessary frequency to generate a standing wave may differ slightly for each microchip.

As shown in **Figure 2-3A**, when a solution of different particle sizes is flowed through the standing wave, the larger particles experience a stronger primary acoustic radiation force, and are held in place, despite the fluid flow dragging them downstream. This can be visualized by acoustic trapping of fluorescent beads (**Figure 2-3B**), and additionally it is observed that a slight deviation from the resonant frequency leads to a significant decrease in trapping efficiency. Beads are

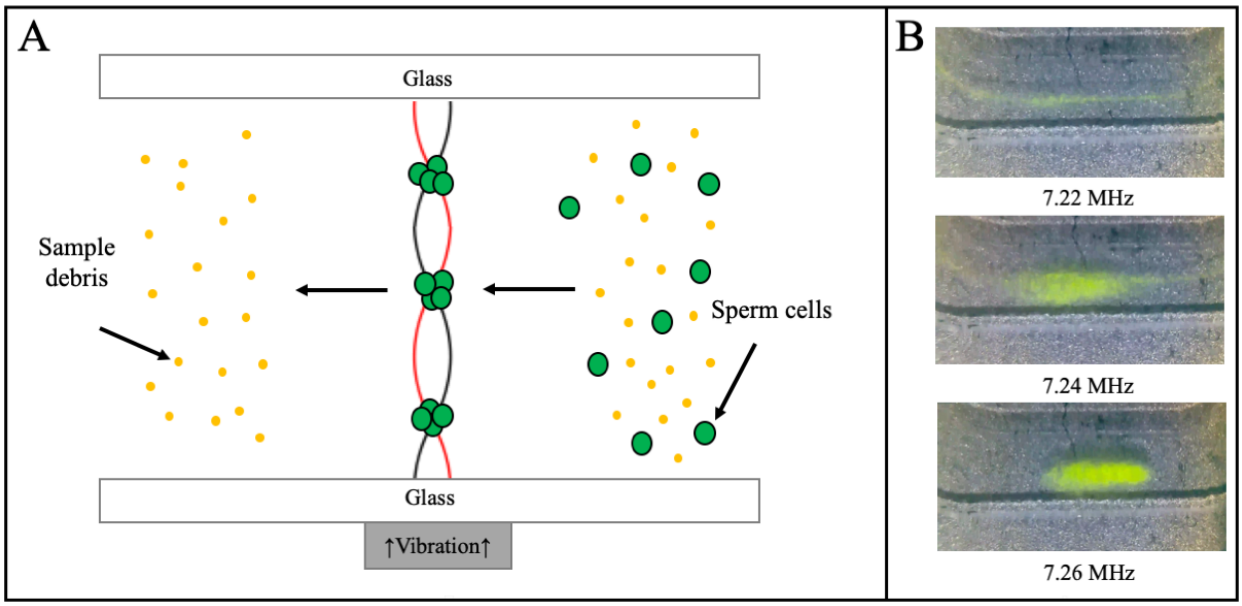


*Figure 2-3. Visualizing acoustic trapping. (A) Acoustic trapping of sperm cells under liquid flow. When subjected to flow in the microchannel, sperm cells are held in place at the acoustic nodes while smaller particles and debris are washed away. (B) Visual monitoring of bead aggregation across three applied frequencies. As the frequency of sound reaches the optimal trapping frequency, 7.26 MHz, a large, dense aggregate of fluorescent beads is formed.*

focused to the channel center, but not trapped at 7.22 MHz, while a loose aggregate is formed at 7.24 MHz. When the applied frequency is increased to 7.26 MHz, a large, stable aggregate of beads is formed that remains held in place under flow. This is exactly how sperm cells are trapped and held in place, as they are the largest particles in solution after a differential lysis is performed on the sexual assault sample.

### *2.2.3 Hardware design*

All necessary components for fluidic control, electronic activation of the piezo, and user operation were integrated into a single prototype instrument shown in **Figure 2-4A**. The acrylic protective shell contained a waveform generator (Hantek DDS-3X25), an oscilloscope (Hantek 6052BE), and a home-built amplifier, all controlled via LabView software. The upper module was 3D printed from polylactic acid (PLA) material, and housed the syringe pumps (LabSmith SPS01), solenoid valves (LabSmith AV201), and rubber O-rings that prevent fluidic contact with any of the hardware outside the microchip. By maintaining pneumatic fluid control, sample is never

exposed to the hardware, and thus, cross-contamination between samples run on the same instrument is mitigated. Also contained in the 3D printed module is the chip manifold, which is

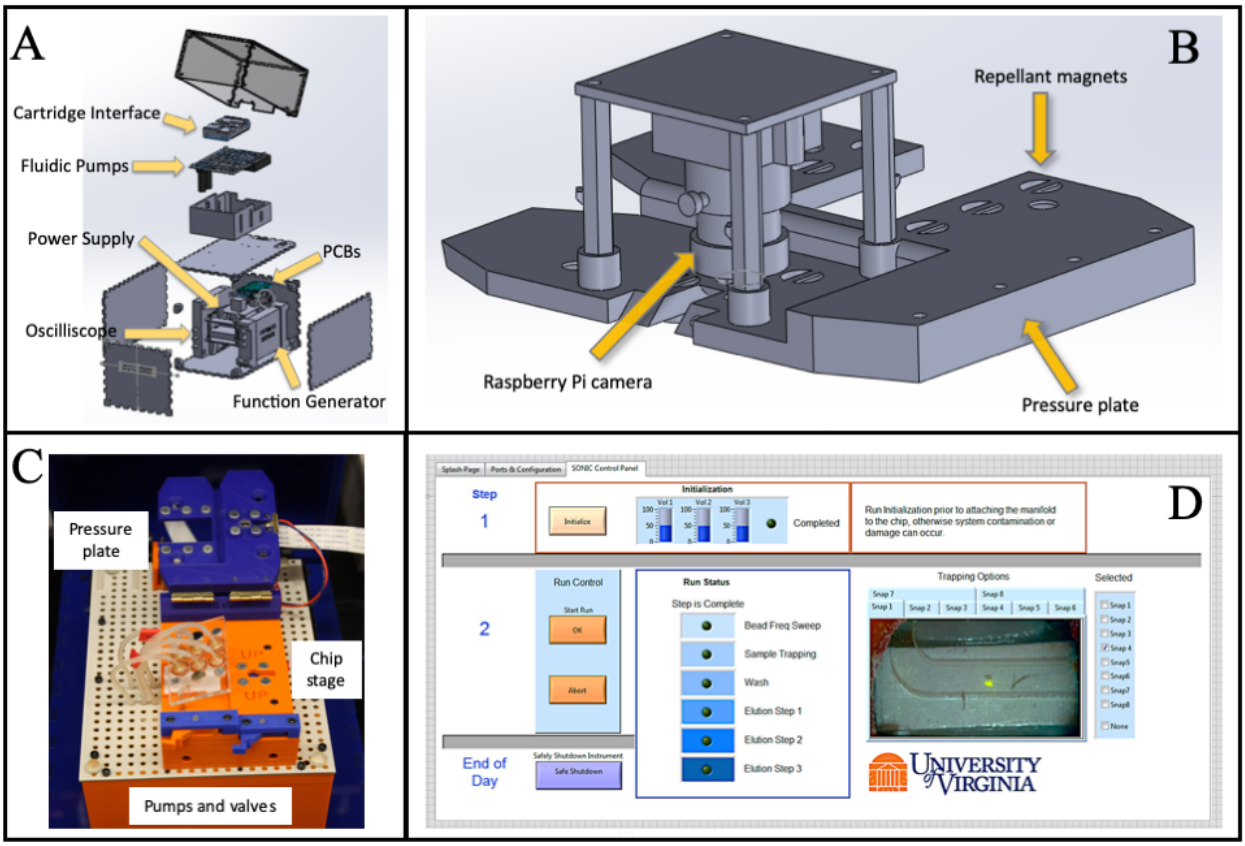


*Figure 2-4. ADE instrumentation. (A) Hardware and electronic components of the ADE prototype. All elements required to induce the standing wave are encased in the ADE box and controlled via external laptop. (B) The chip manifold contains repulsive magnets to apply uniform pressure, as well as a Raspberry Pi camera to monitor trapping in real time. (C) 3D printed chip mounting stage and fluidic control module. The blue pressure plate applied uniform force to the microchip, maintaining pneumatic connection to the pumps and valves housed in the 3D shell beneath the chip stage. (D) The graphical user interface provides status updates on syringe pump volume, valve status, and overall trapping stage.*

comprised of two hinged layers that apply uniform pressure to the top of the microchip (**Figure 2-4B-C**). The chip manifold ensures uniform contact with all 6 O-rings, maintains electrical contact between the piezo and brass pogo pins, and brings the Raspberry Pi camera into focus over the acoustic trapping site. The inclusion of the Raspberry Pi camera provided real time monitoring of acoustic trapping events, which was crucial for development and optimization of this work. Video feedback was also used for quality control testing of each chip to determine the optimal trapping frequency before loading a sample. All of the fluidic and electronic hardware was controlled

through a graphical user interface (GUI) on a laptop. The GUI (**Figure 2-4D**) showed the volume of each syringe pump, valve status, and provided real time video monitoring to the user. The GUI could also be programmed to perform automated acoustic trapping, and contained an advanced menu which allowed the user to change flow rate, trapping time, valve position, and other parameters if desired.

*2.2.4 ADE workflow*

To perform ADE, the following solutions were loaded by the operator in this sequence: 10 μL priming solution (5:1:1 mixture of ethanol, glycerol, and water) to reservoir 1; 110 μL fluorescent bead solution (1:500 dilution of 6 μm diameter yellow fluorescent beads in water) to reservoir 1; 65 μL sample added to reservoir 2; and 43 μL wash buffer to reservoir 3. The microchip was loaded into the instrument, and samples were processed in 4 automated stages: frequency scanning, sample trapping, washing, and elution. The frequency scanning step identified the optimal acoustic trapping frequency for each chip, ensuring resonance was achieved for maximum sperm cell retention. Even though each chip underwent quality control to predict the optimal trapping frequency, environmental conditions such as temperature and humidity can impact the properties of PDMS [12], and lead to minute changes in layer thickness and channel height. The scan was conducted using fluorescent beads by applying 8 different acoustic frequencies at 0.02 MHz increments, holding each one for 5 seconds before releasing the bead aggregate. In this manner, a range of 0.14 MHz could be covered in less than a minute. During each applied frequency, images of the trapped aggregate were saved, computer software measured the size of the aggregated beads, and the optimal trapping frequency was objectively determined based on the largest clump of trapped beads. This is shown in **Figure 2-5**, where frequencies are applied from 8.04 MHz to 8.18 MHz, and the largest aggregate of beads occurred at 8.14 MHz,

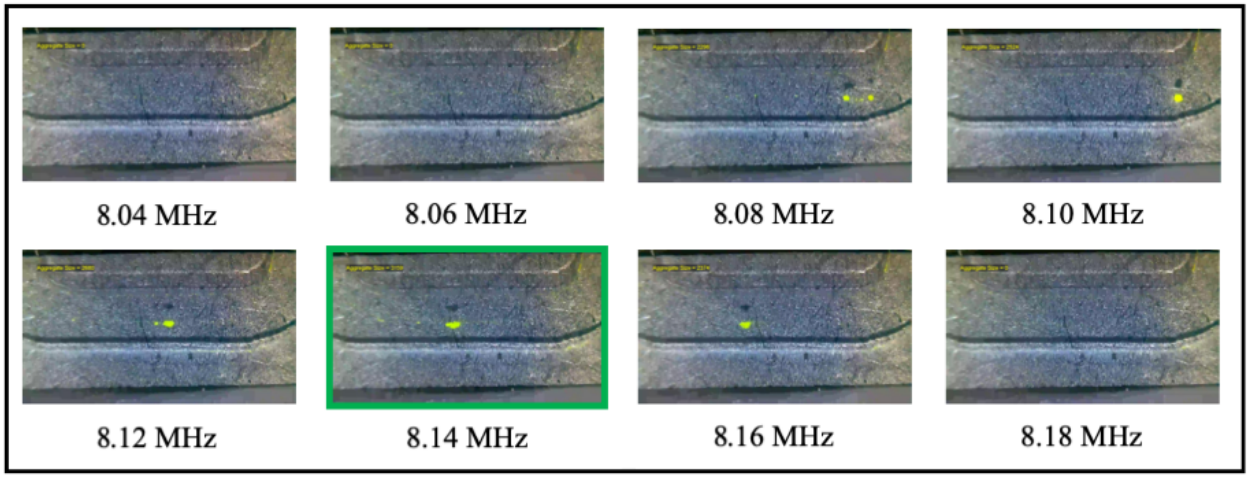


*Figure 2-5. Frequency scan to determine optimal trapping frequency. As the piezo steps up by 0.02 MHz every 5 seconds, the size of the bead aggregate is measured by computer software. The largest bead aggregate occurred at 8.14 MHz, which is selected as the optimal trapping frequency for this test.*

the 6$^{th}$ applied frequency. Using this information, 8.14 MHz would then be applied to trap sperm cells. During sample trapping, the optimal trapping frequency was applied while the sample was flowed from R2 at 45 µL/min. Sperm cells were trapped and held in place, while smaller particles including free DNA and cellular debris were forced out of the trap site and flowed to R5. This proceeded for 60 seconds, after which the sample from R2 was depleted and the aggregate of sperm had been captured. Flow was then switched to R3, which contained the wash buffer. For most experiments this was water, but some tests were conducted using phosphate buffered saline. During this washing stage, the piezo remained activated, at the optimal frequency, to hold the pellet of sperm in place while the wash buffer displaced the surrounding fluid, and removed any residual non-sperm genetic material from the trapping site. Finally, the piezo was deactivated, which eliminated the standing acoustic wave and released all trapped cells. High flow rate (200 µL/min) was used to move the captured cells to R4, where they were pipetted out for DNA extraction and amplification.

### *2.2.5 Chemical processing of samples*

Consistent with forensic protocols, sample handling consisted of a preferential lysis before ADE, followed by a DNA cleanup step, sperm cell DNA extraction, PCR amplification, and electrophoretic separation of DNA fragments [13]. All chemical treatments were performed in-tube. Epithelial cells were preferentially lysed using *prep*GEM (ZyGEM NZ Ltd) with incubation at 75°C for 15 min and 95°C for 5 min. Once ADE was completed and the sperm aggregate eluted from the chip, the pellet was treated with DNase 1 enzyme (ZyGEM NZ Ltd, 0.5 Units enzyme/reaction) and 1X DNase buffer (ZyGEM NZ Ltd) at 37°C for 5 min, followed by 75°C for 5 min to remove any non-sperm DNA that may remain in the sperm fraction. Male DNA was extracted from sperm cells using Acrosolv, *prep*GEM, and 1X Red Plus buffer (ZyGEM NZ Ltd) by incubating at 52°C for 5 min, 75°C for 3 min, and 95°C for 3 min. PCR was conducted using Promega reagents, with either a 5-plex, 6-plex, or 18-plex STR panel, all allele markers are listed in **Table 2-1**.

| Promega amplification kit | Allele-specific PCR markers |
|---|---|
| 5-plex | Amelogenin, D2S1338, D8S1179, D12S391, D21S11 |
| 6-plex | Amelogenin, D18S51, D2S1338, D8S1179, D12S391, D21S11 |
| PP18D | Amelogenin, D3S1358, D1S1656, D21S441, D10S1248, D13S317, Penta E, D16S539, D18S51, D2S1338, CSF1PO, TH01, vWA, D21S11, D7S820, D5S818, D8S1179, D12S391, D19S433, FGA |

*Table 2-1. Allele markers for PCR amplification kits. The custom 5- and 6-plex amplification kits differed by a single allele marker (D18S51). The Promega PP18D kit contained an additional 14 allele markers.*

While national forensic laboratories require 20 loci (or more) for STR profiles that can be used in court, we opted to conduct research and development using custom 5-plex and 6-plex STR kits for reasons of cost. The conclusions drawn from these limited-loci amplification kits are still valid, as we are deciphering the presence or absence of male vs female DNA, not referencing the profiles for a match in a national database. Each amplification kit used a 96°C denaturation step

for 2 min, followed by 30 cycles of 94°C for 10 sec and 60°C for 60 sec, with a final 5 min hold at 60°C. The PCR displayed a linear dynamic range of 0.1-2.5 ng DNA ($R^2$ = 0.9839). After amplification, 1 uL of the DNA fragments, along with an internal lane standard, were injected and separated electrophoretically using a 16-capillary ABI 3130xL. The resulting electropherograms were analyzed using GeneMarker v2.9.2.

*2.2.6 Mock sample formulation*

During development of the ADE prototype, mock samples were tested and analyzed to evaluate acoustic trapping performance. Multiple experts from forensic laboratories were consulted on formulating the most realistic samples possible. Under the UVA Institutional Review Board HSR Protocol #12548, neat semen was donated from healthy males. The semen samples were aliquoted into 50 μL batches and stored at 4°C in a biohazardous materials refrigerator. Under the same IRB protocol, healthy females donated buccal swabs, vaginal swabs, and post-coital vaginal swabs, all collected on cotton, which were stored at room temperature. Post-coital vaginal swabs were donated by the UVA hospital; however, it was not specified if condoms were used, thus the presence of sperm could not be guaranteed. For this reason, 500-2,000 sperm cells were spiked into mock samples generated from these swabs. To recover female epithelial cells, each swab was agitated in 600 μL water for 60 seconds, followed by a spin basket to collect cells. The cell pellet, as well as the semen aliquots, were then diluted and counted via hemocytometry (**Figure 2-6**) using the green fluorescent nucleic acid stain SYTO-11. The respective cellular concentrations recovered for post-coital vaginal and their corresponding buccal swabs are shown in **Figure 2-6**.

For testing the effect of exogenous biological material present on the swab; yeast, *E. coli*, and blood were added to mock samples. Yeast cells were activated by adding 25 mg dry yeast to

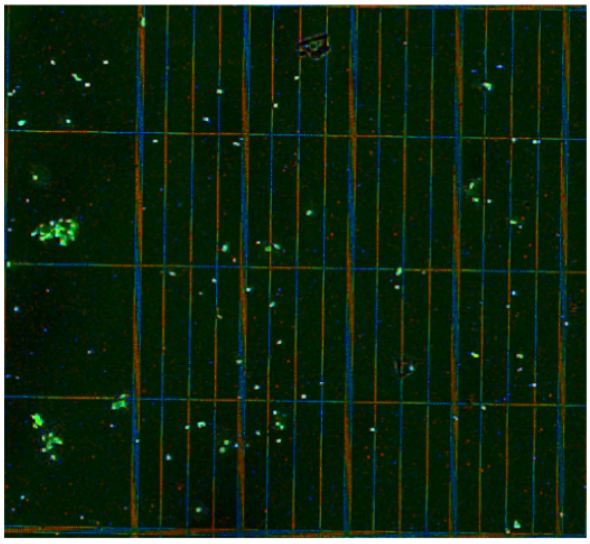

| Sample | Cheek (cells/uL) | Vaginal (cells/uL) |
|---|---|---|
| 003 | 50 | 306 |
| 004 | 239 | 744 |
| 005 | 100 | 2167 |
| 006 | 94 | 588 |
| 007 | 144 | 667 |
| 010 | 89 | 459 |
| 013 | 94 | 405 |
| 015 | 56 | 189 |

*Figure 2-6. Cell counting for donated swabs. The stain SYTO-11 exhibits bright green fluorescence upon binding nucleic acids, and thus can be used to accurately quantify the number of cells present in a sample using microscopy (left). Of the 8 samples collected through the UVA hospital, the range of cell counts on each swab was highly variable (right).*

500 µL water, and diluting 1000X in water. A vaginal swab containing menstrual blood was collected, and the epithelial cell count was measured at 678 cells/µL (including white blood cells, which were not visually distinguishable under SYTO-11 staining). *E. coli* cells (XL1-Blue strain, Stratagene) were cultured in 5 mL of Super Optimal Broth (SOB) medium, and spiked into mock samples. For the addition of yeast and *E. coli* cells, they were added at 20-40% of the concentration of epithelial cells in the sample, a common range for the presence of exogenous cells in the vaginal cavity [14].

## 2.3 Results and discussion

### *2.3.1 Quality control testing*

A crucial aspect for ADE is preventing any possible contamination of one sample with the genetic material of another. The presence of contaminating DNA from a forensic analyst or subject of a separate investigation in a sample could be catastrophic, as it would indicate lack of proper sample handling and cast doubt on all results. For this reason, each microchip was single-use only. However, as a factor of machining tolerances of the purchased materials, complete uniformity in

channel height was not achievable. In order to predict the optimal trapping frequency before testing each microchip, the channel height was measured using EFPI, a fiber-optic technique that can determine the depth of an object based on its light scattering properties [15]. From this data, and the experimental acoustic trapping, a linear relationship ($R^2 = 0.9841$) was established between the optimal resonant frequency and the inverse of the channel height (**Figure 2-7**). Using this predictive formula, the optimal trapping frequency for each chip can be predicted using the

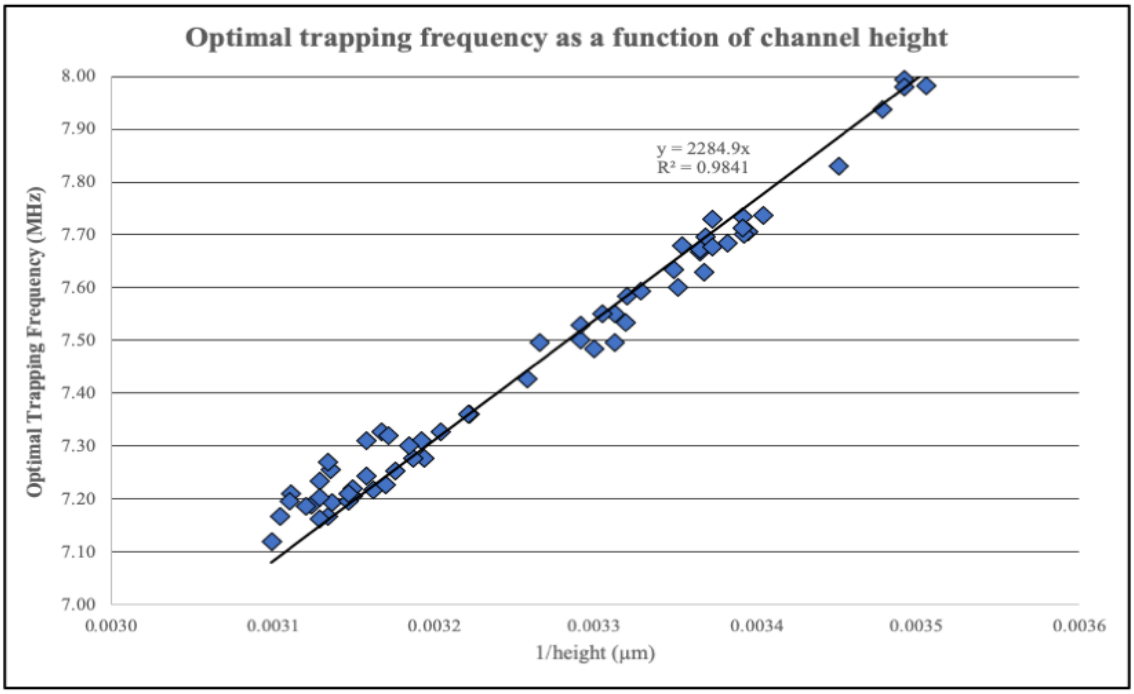


*Figure 2-7. Relationship between channel height and optimal trapping frequency. There is a linear relationship ($R^2 = 0.9841$) between the inverse of the channel height (x-axis) and the optimal trapping frequency (y-axis). This allows for accurate prediction of the optimal trapping frequency without needing to test each individual chip.*

measured height of the channel with high accuracy. As shown in **Figure 2-8**, which plots the experimental optimal trapping frequency (x-axis) against the difference (in MHz) from the predicted optimal frequency (y-axis), these predictions were extremely accurate. The red bars represent ± 0.07 MHz from the predicted frequency, which are the bounds of the 0.14 MHz frequency scan conducted before each test. Of the 93 microchips tested, only 3 fall outside of this scan range. This data clearly shows that accurate channel height measurements can reliably predict

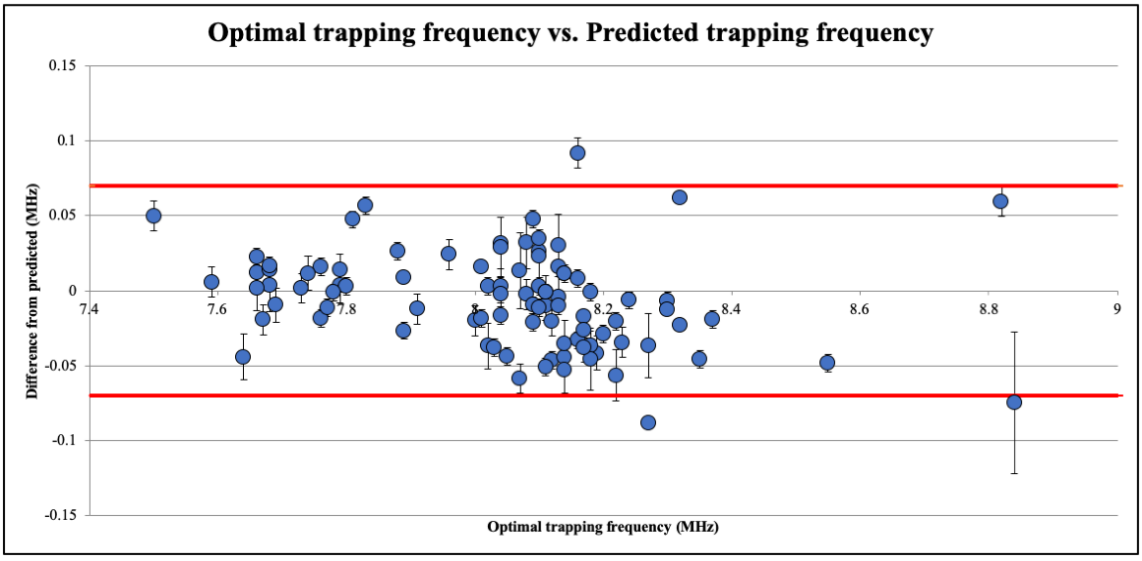


*Figure 2-8. Variability in predicted vs actual optimal trapping frequency. By using testing frequencies across 0.14 MHz (boundaries within red lines), 96% of all microchips fabricated exhibit acoustic trapping within the scan range. Error bars represent ±1 standard deviation, n = 3 for each data point. For the 93 chips tested, all but three displayed optimal trapping frequency within 0.07 MHz of the predicted trapping frequency.*

the optimal trapping frequency, and that a frequency of 0.14 MHz is sufficient for identifying the optimal frequency for the 96% of the ADE microchips.

### *2.3.2 Mock samples from buccal swabs*

This mock sample was generated with buccal cells and sperm cells in equal concentration, and underwent differential lysis prior to ADE. By examining the female reference STR profile (**Figure 2-9A**) and the male reference STR profile (**Figure 2-9B**), it can be seen that the shared alleles are AMEL-X, D2-24, D8-13, and D21-31.2. The remaining alleles are unique to each donor. In the pre-trapping STR profile (**Figure 2-9C**), a 'mixed' profile is observed, where there are roughly equal contributions from both the male and female DNA. This STR profile is insufficient to conclusively identify a suspect, as it could be claimed that one or more alleles of the potential suspect are masked by the significant contribution of the victim's DNA. However, after undergoing ADE, the sperm fraction (**Figure 2-9D**) generated a 'clean male' profile, and exactly matched the reference STR pattern of the sperm cell donor. This demonstrate that ADE

was able to completely isolate sperm cells from all other genetic material in less than 7 minutes, without any hands-on manipulation of the sample.

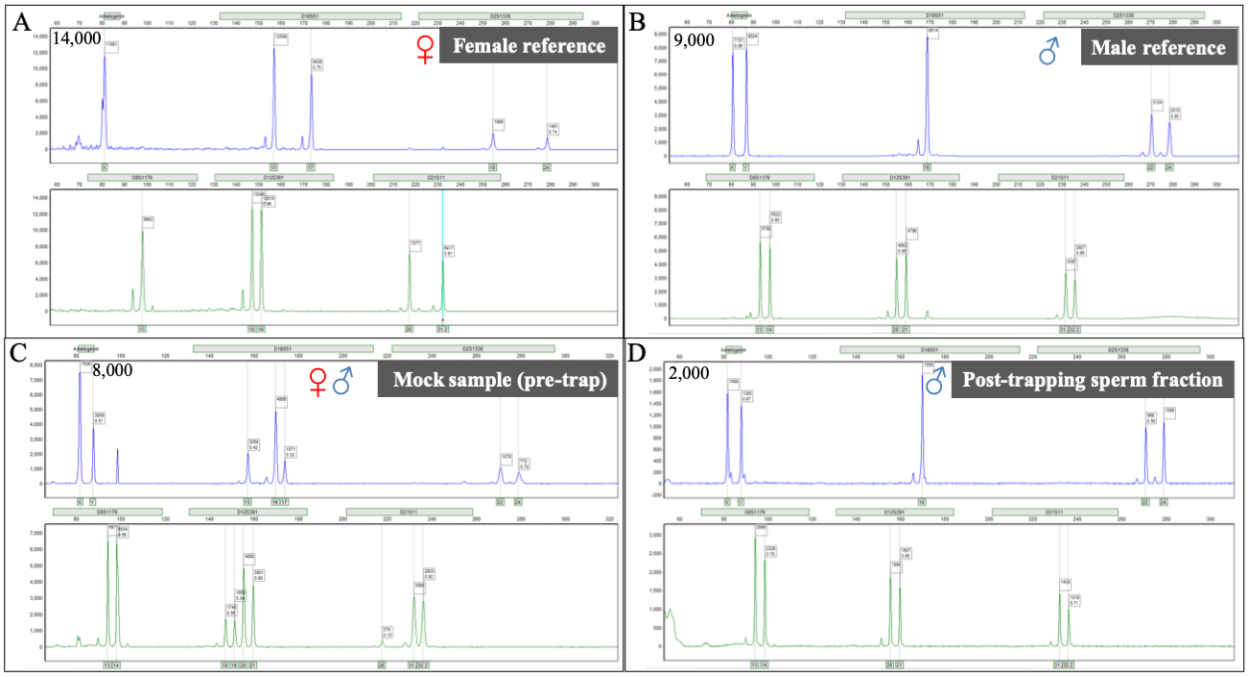


*Figure 2-9. STR profiles from 1:1 mock sample. (A) Female reference profile, obtained from buccal swab. (B) Male reference profile, obtained from anonymously donated semen. (C) STR profile from the mock sample before undergoing ADE. Alleles are present from both the male and female cell donors, constituting a mixed profile. (D) STR profile from the sperm fraction after ADE. All alleles present match the male donor, indicating complete isolation of sperm cells.*

### *2.3.3 Mock samples from post-coital vaginal swabs*

Post-coital vaginal swabs, obtained through collaboration with the UVA Hospital, were used to generate mock samples with a range of epithelial cell:sperm cell (F:M) ratios. The same anonymous sperm donor was used for each sample, but each vaginal swab was provided by a different individual. The data in **Figure 2-10** shows the STR profiles generated from samples 007 and 013, which were formulated at 4:1 and 3.5:1 F:M ratios, respectively, by first quantitating the number of epithelial cells present, and adding a dilution of semen. These ratios of F:M cells are reflected in the pre-trapping STR profiles (**Figure 2-10B and E**), in which a clearly 'mixed' profile is observed. While the female alleles demonstrate stronger peak heights than the male alleles, there is a significant amount of DNA present from both donors, and these samples would require

differential extraction to be probative (usable in court). After ADE, the post-trapping sperm fractions (**Figure 2-10C and F**) are 'clean male' STR profiles, containing alleles only from the sperm donor. While this shows successful ADE for post-coital mock samples at higher cellular ratios, there are concerns over the peak heights of the post-trapping STR profiles. **Figure 2-10C** exhibits peak heights between 100 and 500 RFU, as compared to the 600-2200 RFU peaks seen in **Figure 2-10E**. One conclusion that could be drawn is that not all sperm cells in the mock sample were captured, indicating differences in capture efficiency in each test. However, the video of

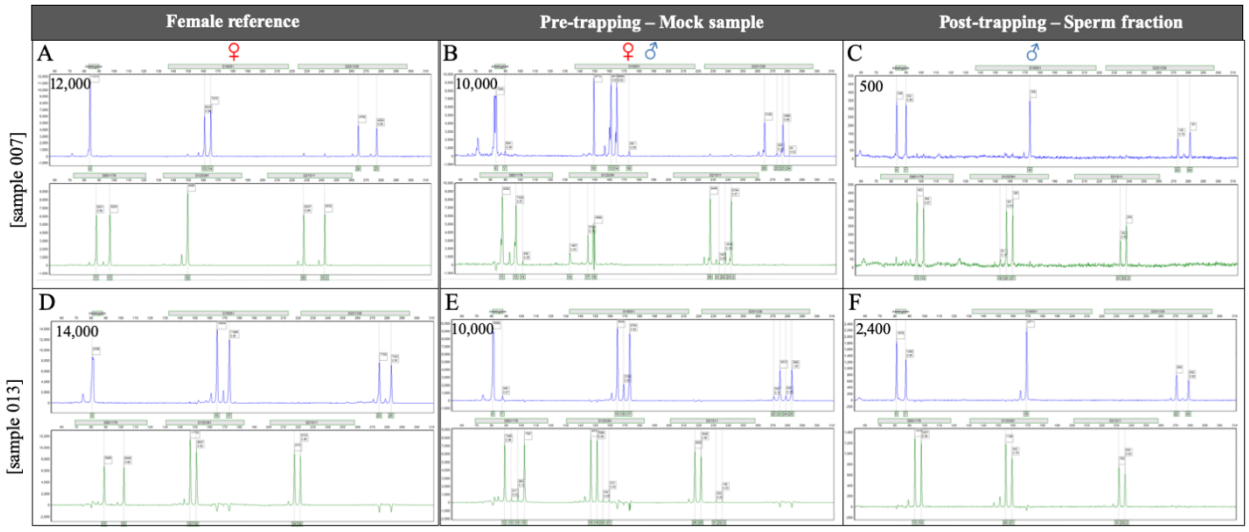


*Figure 2-10. STR profiles from vaginal swab mock samples. (A) Female reference profile for donor 007. (B) STR profile from mock sample containing F:M of 4:1 before ADE. Alleles from both male and female donors are observed. (C) Sperm fraction STR profile from mock sample 007 after acoustic trapping. Only male alleles are seen, which match the reference profile of the semen donor. (D) Female reference profile for donor 013. (E) Pre-trapping profile from mock sample containing F:M of 3.5:1, with both male and female alleles present. (F) Sperm fraction STR profile exactly matches that of the sperm donor, indicating successful separation of sperm cells from female epithelial cells.*

sample trapping showed large aggregates of sperm collected for each sample, suggesting that acoustic trapping performance was not impaired. Another possible explanation is that the sperm cells used for sample 007 had degraded, or been damaged over long term storage. Any sperm cell degradation would make them susceptible to rupture during the first preferential lysis step, resulting in removal of male DNA during the DNase 1 treatment, and subsequently low peak heights in the STR profile.

Additional post-coital vaginal swabs were used to generate samples 010 and 015, which were formulated at F:M cell ratios of 5:1 and 2:1, respectively. The pre-trapping profiles (**Figure 2-11B and E**) show 'major female' profiles, where some male alleles are seen, but at significantly lower peak heights than the female alleles. This is unsurprising due to the excess female cells in solution. After ADE, the post-trapping sperm fractions (**Figure 2-11C and F**), again, generated 'clean male' STR profiles, with no observed female DNA after ADE. These promising results show successful capture of sperm cells from a mock sexual assault sample, both in less time and

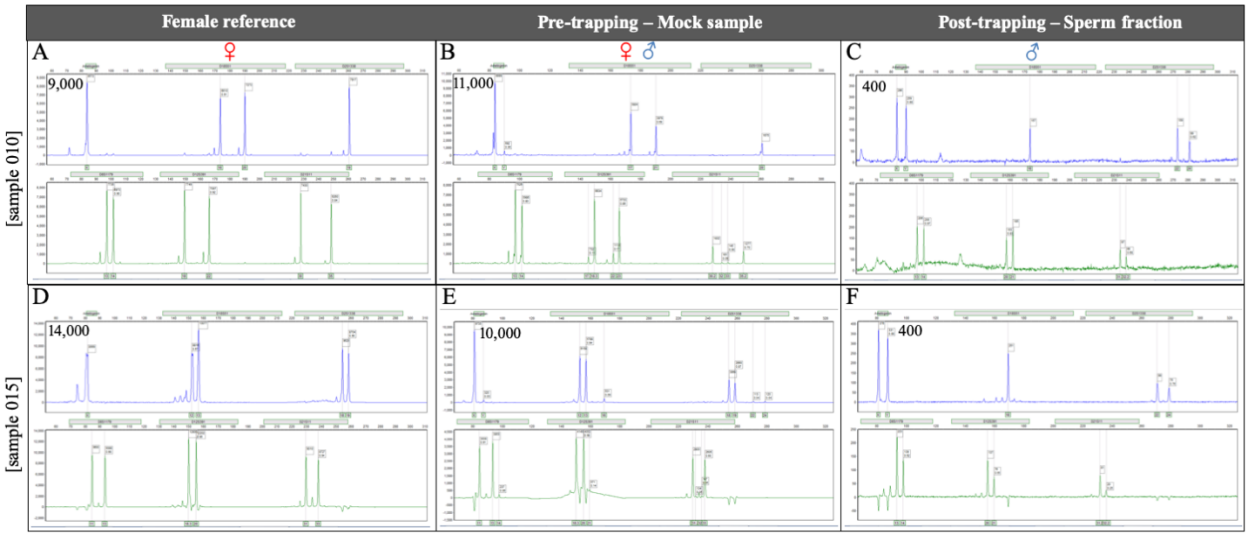


*Figure 2-11. STR profiles from vaginal swab mock samples. (A) STR profile from buccal swab of the female cell donor. (B) The pre-trapping STR profile for sample 010 is mixed, with alleles present from both male and female donors. (C) Sperm fraction STR profile after ADE is entirely male. (D) Female reference profile for donor 015. (E) STR profile of the mock sample 015 before acoustic trapping. (E) STR profile of the sperm fraction is a clean male profile, matching the semen donor.*

with fewer steps than a traditional differential extraction. However, consistent with the previous experiment, relatively low peak heights (<400 RFU) were observed with sperm fractions, which supports the hypothesis of a degraded sperm sample. An alternative theory was that inefficient amplification of DNA was leading to lower peak heights in the resulting STR profiles. This effect is explored and discussed further in section 2.3.6.

### *2.3.4 Effect of other cell types on sperm cell trapping*

Based on our discussions with forensic experts, a necessary consideration for this technology was the potential presence of exogenous material on some sexual assault samples. Swabs, clothing, and other evidentiary materials may also contain blood, or microorganisms such as yeast and bacterial cells, in addition to the sperm and epithelial cells from the suspect and victim. The primary concern regarding the presence of these substances is the possibility of co-trapping with the sperm cells, or even preferential acoustic trapping of the non-sperm particles. This could lead to a loss of sperm cells from the sample, and failure to generate a clean male STR profile after acoustic separation. Specifically, yeast and *E. coli* are microorganisms that commonly appear in these sample types, and are both micron-scale particles that could potentially co-trap with sperm cells. To test the effect of the exogenous materials, mock samples were formulated at 1:1 F:M ratio of epithelial:sperm cells, and then spiked with either yeast, *E. coli*, or blood at 20% of the total cell numbers, as specified in Materials and Methods. From the experiment conducted with yeast spiked into the sample, the pre-trapping STR profile (**Figure 2-12**) is a 'major female' with minor contributions from the male alleles. After ADE, the sperm fraction generated a 'clean male'

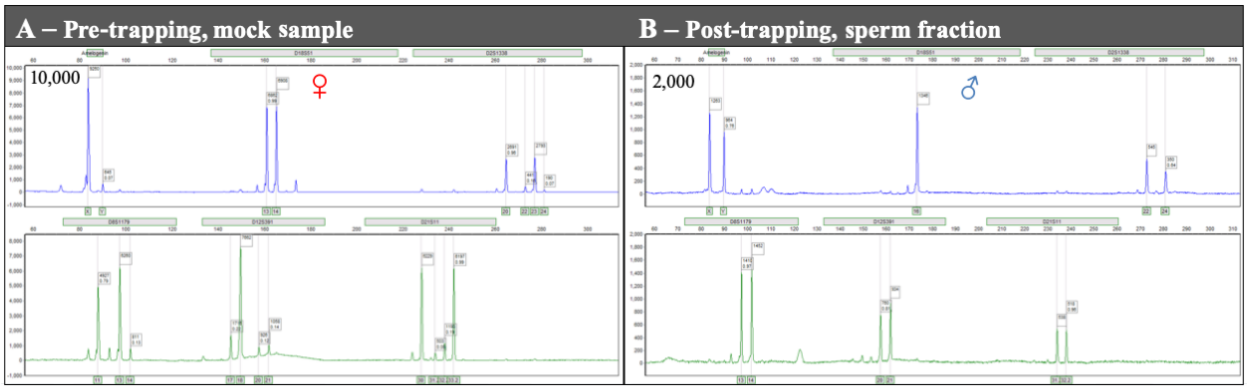


*Figure 2-12. STR profiles from 1:1 mock sample containing yeast. (A) The pre-trapping profile is major female, with minor allele contributions from the male donor. (B) After ADE, the sperm fraction STR profile is entirely male, matching the semen donor.*

profile, indicating that yeast cells did not displace sperm from the trapping site, and do not interfere with acoustic trapping. The results from the *E. coli* experiment are shown in **Figure 2-13**. The

post-trapping sperm fraction STR profiles are shown from samples formulated with 0%, 20%, and 40% bacterial cells as a percent of epithelial cell concentration. A significant decrease in peak height is seen across the three samples, with some larger DNA fragments dropping out entirely from the D21 locus in the 20% and 40% samples, indicative of low initial mass of DNA. This shows that *E. coli* interfered acoustic trapping of sperm cells at biologically relevant concentrations, and may be a concern in some very specific cases [14, 16].

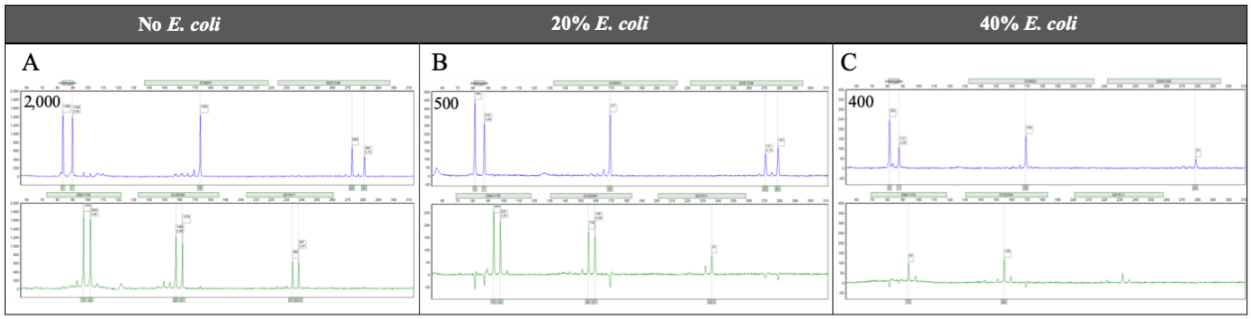


*Figure 2-13. STR profiles from the sperm fraction of 1:1 mock samples containing E. coli cells. (A) Sperm fraction STR profile from a 1:1 sample with no E. coli present. Full male profile with excellent peak heights. (B) Sperm fraction STR profile from a 1:1 sample containing E. coli at 20% the concentration of epithelial cells. Full male profile with low peak heights. (C) Sperm fraction STR profile from a 1:1 sample containing E. coli at 40% the concentration of epithelial cells. Partial male profile with low peak heights and some missing loci.*

A secondary concern with regard to victim's blood is the co-trapping of red blood cells, which are known to contain several PCR inhibiting compounds [17, 18]. If a sample provided by a victim contained significant amounts of blood, and those red blood cells were co-trapped and captured with sperm cells, downstream DNA amplification may be negatively affected. The pre-

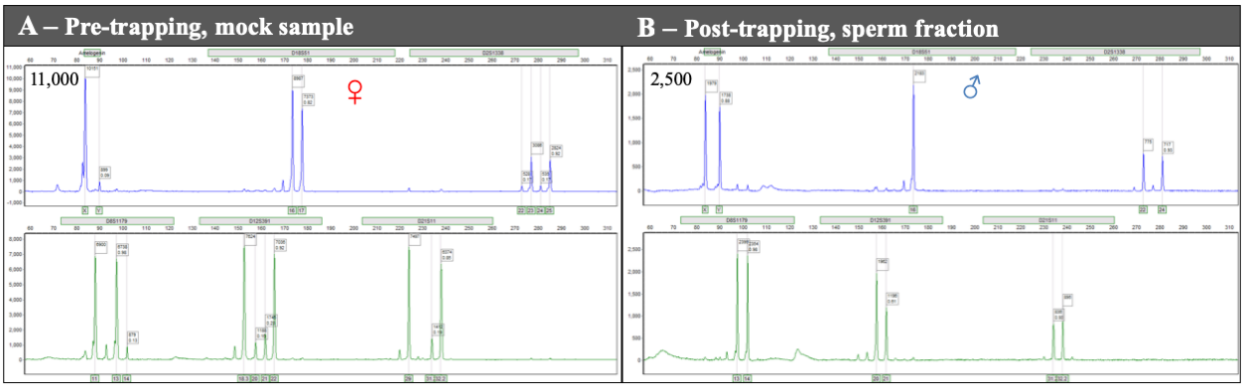


*Figure 2-14. STR profiles from 1:1 mock sample containing blood. (A) The pre-trapping profile is major female, with minor allele contributions from the male donor. (B) After ADE, the sperm fraction STR profile is entirely male, matching the semen donor.*

trapping profile from the sample containing blood (**Figure 2-14**) is a 'major female' STR result, with significantly stronger peak heights for the female alleles than the male alleles. After undergoing ADE, the sperm fraction STR profile is a 'clean male' with no trace of female DNA, and strong peak heights at all loci. This shows that presence of blood on the sample swab did not negatively impact acoustic trapping of sperm cells, and suggests that co-trapping of red blood cells is not a concern for ADE.

### *2.3.5 Impact of sample freshness on DNA amplification*

In section 2.3.4, it was hypothesized that sperm sample degradation was contributing to low STR peak heights. The specific basis for this concern originated from dilution of the sperm cells in water. Due to the extremely high cellular concentration of neat semen, it was necessary to dilute each aliquot up to 1000X prior to addition to the mock samples. However, it has been shown that significant changes in the surrounding liquid medium can lead to osmotic shock, which may impact sperm cell morphology and stability [19, 20]. We hypothesized that by diluting the neat semen in water, and storing those aliquots for several days in between use, inadvertent pre-mature sperm cell lysis was occurring prior to the preferential lysis step. This would then reduce the number of intact sperm cells present in each sample, leading to poor recovery during ADE, and

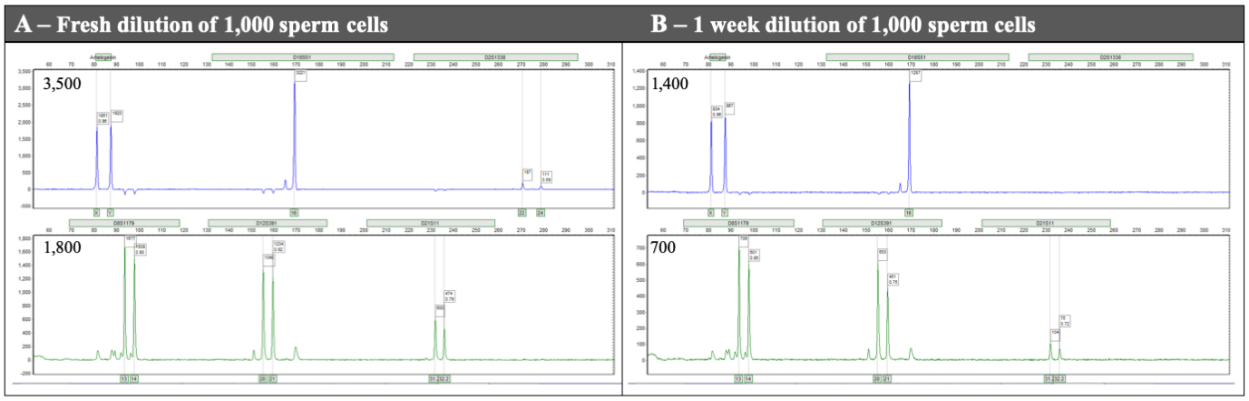


*Figure 2-15. Amplification of 1,000 sperm cells. (A) STR profile from a fresh dilution of 1,000 sperm cells, extracted and amplified the same day. (B) The STR profile from a 1-week old sperm cell dilution has significantly lower peak heights, and one missing loci. This indicates degradation of sperm cells over time once diluted.*

thus, weaker amplification of male DNA. To test this, a freshly diluted aliquot of 1,000 sperm cells and a 7-day old aliquot of 1,000 sperm cells were extracted and amplified. Their resulting STR profiles are shown in **Figure 2-15**, and a reduction in peak height by nearly half-fold is observed between the fresh and aged samples. This result clearly shows that aged dilutions suffer from loss of sperm cell integrity, believed to be due to osmotic shock, and that, in turn, impacts the cellular concentration in each mock sample. Moving forward from this test, each semen aliquot was both re-counted and aliquoted fresh for every mock sample generated.

### *2.3.6 Removal of the D18S51 primer*

One additional theory regarding the low peak heights observed in some sperm fractions after ADE was that inefficient amplification of the target DNA was occurring. When compiling an amplification kit, care must be taken to ensure compatibility of each primer set (in terms of sequence complementarity), in order to produce robust amplification [21]. Previous work in our lab had found success by eliminating the D18S51 primer set from the custom 6-plex amplification kit provided by Promega, and when implemented with our testing, drastic improvement in DNA amplification was observed. **Figure 2-16** shows the STR profiles from the *exact same sperm fraction* collected post-ADE, amplified with the original 6-plex kit (**Figure 2-16A)**, or a 5-plex

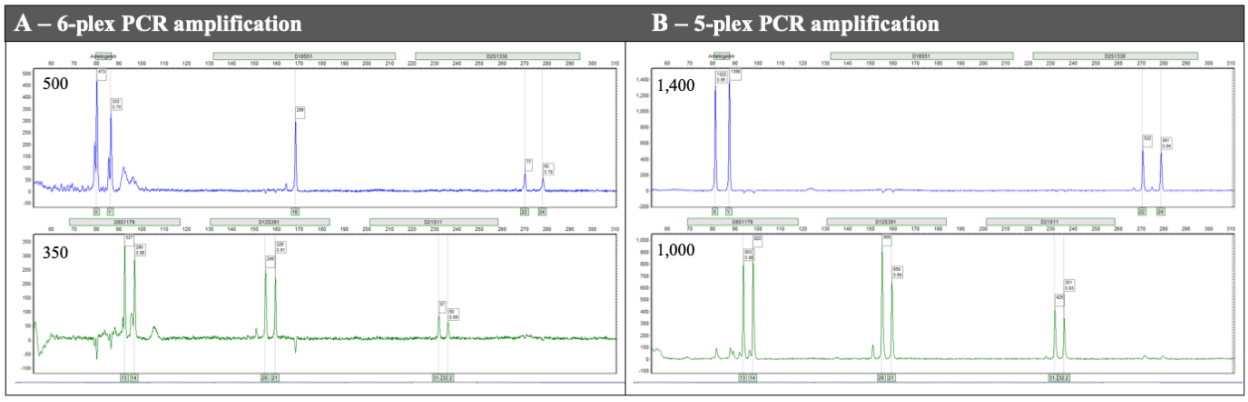


*Figure 2-16. Amplification of the same post-ADE sample with 6-plex or 5-plex STR kits. (A) STR profile of the post-ADE sperm fraction amplified with a custom 6-plex kit. A clean male profile with low peak heights is observed. (B) The same post-ADE sperm fraction was amplified with a 5-plex kit, lacking the D18S51 primers. The resulting STR profile is completely male, and has significantly higher peaks.*

kit which had the D18S51 primers removed (**Figure 2-16B)**. The peak heights are tripled in the 5-plex results, giving clear indication that the primers for the D18 locus were limiting the DNA amplification efficiency of the sample. The same test was conducted with a 20:1 F:M ratio sample, which had previously undergone ADE. **Figure 2-17** compares the amplification of post-ADE male fraction using either 6-plex (**Figure 2-17A**) or 5-plex (**Figure 2-17B**). Consistently, a distinct improvement in peak height is observed with the removal of the D18S51 primers. Moving forward, the modified 5-plex amplification kit was used for all testing.

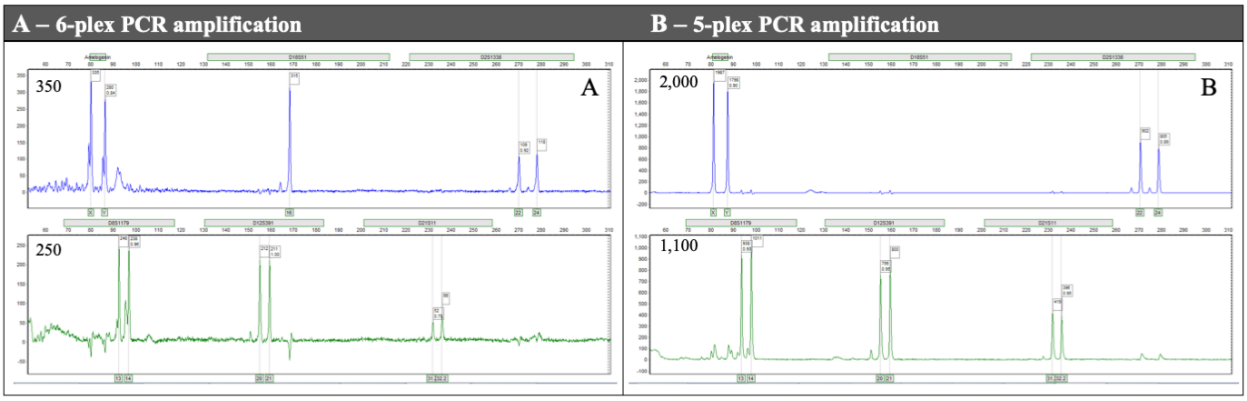


*Figure 2-17. Amplification of the same post-ADE sample with two different PCR kits. (A) This STR profile was collected after amplification of the sperm fraction from a 20:1 sample, PCR conducted with 6-plex kit. Peak heights are low, but a clean male profile is obtained. (B) STR profile from the same sperm fraction sample, but amplified with a 5-plex kit lacking the D18 primers. The peak heights are significantly higher at all loci.*

### *2.3.7 Mock sample testing with modified amplification kit*

After establishing new protocols for preparing sperm cells, and more efficient DNA amplification by removing the D18S51 primer, mock samples were generated from two post-coital vaginal swabs. With the expectation that these changes would significantly improve our capture of sperm cells and subsequent DNA amplification, higher F:M ratio samples were tested. To generate the data shown in **Figure 2-18**, sample 012 was formulated at 20:1 F:M ratio, while sample 017 was formulated at 10:1 F:M ratio. In both cases the pre-trapping STR profiles (**Figure 2-18B and E**) show a 'major female' profile, with peak heights of the female alleles up to 20X higher than the male alleles. This indicates the presence of significantly more female DNA than

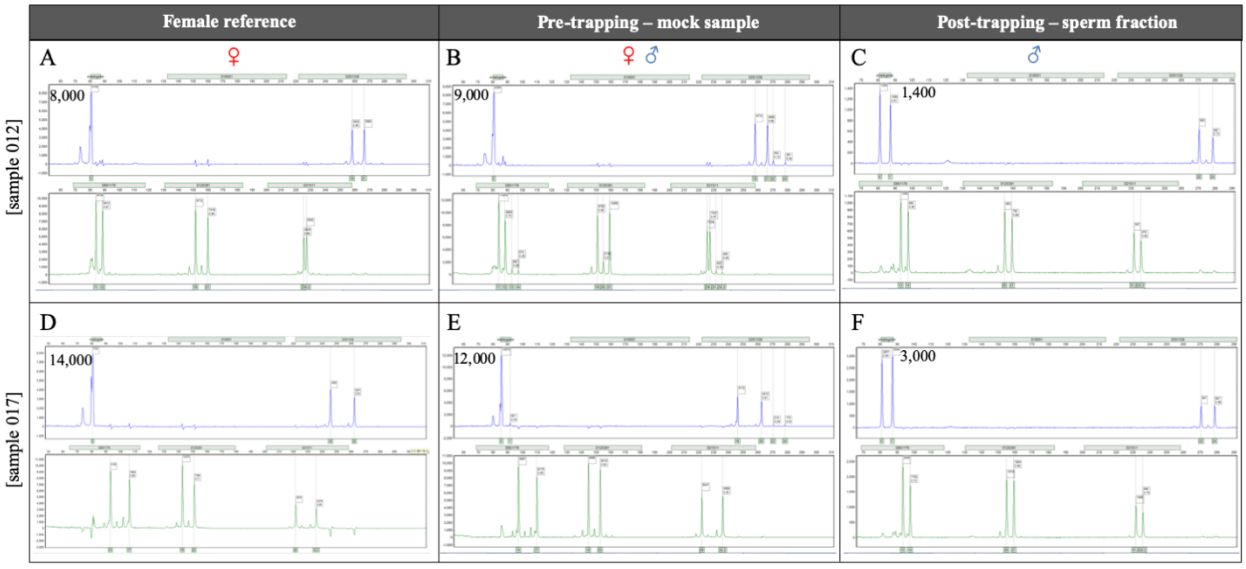


*Figure 2-18. STR profiles from vaginal swab mock samples. (A) The female reference STR profile of donor 012. (B) The pre-trapping STR profile is major female, with much stronger peak heights for the female alleles than the male alleles. (C) STR profile from the sperm fraction post-ADE is entirely male, matching the semen donor. (D) STR profile from a buccal swab of donor 017. (E) Pre-strapping STR profile of this mock sample is major female, with minor male allele contributions. (E) Sperm fraction STR profile is clean male.*

male DNA, and would necessitate a differential extraction in a criminal investigation. After sperm cell capture through ADE, the post-trapping STR profiles (**Figure 2-18C and F**) are 'clean male' profiles with strong peak heights and no trace of female DNA, suggesting sufficient capture of sperm cells from these mock samples using ADE. Furthermore, the peak heights are much higher than previously observed and are indicative of more efficient DNA amplification with the modified STR kit.

### *2.3.8 Sperm cell capture from high F:M ratio mock samples*

Our collaborators at forensic laboratories made it clear that, while there is no 'typical' sexual assault sample, the vast majority will exhibit F:M cell ratios between 1:10 and 50:1. The results reported in sections 2.3.2 through 2.3.7 show that ADE can capture and purify sperm cells from mock samples at the low end of this range, but do not address more challenging, higher F:M ratio samples. Two high ratio samples were formulated at a F:M ratio of 40:1, one containing 1,000 total sperm and the other containing 500 total sperm. Both were prepared with a vaginal

swab from the same anonymous donor, freshly counted and diluted sperm cells, and amplified with the new 5-plex kit. The results in **Figure 2-19** for the 1,000 sperm sample show a 'clean female' STR profile from the pre-trapped sample, as the excess female DNA completely masks the low concentration of male DNA. However, after ADE, a 'clean male' STR profile was generated from the sperm fraction, showing that complete separation of sperm cells is possible even from high F:M ratio samples. The 500 sperm sample results are shown in **Figure 2-20**, and the same conclusions can be reached. From an initial female-dominated sample, ADE can capture enough sperm cells to generate a 'clean male' STR profile capable of identifying a suspect. As expected, the peak heights in the sperm fraction are lower for the sample containing half the quantity of sperm cells.

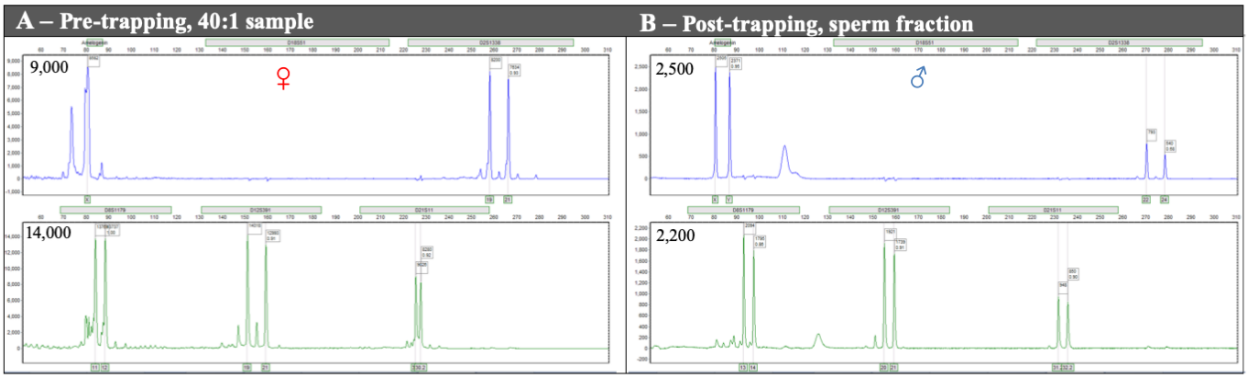


*Figure 2-19. STR profiles from a 40:1 vaginal swab mock sample containing 1,000 sperm cells. (A) STR profile from the mock sample before ADE. The profile is clean female, as no male peaks are observed. (B) Post-ADE sperm fraction STR profile is clean male, with strong peak heights, showing no female DNA contribution.*

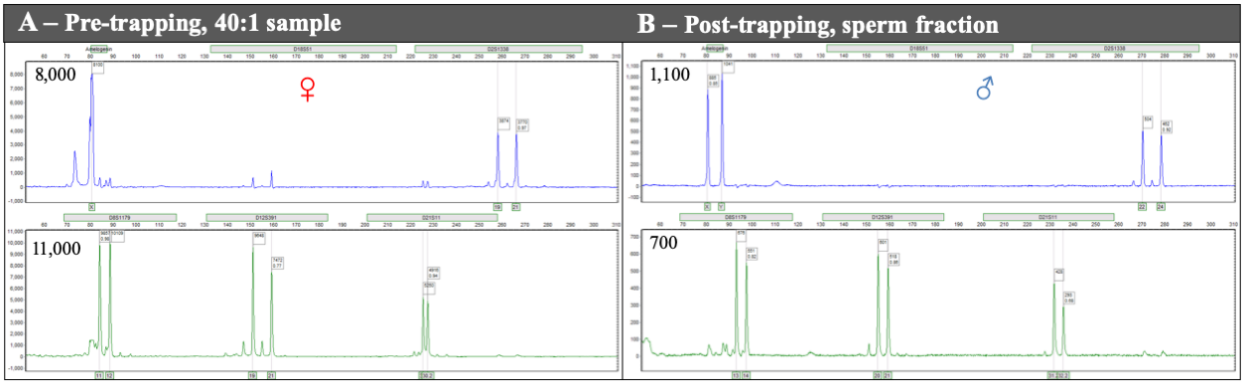


*Figure 2-20. STR profiles from a 40:1 vaginal swab mock sample containing 500 sperm cells. (A) Before ADE, the STR profile of the mock sample is entirely female. (B) After ADE, the sperm fraction STR profile is a clean male profile, with no female alleles present.*

### *2.3.9 ADE of extreme F:M mock sample*

To go well beyond the scope recommended by our forensic collaborators, a sample was prepared containing 100 times as many vaginal epithelial cells as sperm cells in solution. There were 250 sperm cells in the mock sample, and the results from ADE are shown in **Figure 2-21**. As expected, the pre-trapping STR profile is 'clean female' with no trace of male DNA present due to the masking effect. The post-trapping sperm fraction shows a 'mixed' STR profile, with contributing peaks from the male and female cell donors at the Amelogenin, D8S1179, and D12S391 loci, and only male alleles appearing at the D2S1338 and D21S11 loci. However, low peak heights are exhibited at the male-only loci, indicating low total sperm cell capture. While this ADE test did not completely purify sperm cells from the sample, it is still a promising result. From a sample completely overwhelmed with female DNA, acoustic separation isolated enough sperm cells that a partial male profile was obtained. Using modern software and mathematical approaches, mixed STR profiles can be deconvoluted even when female DNA is the major

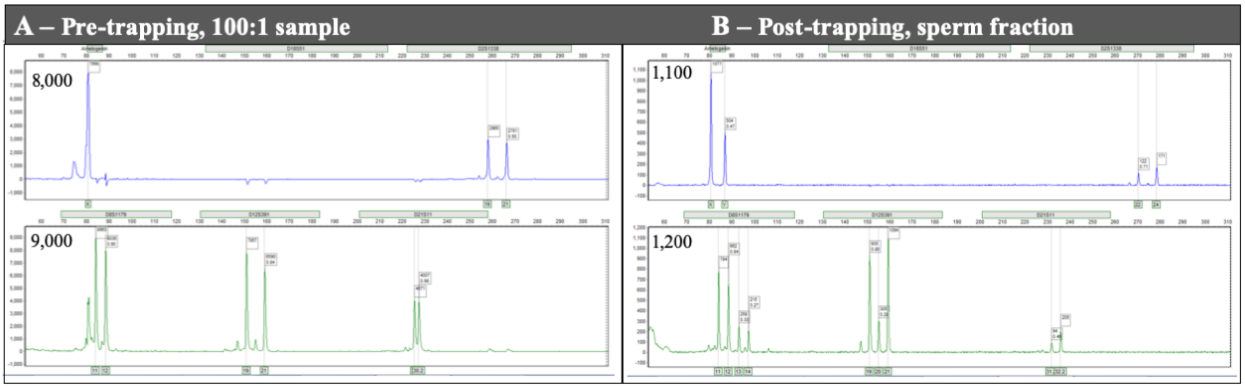


*Figure 2-21. STR profiles from a 100:1 mock sample from a vaginal swab, 250 sperm cells. (A) STR profile from the mock sample before ADE is entirely female. (B) The post-trapping sperm fraction STR profile is mixed, with contributions from both the female and male cell donors.*

contributor [22], and thus, even this partial result could provide valuable identifying information. This experiment was replicated with additional samples at F:M of 100:1, and similar results were obtained.

*2.3.10 Trapping effectiveness demonstrated with the CODIS STR loci*

During the research and development stage of this project, the custom 6-plex and 5-plex amplification kits were cost-effective ways to analyze results and determine experimental directions. However, the long-term goal of this project was always to place instruments in active forensic laboratories for evaluation, and thus an experiment was conducted to demonstrate a full 18-plex amplification of a mock sexual assault sample that had undergone ADE. To demonstrate the compatibility of this technology with already validated forensic chemistries, PowerPlex 18D amplification kit was used for pre- and post-trapped sample fractions. A 20:1 F:M sample was prepared with vaginal swabs and diluted semen, and the resulting STR profiles are shown in **Figure 2-22**. The pre-trapping profile shows only female alleles (**Figure 2-22A)**, as the male DNA was not concentrated enough before acoustic separation to influence the profile. The post-trapping sperm fraction (**Figure 2-22B**) is a 'clean male' STR profile, with all male alleles present and no

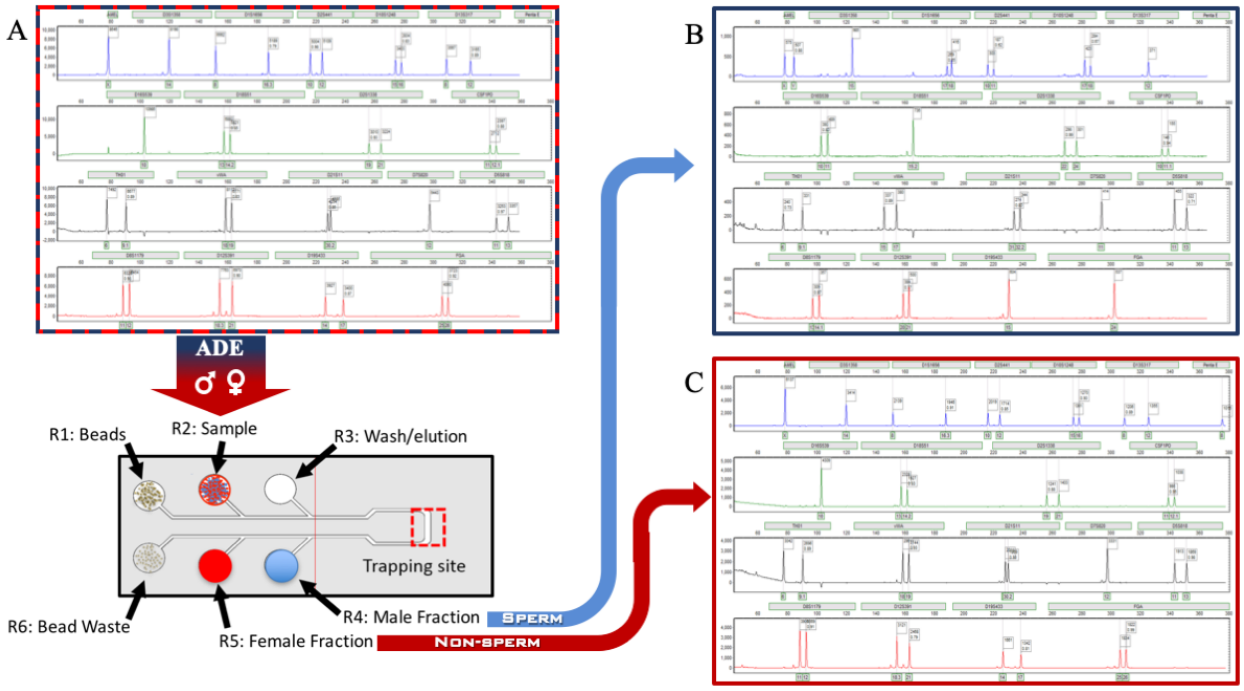


*Figure 2-22. PowerPlex 18D STR profiles from a 20:1 mock sample from a vaginal swab. (A) Pre-trapping STR profile shows only female alleles. (B) The post-trapping sperm fraction STR profile is entirely male, matching the semen donor. (C) Liquid collected from the non-sperm fraction was amplified, and the STR profile matches the female cell donor with no male alleles present.*

extraneous peaks appearing in the profile. Finally, **Figure 2-22C** shows the non-sperm fraction, collected from R5 on the microchip, and is a 'clean female' STR profile that matches the anonymous donor. This experiment demonstrated, beyond a doubt, that this technology can successfully capture sperm cells acoustically from a mock sexual assault sample, and that full amplification of the federally mandated panel of genetic loci is possible from the sperm fraction.

## 2.4 Summary

The continued development of ADE culminated in a fully functioning prototype instrument and microchip, capable of rapidly capturing sperm cells from mock sexual assault samples. This was validated using buccal cells, vaginal cells, a variety of exogenous biological materials, and a wide range of F:M cell ratios. To overcome obstacles encountered with inefficient amplification and degradation of sperm cells, several changes were made to sample formulation, STR protocols, and acoustic trapping parameters, ultimately reaching the point where the instrument could be sent to forensic laboratories for external evaluation with authentic sexual assault samples.

## 2.5 References

1. K. Xu, C.P. Clark, B.L. Poe, J.A. Lounsbury, J. Nilsson, T. Laurell, and J.P. Landers, *Analytical Chemistry*, 2019, **91**, 2186-2191.
2. C.P. Clark, K. Xu, O. Scott, J. Hickey, A. Tsuei, K. Jackson, and J.P. Landers, *FSI: Genetics*, 2019, **41**, 42-49.
3. T. Laurell, F. Petersson, and A. Nilsson, *Chemical Society Reviews*, 2006, **36**, 492-506.
4. C.M. Cousins, P. Holownia, J.J. Hawkes, M.S. Limaye, C.P. Price, P.J. Keay, and W.T. Coakley, *Ultrasound in Medicine and Biology*, 2000, **25**, 881-888.

5. M.S. Limaye, J.J. Hawkes, and W.T. Coakley, *Journal of Microbiological Methods*, 1996, **27**, 211-220.
6. B. Hammarström, T. Laurell, and J. Nilsson, *Lab on a Chip*, 2012, **12**, 4296-4304.
7. M. Evander, K. Horsman, C. Easley, J. Nilsson, T. Laurell, *Proceedings of uTAS 2006 Conference*, 2006, 1055-57.
8. J. Norris, M. Evander, K. Horsman-Hall, J. Nilsson, T. Laurell, J. Landers, *Analytical Chemistry*, 2009, **81**, 6089-95.
9. M. Evander, and J. Nilsson, *Lab on a Chip*, 2012, **12**, 4667-4676.
10. A. Lenshof, M. Evander, T. Laurell, J. Nilsson, *Lab on a Chip*, 2012, **12**, 684-95.
11. A. Manbachi, R. Cobbold, *Ultrasound*, 2011, **19**, 187-96.
12. A. Kuo, *Polymer Data Handbook*, 1999, 411-435.
13. VA DFS, *Forensic Biology Procedures Manual*, 2017, 1-42.
14. D. Eschenbach, S. Hillier, C. Critchlow, C. Stevens, T. DeRouen, and K. Holmes, *American Journal of Obstetrics and Gynecology*, 1988, **158**, 819-828.
15. M.R. Islam, M.M. Ali, M. Lai, K. Lim, and H. Ahmad, *Sensors*, 2014, **14**, 7451-7488.
16. T. Vrolijk-Bosschaart, S. Brilleslijper-Kater, M. Benninga, R. Lindauer, A. Teeuw, *European Journal of Pediatrics,* 2018, **177**, 1343-50.
17. A. Akane, K. Matsubara, H. Nakamura, S. Takahashi, K. Kimura, *Journal of Forensic Science*, 1994, **39**, 362-72.
18. W. Al-Soud, P. Radstrom, *Journal of Clinical Microbiology*, 2001, **39**, 485-93.
19. J.V. Abraham-Peskir, E. Chantler, E. Uggerhoj, and J. Fedder, *Human Reproduction*, 2002, **17**, 375-382.

20. P.N. Zarmakoupis-Zavos, J.R. Correa, P. Aslanis, S. Antypas, and P.M. Zavos, *Middle East Fertility Society Journal*, 1998, **3**, 66-72.

21. S.J. Green, R. Venkatramanan, and A. Naqib, *PLOS One*, 2015, 1-21.

22. N. Novroski, F. Wendt, A. Woerner, M. Bus, M. Coble, B. Budowle, *FSI: Genetics*, 2019, **38**, 121-29.

# Chapter 3: Evaluation of a prototype acoustic differential extraction instrument in forensic laboratories

## 3.1 Introduction

This inability of conventional differential extraction (DE) to keep up with the rising demand for DNA analysis of sexual assault kits (SAKs) has led to research from the academic and commercial sectors for alternative approaches. Several research groups and companies have tackled the issue of improving DE, leading to excellent developments and new technologies. Some of these techniques have been productized [1, 2], while many more are undergoing validation in independent laboratories [3, 4], a crucial step for gaining traction in the forensic community. Internal validations are required before any new procedure can be applied in a forensic laboratory, public or private, and can require months, to years, before gaining acceptance [5, 6]. This testing is important for ensuring that high-quality, reproducible results will be generated from every technique that is approved for criminal investigations. The previous chapters describe acoustic differential extraction (ADE) as our approach to supplanting the laborious conventional DE, but several other promising methods have been developed.

While conventional DE (described in Chapter 1, section 1.2.2) remains the gold standard for sexual assault sample processing in forensic laboratories, there have been significant efforts to provide alternative approaches. One method uses a preferential lysis to sequentially break open all non-sperm cells, but does not isolate or purify the sperm. A secondary lysis degrades the sperm cells, and probabilistic DNA analysis is performed to compare the pattern of short tandem repeats (STR), and identify the major contributors in each profile [7, 8]. This is an intriguing technique, but fails when testing samples with extremely low concentrations of sperm cells, as the male DNA

contribution is masked by the excess female DNA. A similar approach does not physically separate the sperm cells, but instead, relies on a protease and DNase 1 enzyme to completely remove all female DNA from the sample before lysing the sperm cells [9]. This method shows promise for its simplicity and effectiveness, but has yet to gain acceptance in many forensic crime laboratories. One alternative to conventional DE uses pressure cycling to selectively lyse epithelial cells without rupturing the sperm, followed by an alkaline lysis to break open sperm cells, which can improve DNA recovery [10]. This significantly reduces the handling time per sample; however, it still requires repeated manual centrifugation steps by an analyst, and fails to produce clean separations of male and female DNA at cellular ratios of higher than 5:1 epithelial-to-sperm cells [11]. There have been several commercialized systems for improved DE, some of which may soon be adopted by forensic laboratories. One such system is the DEPArray™, which uses dielectrophoresis to manipulate and capture individual sperm cells, providing incredible sensitivity and selectivity. The major drawbacks of DEPArray™ are that it requires more time and operator steps than most other methods, and includes cell staining/fixation and lengthy incubations [1]. However, this approach is incredibly exciting for its application to trace evidence samples with low numbers of sperm, or instances where there are sperm cells from multiple attackers in a single sample. In either of those example cases, traditional DE would fail to produce a single-source male STR profile that could be used to identify a suspect, but DEPArray™ may succeed due to its ability to capture individual sperm based on minute differences in electric polarization. Another system immobilizes sperm cells using antibodies tagged to magnetic beads, which can then be removed from the sample lysate and provide clean separations, even in extreme cases of overwhelming amounts of epithelial cells [2]. However, this procedure also suffers from complex handling and preparation steps, and can fail to capture significant amounts of sperm from samples

more dilute than $10^3$ cells/mL [2]. Laser capture microdissection (LCM), another very precise technology, harvests sperm cells, or other particles of interest, by individually cutting them out of the substrate. LCM can effectively separate sperm cells from mixed samples, but routinely provides sperm fractions with a low number of cells, and like other systems, struggles with laborious and time-consuming steps [12]. In addition, the highly manual nature of LCM makes it unlikely that this technique can be automated in the future [13]. One of the simpler, but non-commercialized alternatives to conventional DE uses filtration to sift out sperm cells from the larger epithelial cells. However, as would be expected, this approach is subject to clogging of the membrane with high number of cells, as well as, failure to filter out free DNA from the sample that could influence the downstream STR profile [14, 15].

Each of these novel approaches offer advantages over conventional DE, but none can fully address the issues with current protocols, namely the need for *faster*, more *automated*, and *robust* capture of sperm cells from any type of sexual assault sample. It was our hope that ADE, developed over several years, would meet these needs and fit seamlessly into existing forensic protocols. In order to evaluate ADE with authentic sexual assault samples, tested by professional forensic analysts, we established connections at six state-run forensic laboratories across the country. From these labs, we inquired about the average sample composition of sexual assault evidence, the recovery rate of sperm cells from a conventional DE, and expected ratios of epithelial:sperm cells. This information was used to plan for and execute an external evaluation of the ADE technology, where the prototype instrument and microchips were tested by forensic analysts in two government laboratories.

## 3.2 Materials and methods

### *3.2.1 Selection of off-site laboratories*

During development of the ADE microchip and instrument, many forensic experts around the country provided valuable insight and recommendations. Of these experts, two groups in particular expressed interest in remaining involved throughout the project. The forensic biology units from Palm Beach County Sheriff's Office (PBSO) and Mesa Police Department (Mesa PD), spearheaded by Dr. Julie Sikorsky and Dr. Kim Meza, respectively, each agreed to facilitate the validation of an ADE prototype in their facility. Drs. Sikorsky and Meza are well respected in the forensic field, and their team of analysts possessed the skills, knowledge, and access to authentic samples required for a true analysis of the capabilities of ADE.

### *3.2.2 Non-probative sexual assault samples*

Available at the PBSO forensic biology unit for testing was a large collection of adjudicated samples, all of which originated from investigations that had already concluded. These non-

| Submission # | Substrate? | no. sp cells | Clean Separation? (yes/no) | SP Profile quality (partial/mixture/full) | AP (+/-) | PSA (+/-) |
|---|---|---|---|---|---|---|
| 1Ans | vag sw | 5 | yes | full female | + | |
| 1Asp | | | no | good mix M/F | | |
| 3-3ns | tank top | >10 | yes | full female | + | |
| 3-3sp | | | yes | full male | | |
| 3B-1ns | shirt | 10 | no | full male | + | |
| 3B-1sp | | | yes | full male | | |
| 1Ans | vag sw | 5 | yes | full female | + | |
| 1Asp | | | no | good mix M/F | | |
| 2A-4ns | underwear | ++ | no | mix @1 major male | + | |
| 2A-4sp | | | yes | full male | | |
| 5A-1ns | panties | 0 | yes | full female | + | + |
| 5A-1sp | | | no | mix no Y called | | |
| 5B-1ns | boxers | <10 | no | full male | + | |
| 5B-1sp | | | yes | full male | | |
| 5B-5ns | boxers | 0 | | | + | + |
| 5B-5sp | | | | | | |
| 2B-1ns | shorts | 50 | no | good mix no Y called | + | |
| 2B-1sp | | | yes | full male | | |
| 2B-6ns | shorts | 30 | no | ~ mix maj female w/ Y | + | |
| 2B-6sp | | | yes | full male | | |
| 1Ans | vag sw | 6 | yes | full female | + | |
| 1Asp | | | no | mix of 3 w/ Y | | |
| 2Ans | vag sw | 1 | yes | full female | + | |
| 2Asp | | | no | mix no Y | | |
| 1Ans | vag sw | 40 | yes | full female | - | |
| 1Asp | | | no | mix 2 major male | | |
| 1Bns | oral sw | 2 | yes | full female | - | |
| 1Bsp | | | no | full female | | |
| 5-6ns | jeans | 12 | no | mix w/ Y called | + | |
| 5-6sp | | | yes | full male | | |
| 5-13ns | jeans | 15 | no | mix w/ Y called | + | |
| 5-13sp | | | yes | full male | | |
| 5-18ns | jeans | 5 | | | + | |
| 5-18sp | | | | | | |
| 2A-1ns | shirt | 50 | no | mix 2 major male | + | |
| 2A-1sp | | | yes | full male mix @1 | | |
| 5-2ns | paper towel | 25 | no | mix 2 major female | + | |
| 5-2sp | | | no | mix 2 1:1 | | |
| 5-3ns | paper towel | <10 | | | + | |
| 5-3sp | | | | | | |
| 3-1ns | condom outside | 7 | no | good mix w/ Y called | + | |
| 3-1sp | | | yes | full male | | |
| 3-2ns | condom inside | +++ | | full male | + | |
| 3-2sp | | | yes | full male | | |

*Table 3-1. Catalog of PBSO authentic sexual assault samples. The PBSO forensic biology unit samples varied in terms of substrate, number of sperm cells, previous separation quality, and presence or absence of acid phosphatase (AP) prostate specific antigen (PSA).*

probative, excess materials offered the chance to test authentic sexual assault evidence, and compare ADE results to the actual findings from conventional DE. A catalog of the available samples from PBSO is shown in **Table 3-1**; these pieces of evidence were collected between 2006-2009. Additional samples were tested as they became available, with a priority placed on testing samples from a wide range of substrates that contained a variable amount of sperm cells in order to challenge the ADE technique and gain a true appraisal of its robustness. At the Mesa PD lab, analysts first tested the ADE prototype using diluted semen deposited onto an array of fabrics. They also prepared mock samples from vaginal swabs and semen, and used the mock samples to evaluate ADE as a sperm cell capture technique. At both laboratories, forensic analysts were asked to track each sample using the chart shown in **Table 3-2**. By tracking sample information, visual observations from the acoustic trapping, and STR profile interpretation, comprehensive data was collected for each non-probative sample evaluated.

| Sample # | Sample Code | Operator Initials | MIC Chip # | sample type | Info on [Sperm Cell]? | Beads trapped | Sample trapped | Pellet captured | M profile; F peaks seen | M profile; no F contribution | M profile; no F peaks; strong PH | OPERATOR COMMENTS |
|---|---|---|---|---|---|---|---|---|---|---|---|---|
| 3 | 844_1-9 | JCS | B063 | swabs of sheet | 100 sp, ECs noted | Y | Y | Y | | | Y | SP fraction: single source male contributor. NS fraction: major male contributor with 2 additional low level peaks called. Sample from 2009 |

*Table 3-2. Operator feedback chart. For each sample tested, the operator tracked if the ADE microchip showed bead trapping, sample trapping, and the visual pellet captured and eluted to the sperm reservoir.*

### *3.2.3 Microchips and reagents for external evaluation*

In anticipation of testing a wide range of non-probative samples, each forensic laboratory was provided with 20 ADE microchips. The chips were fabricated as described in Chapter 2, section 2.2.2, and underwent quality control testing to ensure adequate acoustic trapping of sperm-like particles (6 μm diameter beads). In addition, the following solutions were prepared for each lab: a priming solution (5:1:1 ratio of water:ethanol:glycerol), a fluorescent bead solution (1:500 dilution of 6 μm fluorescent beads in water), and an assisting bead solution (1:75 dilution of 6 μm black beads in 20% Tween 20; beads were sourced from Polysciences). The assisting bead solution

is crucial for 'seeding' the acoustic trapping site, which initiates aggregation of particles [16]. This is especially important for samples which may contain a low number of total sperm cells, as the beads will initiate trapping and allow sperm to collect [17]. The chemical reagents supplied to each forensic lab were: *Prep*GEM and 10X Blue Buffer (ZyGEM NZ Ltd), a 5% sarkosyl solution in water, DNase 1 enzyme and 10X DNase 1 Buffer (ZyGEM NZ Ltd, 0.5 Units of enzyme/reaction), and the sperm lysis reagent Acrosolv and 1X Red+ Buffer (ZyGEM NZ Ltd). All DNA amplification was performed with Promega or Qiagen polymerase chain reaction (PCR) reagents, as specified below, provided by each forensic laboratory.

### *3.2.4 Workflow and sample protocol*

For each mock sample, a portion of the substrate (1/4 of a cotton swab, or 3 $mm^2$ fabric cutting) was added to a polypropylene tube with 1U *Prep*GEM, 1X Blue Buffer, sarkosyl (0.2% final concentration), and water to 100 uL, and incubated at 75°C for 15 min, 95°C for 5 min. This liberated cells and genetic material from the substrate cutting, while also lysing epithelial cells and leaving sperm cells intact. The sample cutting was placed in a spin basket and piggy-back centrifuged to collect the excess liquid, which was added to the sample lysate. Assisting bead solution was also added to the lysate, and the sample was loaded into the ADE chip. After performing ADE as described in Chapter 2, section 2.2.4, the sperm and non-sperm fractions were collected from the microchip. Prior to sperm cell extraction with Acrosolv and Red+ Buffer, the non-sperm fraction was treated with DNase 1 to remove any residual free DNA. The sperm and non-sperm fractions were then quantified using quantitative polymerase chain reaction (qPCR) with the Promega *PowerQuant* AB7500, DNA amplified with the Promega PowerPlex *Fusion* 5C kit (1 ng DNA per reaction), STR profiles were generated on the ABI 3500xL (Applied Biosystems), and analyzed using GeneMapper ID-X 1.5 software. The stochastic threshold for

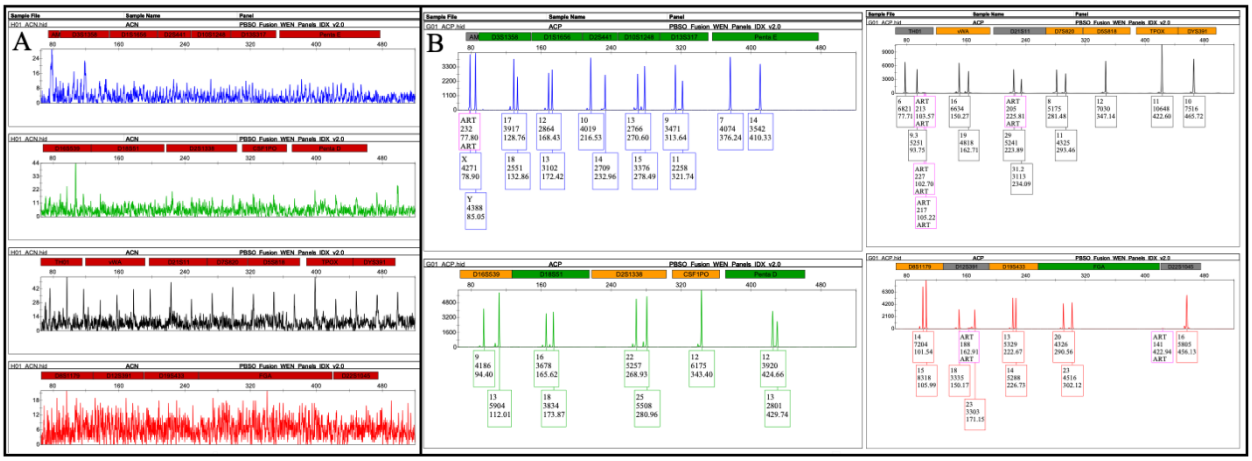


*Figure 3-1. (A) Negative control for PBSO amplification kit. No extraneous alleles are observed, indicating no contamination from reagent or environmental sources. (B) Positive control from PBSO amplification kit. Template male DNA was amplified using Promega PowerPlex Fusion 5C kit, strong peak heights and acceptable balance at all loci indicate successful amplification.*

this instrument and amplification chemistry was 150 RFU. A negative and positive control (2800M control DNA, 1 ng) for the PCR amplification is shown in **Figure 3-1**, demonstrating no contamination or extraneous peaks in the negative control, and a full male profile with strong peak heights for the positive control.

## 3.3 Results and discussion

### *3.3.1 Condom swab sample*

The first sample tested at PBSO was number 758, obtained by swabbing the inside of a condom collected during a sexual assault investigation in 2008. In the initial processing and DE conducted by PBSO, analysts noted greater than 100 sperm cells present, with few epithelial cells visible during microscopy of a 1/8 swab cutting. After their conventional DE (as performed at time of sample collection), both the sperm and non-sperm fractions generated full male STR profiles. When processed using ADE, our results matched those obtained by conventional DE. The STR profiles shown in **Figure 3-2** (non-sperm fraction) and **Figure 3-3** (sperm fraction) both show full male profiles, with strong peak heights and no contribution from female alleles. The strong peak heights (500-14000 RFU) indicate that an abundance of sperm cells was present in the initial sample, and that ADE successfully captured enough sperm to generate a full male profile.

*Figure 3-2. STR profile from the non-sperm fraction of a condom swab sample. The non-sperm fraction from reservoir 5 was collected and amplified, resulting in an STR profile that is entirely male. This indicates lack of epithelial cells present in the initial sample. NOTE: all 4 panels are from the same STR profile, each representing a different fluorescent dye channel that detects different primer sets.*

*Figure 3-3. STR profile from the sperm fraction of a condom swab sample. This post-trapping profile shows all of the male-associated alleles, with peak heights exceeding the PSBO stochastic threshold. This confirms that ADE can capture a sufficient number of sperm cells for DNA profiling from a sexual assault sample containing an abundance of sperm.*

Based on the full male profile acquired from the non-sperm fraction (**Figure 3-2**), this result also shows that when excess sperm are present, a significant number of cells will escape to the non-

sperm fraction. The generation of a full male STR profile from the sperm fraction was a positive, yet unsurprising result, as it was the first demonstration that ADE can capture sperm cells in an automated fashion from an authentic, non-probative sexual assault sample.

### *3.3.2 Sheet cutting sample*

Sample 844 from PBSO was a piece of fabric, cut from sheets that were collected as evidence from an investigation conducted in 2009. During initial cataloging, over 100 sperm cells were observed with microscopy, with some epithelial cells present. The 3 $mm^2$ fabric cutting was processed in the same manner as a cotton swab, with cells eluted and lysed from the substrate prior to ADE. Our ADE results showed a full male STR profile from both the non-sperm fraction, **Figure 3-4**, and the sperm fraction, **Figure 3-5**. Each locus in the sperm fraction profile shows peak heights well exceeding the stochastic threshold, indicating an abundance of sperm, enough of which were trapped acoustically to generate a full male profile. This is similar to the conventional DE result obtained by PBSO during their initial investigation. Their DE in 2009 also yielded a full male profile from the sperm fraction, whereas the non-sperm fraction yielded a

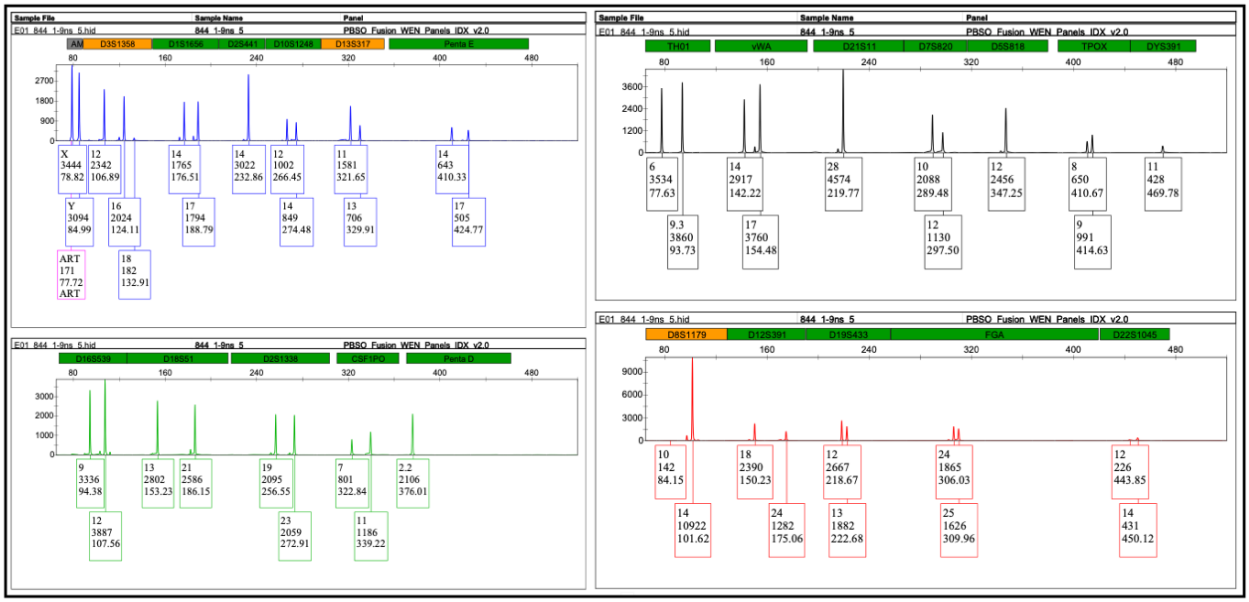


*Figure 3-4. STR profile from the non-sperm fraction of a sheet cutting sample. A full male profile is observed, with no significant contribution observed from female alleles.*

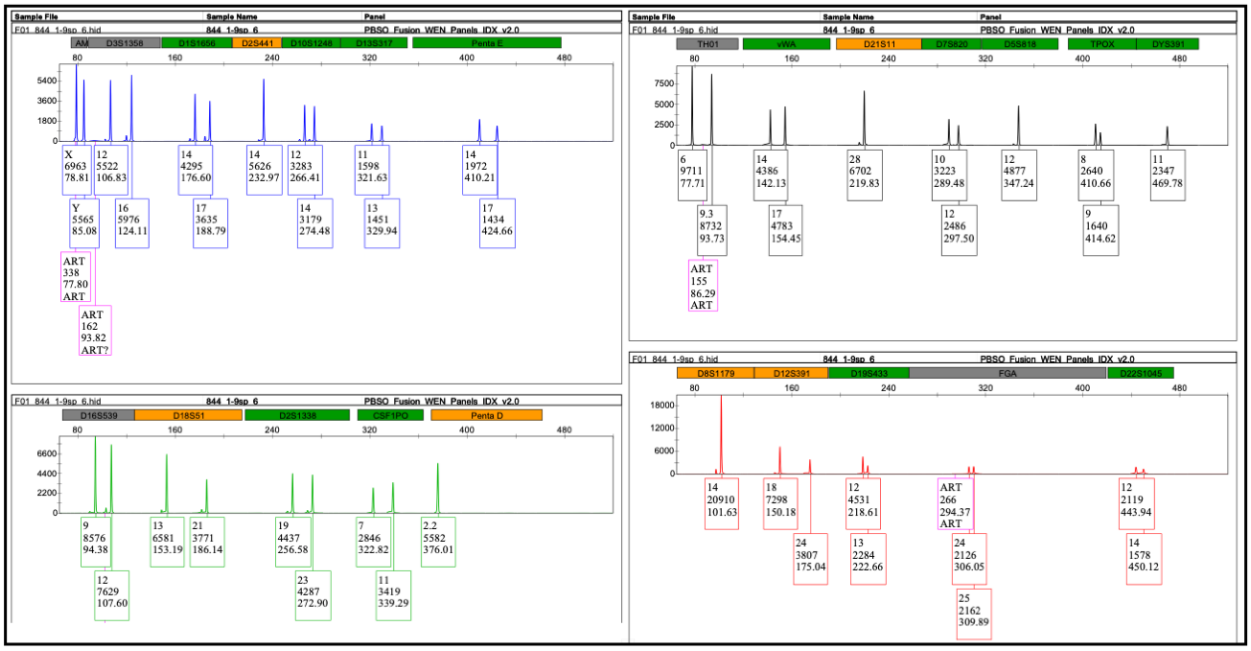

*Figure 3-5. STR profile from the sperm fraction of a sheet cutting sample. The sperm fraction generated a full male profile, with no contributing female alleles. This matches the conventional DE result obtained by PBSO in 2009.*

'mixed profile' with major male contributor. A 'mixed profile' means that some DNA was present from both the victim and suspect, but with a higher concentration of male DNA. We believe this is due to conventional DE's ability to repeatedly purify and wash each sample, which resulted in fewer sperm cells in the non-sperm fraction compared to our results. While ADE lacks this capability, the priority was to isolate sperm to generate a male profile, which was clearly achieved (**Figure 3-5**). Additionally, by examining the relative peak heights seen in each STR profile from ADE, it can be deduced that more sperm cells were captured in the sperm fraction than the non-sperm fraction.

### *3.3.3 Vaginal swab sample*

A vaginal swab (PBSO sample 412) from 2008 was selected for ADE testing, with 100+ sperm cells and significant amounts of epithelial cells noted during microscopy. When initially processed through conventional DE, analysts obtained a full female profile from the non-sperm fraction, and a full male profile from the sperm fraction. When tested with ADE, a full female

profile was obtained for the non-sperm fraction, **Figure 3-6**, but the sperm fraction results deviated from PBSO's findings. When subjected to ADE, this sample produced a major female STR profile, **Figure 3-7**, indicative of predominantly female DNA in solution. While there are some male

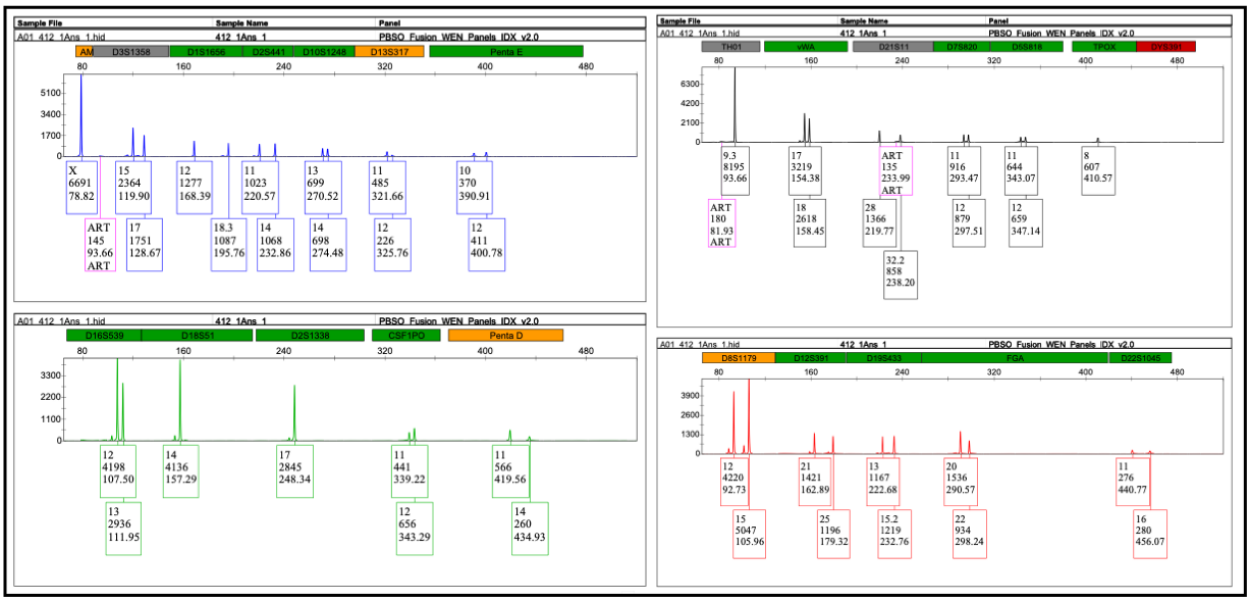

*Figure 3-6. STR profile from the non-sperm fraction of a vaginal swab sample. This result is a full female STR profile, indicative of no sperm present in the non-sperm reservoir. This matches the conventional DE result from PBSO.*

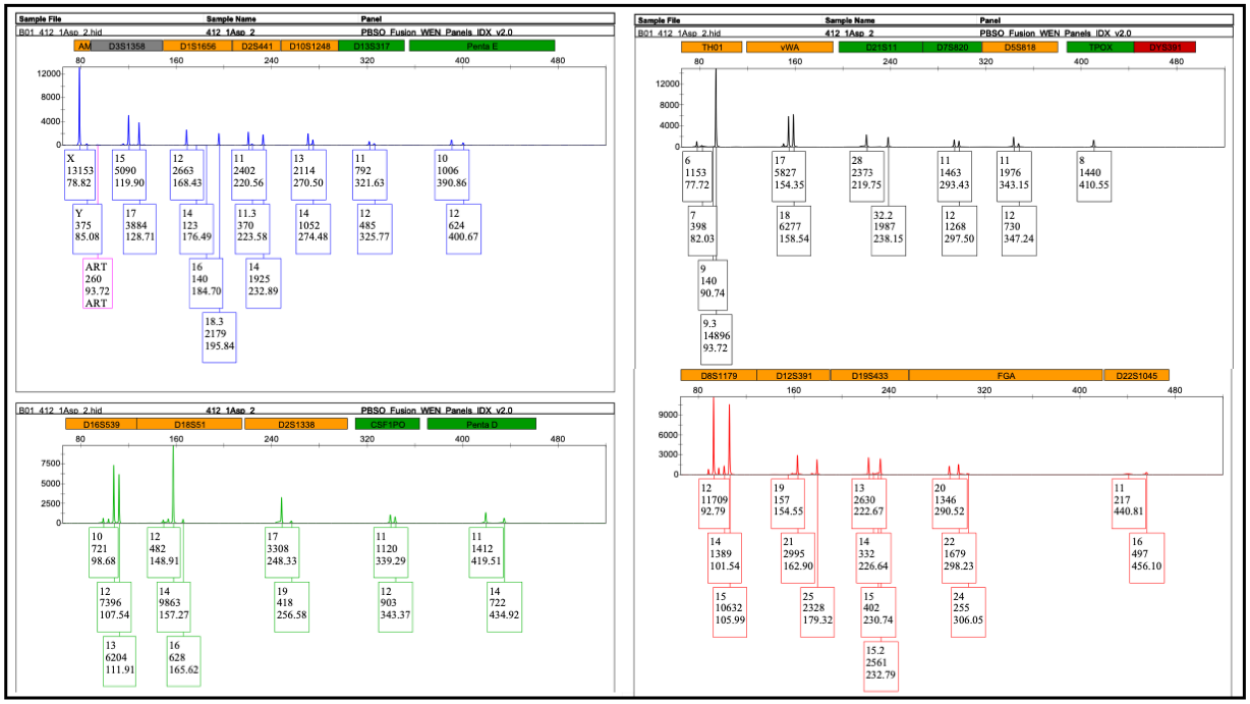

*Figure 3-7. STR profile from the sperm fraction of a vaginal swab sample. This sample generated a mixed profile with major female contribution. This indicates capture of some sperm cells during ADE, but failure to remove all epithelial cells and female DNA.*

alleles observed, they have much lower peak heights than the female alleles. This showed that ADE did not capture enough sperm cells to generate a male profile, nor did it fully eliminate female epithelial cells and/or free DNA during acoustic trapping. This result would suggest that ADE may struggle to isolate sperm cells from samples that contain a high total number of cells, with excess female epithelial cells as compared to sperm.

### *3.3.4 Shorts cutting sample*

In order to test the lower limits of ADE, two challenging samples were chosen from PBSO which contained few total sperm cells. The first sample, a swab of fabric shorts, submitted as evidence in 2009, contained no observable sperm cells during microscopy, but did test positive for prostate specific antigen (PSA), which can be used to predict the presence of semen in a sample [18]. When processed using conventional DE, the analysts were unable to obtain a clean separation of female and male DNA, which resulted in a mixed profile for both the non-sperm and sperm fractions. When processed with ADE, the non-sperm fraction generated a partial STR profile (incomplete profile with allele 'dropouts'), as shown in **Figure 3-8**. The alleles that are present can be assigned to the female victim, but conclusive identification was not possible from this profile. A partial profile was also generated from the sperm fraction, **Figure 3-9**, with only 3 loci

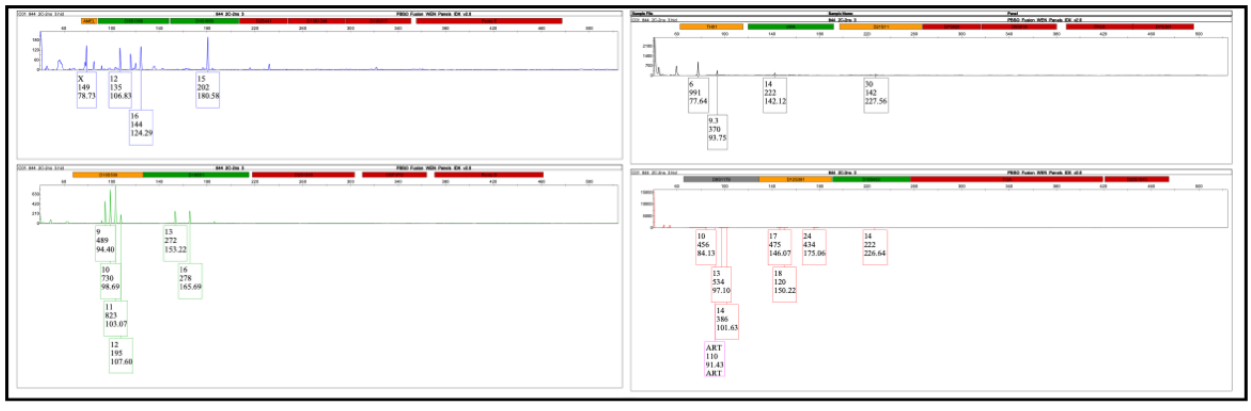

*Figure 3-8. STR profile from the non-sperm fraction of a shorts swab sample. This sample generated an incomplete STR profile from the non-sperm fraction, yielding at best a partial female result, indicating very low DNA concentration in the non-sperm fraction.*

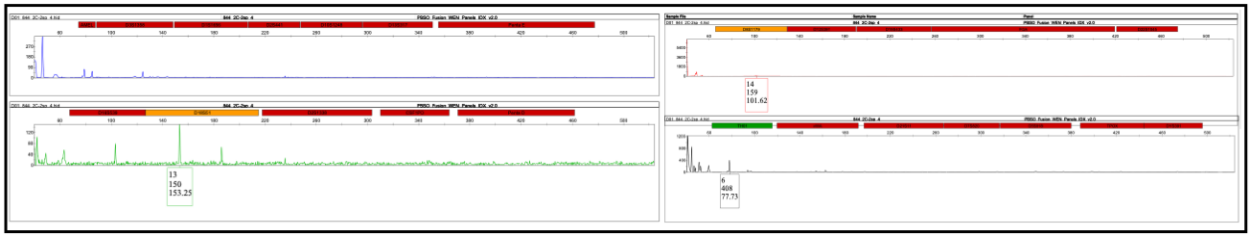

*Figure 3-9. STR profile from the sperm fraction of a shorts swab sample. This sperm fraction yielded an incomplete profile, with only three discernable peaks appearing across all loci. This indicates an almost complete absence of any DNA in the sperm fraction.*

reaching the stochastic threshold (out of 24 loci) . This indicates that almost no DNA was present in the non-sperm fraction and that few, if any sperm cells, were captured. This result showed that when conventional DE could not obtain a male profile from a challenging, low-cell count sample, it is unlikely that ADE would be able to succeed as an alternative method.

### *3.3.5 Rectal swab sample*

The second challenging PBSO sample, a rectal swab from 2008, contained 3 sperm cells observed during microscopy along with epithelial cells and debris. When processed with ADE, the non-sperm fraction generated an incomplete STR profile, with significant dropout at multiple alleles (**Figure 3-10**). The alleles that were present are predominantly female, indicating a 'partial female' profile with minor contributions from male DNA. The sperm fraction from this sample is shown in **Figure 3-11**. While also a partial profile with many allele dropouts, the peak balance at various loci (e.g., Amelogenin, D18S51) indicate that this is a mixed profile, with similar amounts

*Figure 3-10. STR profile from the non-sperm fraction of a rectal swab sample. The resulting partial profile is lacking larger fragment peaks in the electropherogram. The peaks that do appear, indicate that this is a major female profile, with predominantly female DNA present.*

*Figure 3-11. STR profile from the sperm fraction of a rectal swab sample. After ADE, the sperm fraction also generated a partial, mixed profile, with similar amounts of male and female DNA present in the sample.*

of both male and female DNA present. However, the overall peak heights are low, and PBSO forensic analysts noted that significant degradation appears to have occurred. This conclusion is based on the observed ski slope effect (reduction in peak height from left-to-right in the STR profile), and loss of larger fragments in the electropherogram. When originally processed via conventional DE, analysts generated a full male STR profile from the sperm fraction, showing that ADE could not replicate the conventional result for this challenging sample. The reasons for the inability of ADE to replicate conventional DE results are discussed in the following sections.

### *3.3.6 Inhibition of PCR*

When analyzing the data collected from these initial ADE tests, several observations were made. Most importantly, there appeared to be significant dropout (missing loci) and degradation (decline in peak height at larger fragments) in many post-ADE samples. While this could be attributed to old samples, it was hypothesized that incompatibility between reagents could also be causing these issues. As detailed in materials and methods, all pre-ADE lysis and post-ADE DNase/extraction was carried out with ZyGEM reagents, which were not validated by PBSO, whereas qPCR and STR amplification were carried out by validated Promega reagents. Upon recommendation by the PBSO analysts, an additional 5 samples were processed using only

reagents previously validated by PBSO (lysis and extraction). All samples were then analyzed by *PowerQuant* to assess DNA quantities, quality, extraction efficiency, and potential contamination.

| | Sample Name | IPC Shift | IPC Threshold | [Auto]/[Y] | [Auto]/[Y] Threshold | [Auto]/[D] | [Auto]/[D] Threshold |
|---|---|---|---|---|---|---|---|
| 01-30-17 SONIC Training | 412_1Ans_1 | -8.403 | Below | 142.104 | At or Above | 7.134 | At or Above |
| | 412_1Asp_2 | 2.3400 | At or Above | 21.5548 | At or Above | 7.5673 | At or Above |
| | 758_2-2ns_3 | -0.5249 | Below | 1.4534 | Below | 3.2417 | At or Above |
| | 758_2-2sp_4 | | At or Above | 0.6802 | Below | 5.6017 | At or Above |
| | 844_1-9ns_5 | -1.6596 | Below | 3.0550 | At or Above | 6.0136 | At or Above |
| | 844_1-9sp_6 | | At or Above | 1.0281 | Below | 4.7976 | At or Above |
| 01-31-17 SONIC Training | 412_1Cns_1 | 0.516 | At or Above | 8.978 | At or Above | 40.069 | At or Above |
| | 412_1Csp_2 | 0.4719 | At or Above | 3.8127 | At or Above | 15.9542 | At or Above |
| | 844_2C-2ns_3 | 0.0882 | Below | 21.4504 | At or Above | 62.5470 | At or Above |
| | 844_2C-2sp_4 | 0.2287 | Below | 10.3666 | At or Above | Undetermined | At or Above |
| 02-06-17 Non SONIC - used conventional methods to compare samples to SONIC (age) | 412_1Cns_1 | -0.002 | Below | 16.169 | At or Above | 17.521 | At or Above |
| | 412_1Csp_2 | 0.1160 | Below | 1.6424 | Below | 4.8121 | At or Above |
| | 844_2C-2ns_3 | -0.1139 | Below | 9.9633 | At or Above | 10.2535 | At or Above |
| | 844_2C-2sp_4 | -0.1114 | Below | 1.4265 | Below | Undetermined | At or Above |
| | RCNS_5 | -0.1680 | Below | | | | |
| | RCSP_6 | -0.0902 | Below | | | | |
| 04-17-17 Used PBSO reagents in combination with SONIC instrument; post-SONIC purification with EZ1 | 469_3-3ns_1 | 0.123 | Below | 4.811 | At or Above | 5.988 | At or Above |
| | 469_3-3sp_2 | -0.2632 | Below | 4.0371 | At or Above | 4.6574 | At or Above |
| | 289_3-1ns_3 | 0.1175 | Below | 7.7650 | At or Above | 3.5126 | At or Above |
| | 289_3-1sp_4 | -0.1312 | Below | 7.0450 | At or Above | 3.1765 | At or Above |
| | 412_1Ans_5 | -0.1809 | Below | 599.1305 | At or Above | 6.7913 | At or Above |
| | 412_1Asp_6 | -0.1155 | Below | 386.3917 | At or Above | 5.5325 | At or Above |
| | 376_14-1ns_7 | 0.0138 | Below | 224.9058 | At or Above | 11.8926 | At or Above |
| | 376_14-1sp_8 | 0.1497 | Below | Undetermined | | 7.8943 | At or Above |
| | 980_6Cns_9 | -0.150 | Below | 782.654 | At or Above | 5.499 | At or Above |
| | 980_6Csp_10 | 0.0335 | Below | 115.4203 | At or Above | 4.2447 | At or Above |
| | RCNS_11 | -0.4478 | Below | | | | |
| | RCSP_12 | -0.3833 | Below | | | | |
| 04-19-17 All SONIC | 957_5-13ns_1 | 0.182 | Below | 2.046 | At or Above | 7.365 | At or Above |
| | 957_5-13sp_2 | 0.4147 | At or Above | 2.0227 | At or Above | 9.8539 | At or Above |
| | 844_1-5ns_3 | -0.3802 | Below | 2.9712 | At or Above | 3.4705 | At or Above |
| | 844_1-5sp_4 | 0.2790 | Below | 4.9959 | At or Above | Undetermined | At or Above |
| | 980_6Ans_5 | 0.3640 | At or Above | 90.4568 | At or Above | 5.1132 | At or Above |
| | 980_6Asp_6 | 0.8189 | At or Above | 91.8752 | At or Above | 12.7976 | At or Above |
| | 976_1Gns_7 | 0.4562 | At or Above | 69.6473 | At or Above | 15.4556 | At or Above |
| | 976_1Gsp_8 | 1.4383 | At or Above | 62.3771 | At or Above | 31.1777 | At or Above |
| | 839_2B-6ns_9 | 0.389 | At or Above | 24.587 | At or Above | 46.624 | At or Above |
| | 839_2B-6sp_10 | 0.2057 | Below | 10.8427 | At or Above | 20.6097 | At or Above |
| | 039_1Gns_11 | -0.2018 | Below | 9.5491 | At or Above | 77.6139 | At or Above |
| | 039_1Gsp_12 | 0.3186 | At or Above | 1.7321 | Below | Undetermined | At or Above |

| IPC shift = At or Above 0.3, Possible inhibitor present | At or Above 2 indicates possible Male/Female mixture; Auto/Y ratio is ≥ 200 = PBSO direct to Y-STR | Auto/Degradation = At or Above 2.0, Possible degraded sample |
|---|---|---|

*Table 3-3. qPCR data from PBSO samples. "SONIC" was the name of the prototype instrument, and "All SONIC" refers to use of ZyGEM reagents. The IPC shift is used to indicated possible inhibition of DNA amplification. IPC above 0.3 may signify presence of an inhibitor. Elevated IPC threshold was observed only in samples which used UVA-provided extraction reagents in combination with PBSO amplification chemistry. When IPC shift exceeded 2.5, detection was maxed out, and thus, no value was recorded.*

During qPCR, the internal positive control (IPC) threshold is often used as an indicator for potential inhibition of DNA amplification [19]. *PowerQuant* data shown in **Table 3-3** demonstrates a clear pattern: an elevated IPC threshold (second and third columns) only occurs in samples that were lysed and extracted using ZyGEM reagents from UVA, and never occurs in the all-PBSO processed samples. While not every ZyGEM sample displays potential PCR inhibition, it is evident that there is some incompatibility between the ZyGEM and Promega reagents, leading to less efficient amplification of the target DNA. With these new data and hypothesis, additional samples were tested using all PBSO extraction and amplification chemistries, and some previous samples were retested under new conditions.

### *3.3.7 Rectal swab sample, retested*

One PBSO sample that was flagged for inhibition was 412-C, the rectal swab which generated partial STR profiles from the non-sperm and sperm fractions after ADE (**Figures 3-10, 3-11**). This sample, having already undergone ADE, was re-extracted using the validated Qiagen

*Figure 3-12. Re-extracted STR profile from the sperm fraction of a rectal swab sample. Upon DNA extraction with EZ1 reagents, a full male STR profile is seen from the sperm fraction. A minor ski slope effect is observed at larger fragments, indicating possible degradation of the sample. NOTE: y-axis has been zoomed in to display smaller peaks at larger fragments.*

*EZ1 Investigator Kit*, and significantly different results were observed. **Figure 3-12** shows the sperm fraction from the rectal swab sample after ADE, where a *full male STR profile* is observed. This suggests that ADE did, in fact, capture enough sperm cells from this challenging sample to conclusively identify a suspect. In addition, the resulting profile contains no female alleles, and demonstrates strong peak heights at all loci. Some degradation concerns remain, due to lower peak heights at larger fragments, but those may be attributed to age of the sample or low total sperm cell concentration. While the exact cause of PCR inhibition was not determined, it is clear that some combination of the ZyGEM lysis/extraction reagents and Promega amplification kits were incompatible, leading to inefficient extraction and amplification of male DNA from the captured sperm cells. This promising result of a full male STR profile obtained from a rectal swab with low total sperm cells shows that ADE may be viable for a wide range of sexual assault samples.

### *3.3.8 Delayed collection vaginal swab*

The feedback from our initial evaluation at PBSO was positive, and the laboratory director requested that the prototype ADE instrument be subjected to further testing. Additional samples were collected, including a 'time-delayed' vaginal swab sample collected 5 hours after intercourse. There was no microscopy data for this sample, but *PowerQuant* results gave an estimate of 16:1 ratio of female:male cells. There was no information on the total number of cells, but based on prior sample collection at PBSO, it is likely that the sample contained significantly more epithelial cells than a buccal or rectal swab. When processed using ADE (with validated reagents), the non-sperm fraction resulted in a full female STR profile (**Figure 3-13**). The sperm fraction STR profile, shown in **Figure 3-14**, was considered mixed, with significant contributions from both the victim's and suspect's DNA. Compared to the non-sperm fraction, the sperm fraction profile showed a clear increase in sperm cell concentration and improvement in purification (i.e., an enrichment in

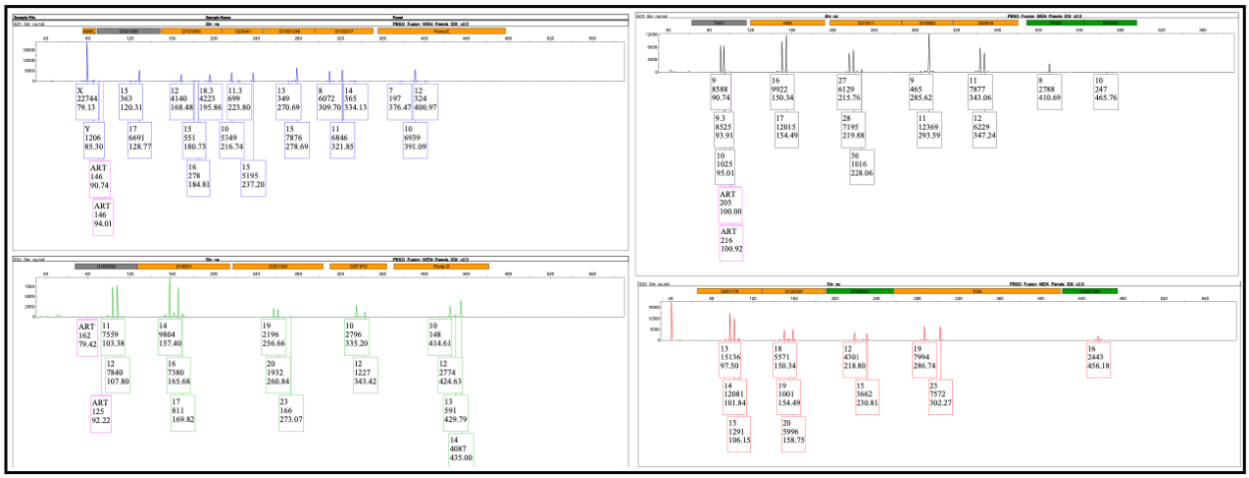

*Figure 3-13. STR profile from the non-sperm fraction of a delayed vaginal swab. This profile is full female, with no significant contributions from any male alleles.*

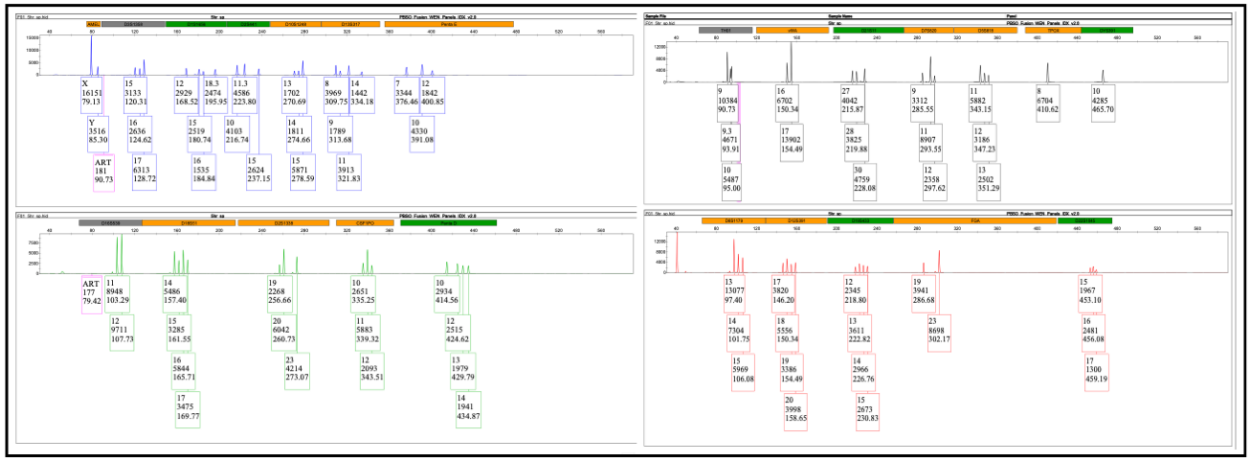

*Figure 3-14. STR profile from the sperm fraction of a delayed vaginal swab. After ADE, the sperm fraction generated a mixed profile, with major female contributions. This profile shows alleles from both the victim and suspect, with more female DNA present than male DNA.*

suspect's DNA), even though ADE was not able to fully isolate sperm cells and remove all female DNA from the sample. However, with recent software advancements, STR mixtures can be deconvoluted to their individual sources, so even a mixed profile is a valuable improvement over pre-ADE results.

### *3.3.9 Analysis of failed trapping tests*

The most important takeaway from this external evaluation was discovered during data analysis, when the real-time trapping videos were reviewed in conjunction with analyst records. For each sample tested, the operator noted successful fluorescent bead trapping during the

frequency scan step. This was important, as it demonstrated that each microchip and piezo were operating correctly, and generating a standing acoustic wave for particle trapping. However, during the sperm cell trapping stage of many tests, aggregation was difficult to observe. Upon reviewing the videos of each run, it became apparent that a large aggregate of beads was trapped to determine the optimal frequency, as expected, but upon switching from bead solution to actual sample, a rapid loss of trapping occurred. This unpredicted effect is illustrated in **Figure 3-15**,

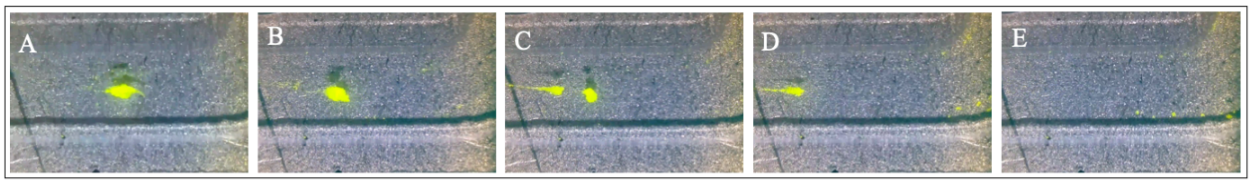


*Figure 3-15. Snapshots from scanning vs trapping of time-delayed samples. (A) Beads trapped during frequency scanning; sample flow is from right to left. (B) Sample trapping 5 seconds after scan, full aggregate is retained. (C) Sample trapping 6 seconds after scan, aggregated has broken into two and shifted downstream of the optimal trapping site). (D) Sample trapping 7 seconds after scan. Smaller aggregate remains trapped, but is further downstream. (E) Sample trapping 8 seconds after scan, entire aggregate has been washed away. Using the same frequency that optimally trapped beads in (A), the entire aggregate is lost within 8 seconds.*

which shows the decrease in aggregate size and shift in trapping location over the course of 8 seconds. These images were collected during ADE of a non-probative sample at PBSO, while switching between the frequency scan and the sample trapping stages. We hypothesized that physical differences in the density, viscosity, and compressibility of the scanning solution, as compared to the non-probative sample, led to variability in optimal acoustic trapping conditions. This loss of acoustic trapping resulted in poor sperm cell capture, which in turn led to less male DNA in the sperm fraction, and fewer full male STR profiles generated. This effect was observed in many samples upon reviewing the run data, and was identified as a clear area that needed improvement for future iterations of this technology.

### *3.3.10 Mesa PD: Cotton fabric sample*

The Forensic Biology Unit at Mesa PD did not have any non-probative samples available to test with ADE, instead, their analysts prepared mock samples on realistic substrates. The first was a dilution of semen deposited onto cotton fabric. The only difference from the ADE protocol

described in section 3.2.4 was the use of Qiagen *Investigator* 24Plex kit for DNA amplification, as opposed to the Promega *Fusion* kit. A cutting of the fabric was subjected to the ADE workflow, carried out by Mesa PD analysts. The non-sperm fraction resulted in a partial male STR profile, shown in **Figure 3-16**. Due to the lack of female epithelial cells in the mock sample, one would

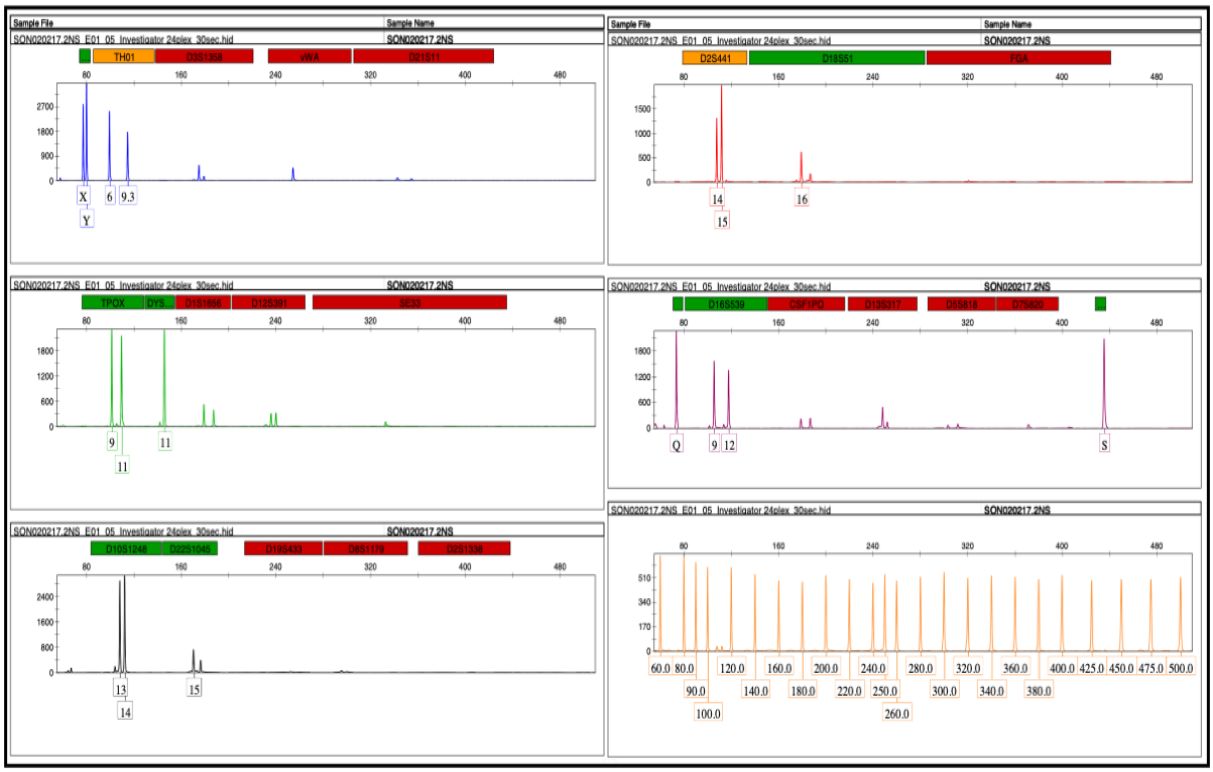

*Figure 3-16. STR profile from the non-sperm fraction of a cotton fabric sample. This is a partial male profile, with only male DNA present, but many loci lacking any peaks.*

expect nothing in the non-sperm fraction. However, the STR result indicates that a low number of sperm cells did escape the trapping site, leading to a partial male profile in the non-sperm fraction. The sperm fraction STR profile from this cotton fabric sample is shown in **Figure 3-17**. This STR profile is a 'clean male' with all loci represented and only male DNA present, indicative of successful separation. This is an unsurprising, but still positive result, showing that ADE can capture sperm cells from a cotton substrate.

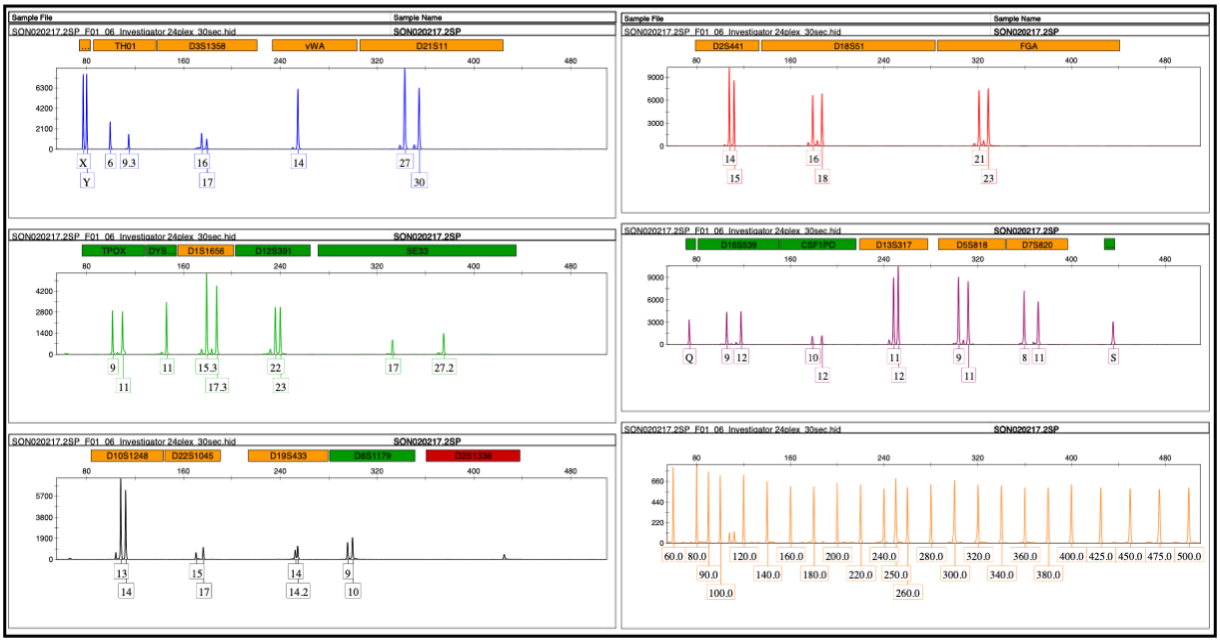

*Figure 3-17. STR profile from the sperm fraction of a cotton fabric sample. This is a full male STR profile, with only male DNA present and peaks appearing at all loci. For the D2 locus (furthest right in the black trace), a single male allele is present, but was not automatically called by the analysis software.*

### *3.3.11 Spandex fabric sample*

The second sample prepared and tested at Mesa PD was semen deposited onto spandex fabric. Similarly, as with the cotton fabric sample, the non-sperm fraction here (**Figure 3-18**) generated a partial male profile, with many allele dropouts and low overall peak heights. This

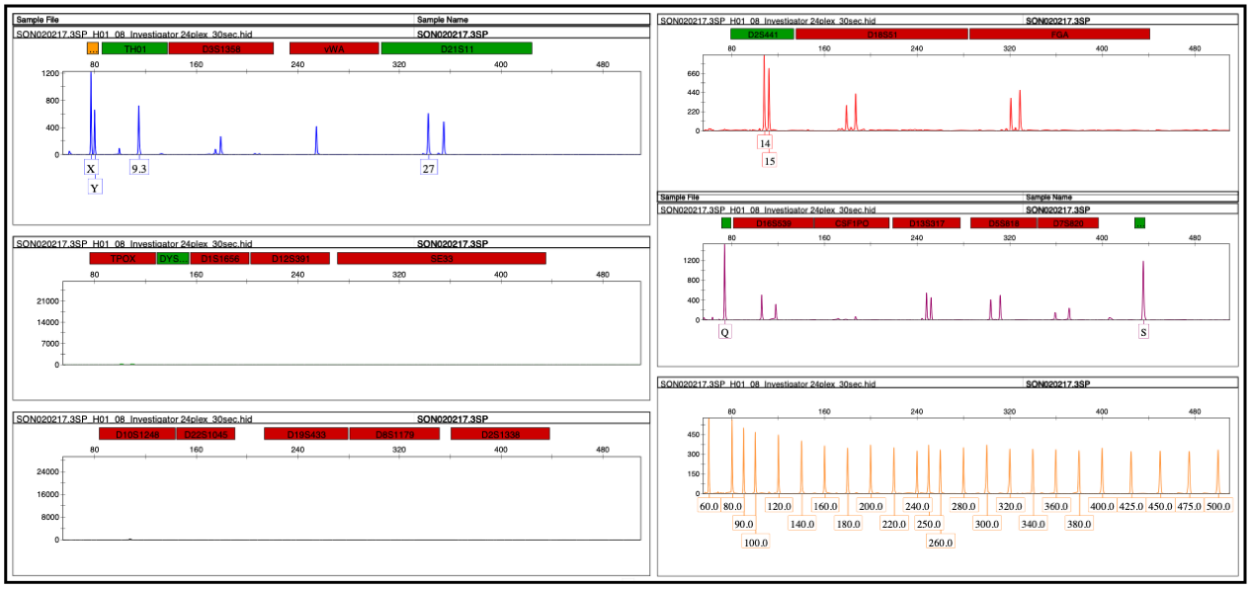

*Figure 3-18. STR profile from the non-sperm fraction of a spandex sample. A partial male profile is observed; this result shows some male DNA present in the non-sperm fraction.*

indicates a small number of sperm cells escaping the acoustic trapping site. The sperm fraction STR profile in **Figure 3-19** is, again, a 'clean male' profile. At two loci, D2S1338 and D7S820, peaks for the male alleles are present, but were not automatically called due to low peak heights. A similar effect was observed with the cotton fabric sample, suggesting that the sperm cells may have been degraded or damaged during storage. However, this test confirms that ADE can capture sperm cells from a variety of substrate materials, and can fit into the existing forensic workflow at a government laboratory.

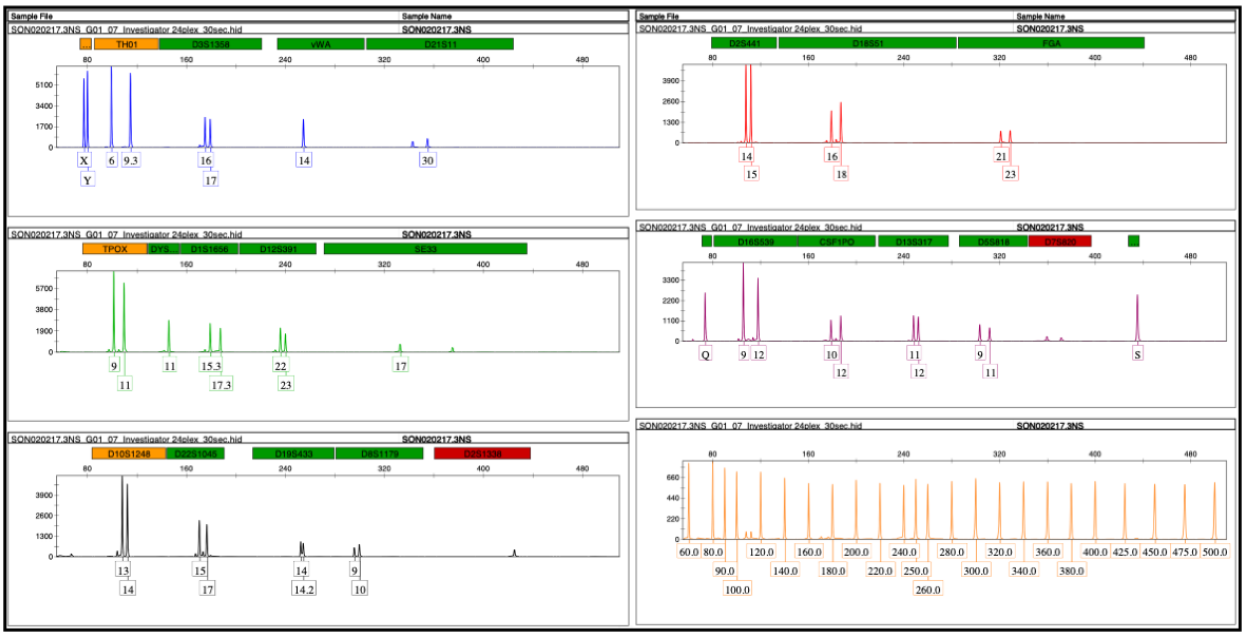

*Figure 3-19. STR profile from the sperm fraction of a spandex sample. This is a full male STR profile, with only male DNA and all loci represented. The D2 locus (furthest right in the black trace) and the D7 locus (second from right in the purple trace) both have male alleles present, but peak heights were too low to be automatically assigned.*

### *3.3.12 Mock sexual assault sample*

A mock sample was prepared at Mesa PD, containing female epithelial cells and male sperm cells deposited on a cotton swab. The concentration range of each cell type was not known, and the sample was processed as described in section 3.2.4. Acoustic trapping was observed for the fluorescent beads and sperm cells, however, a downstream valve failure resulted in complete loss of sample to the non-sperm fraction. This caused unexpectedly high volume of liquid to collect in reservoirs 4 and 5 of the microchip, recombining the sperm and non-sperm fractions,

leading to inconclusive STR profiles. **Figure 3-20** shows the STR profile of the non-sperm fraction, which would be classified as a 'partial male' profile. Despite many allele dropouts, the partial profile can be attributed to the male semen donor, indicating that a significant amount of sperm cells was present in the non-sperm fraction. **Figure 3-21** shows the STR profile of the sperm fraction. There is no DNA present in this sample based on the absence of STR peaks, indicating a total lack of sperm cell capture. This can be attributed to the unexpected hardware

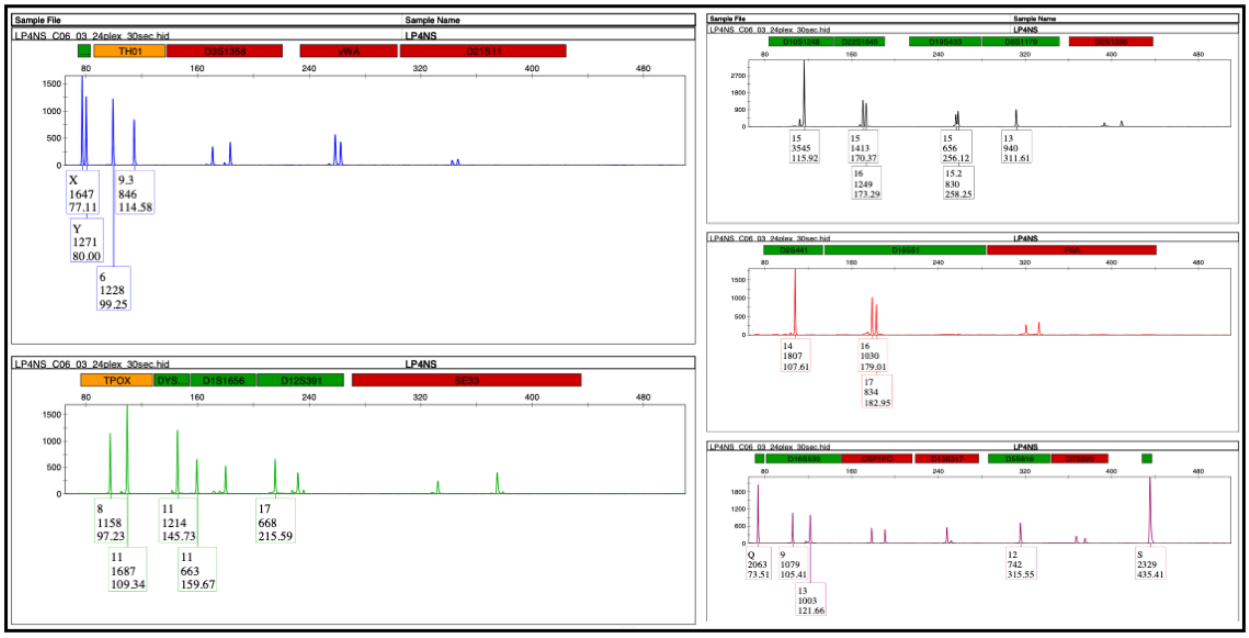

*Figure 3-20. STR profile from the non-sperm fraction of a mock sample. This non-sperm fraction resulted in a partial male STR profile, with male alleles present at most loci.*

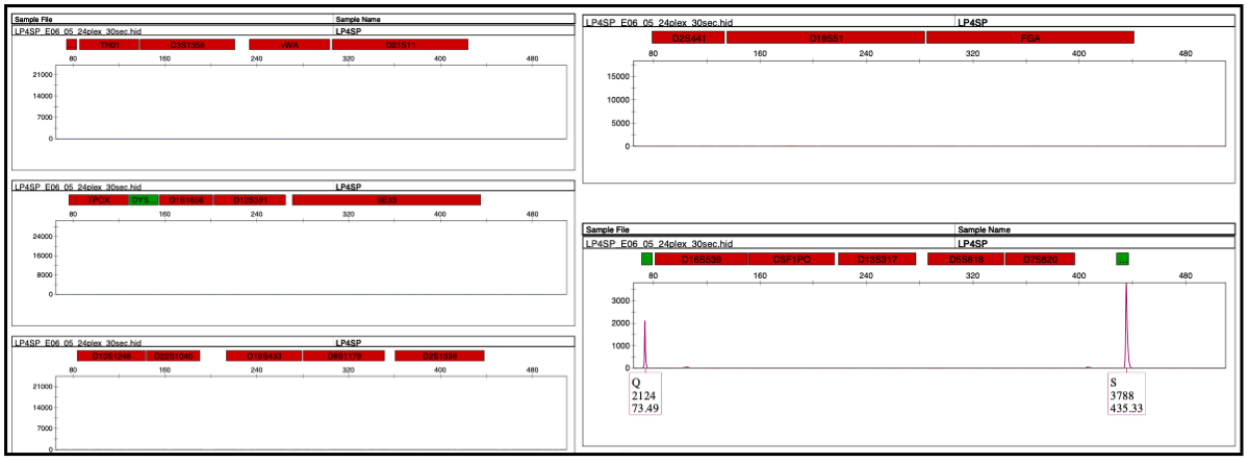

*Figure 3-21. STR profile from the sperm fraction of a mock sample. There is no amplification of target DNA in this sample, resulting in no profile. This is indicative of lack of sperm cells, or any other DNA, in the sperm fraction.*

failure, which resulted in minimal fluid (< 10 μL) collected from reservoir 4 (sperm fraction) of the microchip.

These STR profile results, combined with discrepant volumes in the downstream reservoir, led to the discovery that one of the solenoid valves was malfunctioning, causing the sperm and non-sperm fractions to be combined into a single reservoir. Aside from the obvious impact of failing to separate sperm cells from female DNA, this valve failure also forced excess fluid into reservoir 5, causing sample to flow down into the tubing and valving that connects reservoirs 4, 5, and 6. While onsite in the Mesa PD Forensic Biology Unit, the valve and tubing blockages could not be cleared and the instrument was deemed non-functional. At this point the external testing was halted at the Mesa facilities, and the instrument returned to UVA for repair. The prototype system was not designed to be ruggedized, and therefore we hypothesized that unforeseeable shipping damage caused the valving failure which led to breakdown.

## 3.4 Summary

During extensive testing at two state-run forensic laboratories, the ADE prototype instrument and microchip delivered results that are comparable to conventional DE with some sample types. ADE of the condom, bed sheet, and rectal swab sample from the PBSO lab all resulted in full male STR profiles, matching the previously obtained result via conventional DE. The novel ADE method required far fewer pipetting steps, avoided centrifugation of the sperm cells to separate them from epithelial lysate, was performed faster (50 minutes vs 2+ hours), and in a more automated fashion than conventional DE. However, the testing at PBSO also illustrated several areas in which improvement is needed. First, there was clear incompatibility between the mixed use of non-validated and validated reagents, indicated by the IPC flag. This resulted in poor DNA amplification, possibly skewing the overall results of some samples. Future testing of this

prototype will necessitate better reagent compatibility, either by providing all reagents with the instrument, or fully investigating different reagent combinations in advance. The second, and more impactful takeaway from this evaluation, was that the acoustic trapping effect appears to vary greatly between samples of different cellular composition. This was observed with several samples containing a high number of epithelial cells, where fluorescent beads were successfully trapped, but sperm cells and residual beads failed to be trapped under the same applied acoustic frequency. It is our hypothesis that the complex biofluids present in authentic sexual assault samples significantly change the liquid medium as compared to pure water, and that, in turn, shifts the acoustic frequency that must be applied. This is not a simple issue to resolve, and our attempt to do so is presented in Chapter 4.

The feedback from analysts at Mesa PD and the team at PBSO was extremely positive. Both groups expressed a strong interest in continuing to support development of this technology, as they foresee a clear path to implementing ADE in the processing of sexual assault samples. Dr. Cecelia Crouse, the Crime Laboratory Director from PBSO stated that:

> "*The prototype SONIC-DE instrument was compact, intuitive to use, and provides a new approach for differential extraction. We were impressed with the technology's ability to capture sperm from exemplary sexual assault samples, and with some adjustments to hardware and chemical processes, we believe that this system could also move to address more challenging samples (such as those with low total sperm or excess epithelial cells). We would support the further development and testing of this technology, and would be excited to field-test a second-generation system with the necessary improvements.*"

Such support from a respected and influential figure in the forensic community is vital for advancing this technology, and the partnerships with PBSO and Mesa PD will remain crucial for bringing ADE to a functional role in processing sexual assault samples.

## 3.5 Acknowledgements

I would like to thank the forensic analysts and lab directors at the Palm Beach County Sheriff's Office and the Mesa Police Department for their consultation, recommendations, and for hosting the external evaluation of the ADE prototype.

## 3.6 References

1. V. Williamson, T. Laris, R. Romano, M. Marciano, *FSI: Genetics*, 2018, **34**, 265-76.
2. X. Zhao, L. Wang, J. Sun, B. Jiang, E. Zhange, J. Ye, *PLoS One*, 2016, **11**, 1-9.
3. V. Bogas, A. Bento, A. Serra, P. Brito, V. Lopes, L. Sampaio, N. Gouveia, P. Cunha, F. Balsa, M. Sao-Bento, M. Porto, *FSI: Genetics Supplement Series*, 2017, **6**, 353-4.
4. S. Klein, M. Buoncristiani, *FSI: Genetics*, 2017, **29**, 109-17.
5. Promega Corporation, *Internal Validation Guide of Autosomal STR Systems for Forensic Laboratories*, 2013.
6. European Network of Forensic Science Institutes, *Guidelines for the single laboratory Validation of Instrumental and Human Based Methods in Forensic Science*, 2014.
7. P. Wiegand, M. Schurenkamp, U. Schutte, *International Journal of Legal Medicine*, 1992, **104**, 359-60.
8. I. Voskoboinik, A. Darvasi, *FSI: Genetics*, 2011, **5**, 428-35.

9. S. Garvin, M. Bottinelli, M. Gola, A. Conti, G. Soldati, *Journal of Forensic Science*, 2009, **54**, 1297-1303.
10. D. Nori, B. McCord, *Analytical and Bioanalytical Chemistry*, 2015, **407**, 6975-84.
11. V. Martinez, D. Nori, P. Dimsoski, B. McCord, *Electrophoresis*, 2017, **38**, 2777-85.
12. M. Vandewoestyne, F. Nieuwerburgh, D. Hoofstat, D. Deforce, *FSI: Genetics*, 2012, **6**, 258-62.
13. Z. Budimlija, M Lechpammer, D. Popiolek, F. Fogt, M. Prinz, F. Bieber, *Croatian Medical Journal*, 2005, **46**, 549-55.
14. J. Chen, I. Kobilinsky, D. Wolosin, R. Shaler, H. Baum, *Journal of Forensic Science*, 1998, **43**, 114-118.
15. C. Ladd, E. Carita, E. Pagliaro, A Garvin, A Crumbie, H. Lee, *U.S. Department of Justice*, 2006, 215339.
16. B. Hammarström, T. Laurell, J. Nilsson, *Lab on a Chip*, 2012, **21**, 4296-4304.
17. K. Xu, C. Clark, B. Poe, J, Lounsbury, J. Nilsson, T. Laurell, J. Landers, *Analytical Chemistry*, 2019, **91**, 2186-91.
18. M. Hochmeister, B. Budowle, O. Rudin, C. Gehrig, U. Borer, M. Thali, R. Dirnhofer, *Journal of Forensic Science*, 1999, **44**, 1057-60.
19. C. Strayer, *Understanding the IPC in DNA Quantitation Assays*, 2014, available from http://www.promega.com/resources/profiles-in-dna/2014/understanding-the-ipc-in-dna-quantitation-assays/

# Chapter 4: Real-time electronic feedback for improved acoustic trapping

## 4.1 Introduction

### *4.1.1 Impact of external evaluation testing*

The years-long development of acoustic differential extraction (ADE), described in Chapters 2 and 3, yielded promising results during external evaluation in forensic laboratories. Testing non-probative sexual assault samples showed that ADE performs comparably to conventional differential extraction (DE) in some cases, with far fewer hands-on steps and less time required. However, through testing a wide range of evidentiary materials and analyzing acoustic trapping performance, it became clear that sperm cell capture was not uniform across all sample types. Specifically, it was observed that in samples containing an extremely high number of epithelial cells (greater than approximately 50,000), very few, if any, sperm cells were retained. As discussed in Chapter 3, section 3.3.8, all microchips showed acoustic trapping of fluorescent beads in water during the 'frequency scan' step that identifies the optimal trapping frequency. However, on that same microchip, when fluid flow was shifted from the bead solution to a non-probative sample, particle aggregation was lost over the course of ten seconds, and no sperm cells were captured. This phenomenon occurred with multiple non-probative sexual assault samples during the external evaluation stage, but had not been previously observed during research and development of this technology. Essentially, applying the optimal trapping frequency for a microchip caused aggregation of beads in water, but did not capture sperm cells from a sample. The conclusion drawn from these tests was that variability in the physical characteristics of the

sexual assault sample caused a loss of acoustic trapping. Specifically, differences in sample density, viscosity, and compressibility caused a shift in optimal trapping frequency.

*4.1.2 Sample-to-sample variability*

During previous development and testing of the ADE prototype at UVA, mock samples were formulated to contain between 1,000 and 20,000 female epithelial cells. This was due to a focus on cellular ratio, i.e. epithelial cells:sperm cells, rather than concern with the total number of cells present. However, as it became clear at the Palm Beach County Sherriff's Office and Mesa Police Department, there is no 'typical' sexual assault sample, and evidence can contain hundreds of thousands of total cells. Regardless of sample composition, the first step of ADE or conventional DE is cellular lysis, breaking open all epithelial cells to release their contents. We believe that this lysis significantly changes the physical properties of samples with a high number of epithelial cells, and those changes in density, compressibility, and viscosity of the fluid leads to a loss of acoustic trapping. Multiple studies have shown that when cellular lysis occurs, the cellular content perfuses into the surrounding liquid and causes an increase in viscosity [1-4]. Significant fluidic changes, brought on by cellular lysis and release of proteins, debris, and membrane fragments into solution, subsequently impact the efficiency of acoustic trapping. Acoustic radiation forces are well defined in the literature [5-10] and described in depth in Chapter 1, section 1.2.5. These forces, specifically the primary radiation force, depend heavily on the fluidic properties, as well as the particles being trapped. With regard to the fluidic properties, there is specific literature demonstrating that the viscosity of the surrounding liquid will impact trapping, changing the acoustic radiation force experienced by particles in a standing wave [7, 11]. What has not been reported, however, is if these changes could lead to a shift in the resonant frequency for an acoustic trapping device, resulting in a different required wavelength of sound to create the

standing wave. In short, a frequency of sound that traps particles in one liquid, may not do so in another. This effect could explain the observed loss of trapping during the shift from beads in water to a non-probative sexual assault sample.

The crux of this issue is two-fold: First, due to the wide variability in the cellular content of sexual assault samples, it is impossible to accurately predict their physical properties. Second, the evidence screening process does not quantify the number of cells present on sexual assault sample. Microscopy is used to gather a rough estimate of sperm cell count, and note any presence of epithelial cells, but this is performed quickly on a small cutting of evidence, and samples with high cell counts are simply marked as "+++" to indicate an excess of epithelial cells or sperm [12]. These two factors cause a dilemma, wherein each sexual assault sample may have significantly different fluidic characteristics that cannot be accurately predicted with current techniques. ADE already uses an initial frequency scan to identify the optimal trapping frequency for *each unique microchip*, accounting for differences in channel height and material thickness. However, we must now also account for differences in the physical properties of *each unique sample*. To achieve this, an approach was sought that could measure acoustic trapping performance in real-time, feed that information back into the ADE instrument, and automatically adjust the applied frequency as necessary to account for changes in the liquid medium.

Such a 'feedback system' has been previously described by Nilsson et al. [13], where impedance measurements were used to identify the optimal trapping frequency for a microfluidic acoustic trapping platform. Based on previous literature [14,15], the Nilsson group designed a circuit to calculate a power spectrum from the output impedance of the function generator, which applies the electrical waveform. By identifying the peak power output of the piezoelectric transducer, based on impedance measurements, they determined the optimal trapping frequency

for their system. That information was used to adjust the applied frequency under different conditions, successfully maintaining a resonant standing wave. This approach would meet the necessary criteria for our problem, and provide real-time feedback on the optimal acoustic trapping frequency.

### *4.1.3 Alternate method of detecting optimal trapping frequency*

When conducting an acoustic trapping experiment, the resonance frequency occurs when the piezoelectric transducer most efficiently converts electrical energy into mechanical energy [16]. There is less resistance to vibration as the piezo approaches its resonant frequency, which causes electrical impedance to reach a minimum when resonance is achieved. Taking advantage of this relationship is how Nilsson et al. identified the optimal frequency for their system, using impedance measurements to determine when resistance to vibration was at a minimum. Our approach uses the same principle, seeking to identify the resonant frequency by determining when the minimum resistance to piezo vibration occurs. However, instead of using an impedance analyzer, we directly measured the output voltage of the piezo. Impedance is defined as the opposition a circuit presents to a current when voltage is applied, and Ohm's Law (for AC) states that $V = IZ$, where $V$ = voltage, $I$ = current, and $Z$ = impedance [17,18]. By using this relationship and monitoring output voltage of the piezo, any changes in the voltage represent a change in impedance, and thus, change in resistance to vibration during acoustic trapping. This is an appealing approach for determining the optimal trapping frequency, as voltage measurements are rapid, quantifiable, and more easily interpreted than measuring the aggregation of fluorescent beads. Our testable hypothesis was that a minimum in voltage output from the piezo will correlate with the optimal trapping frequency, and this measurement can be used to adjust acoustic trapping in real-time, preventing the loss of captured particles.

## 4.2 Materials and methods

### *4.2.1 Circuitry for measuring voltage output of the piezo*

A custom printed circuit board (PCB) was designed and fabricated by Vahid Farmehini (UVA Department of Electrical Engineering) to measure the output voltage of the piezoelectric transducer. The objective of incorporating this PCB was to measure, in real-time, any changes in the voltage output from the piezo during ADE. A simplified schematic of the PCB is shown in **Figure 4-1**, which can be broken down into the 'voltage divider' and 'peak detector' units. Together these units provide precise measurement of the AC voltage amplitude across the piezo

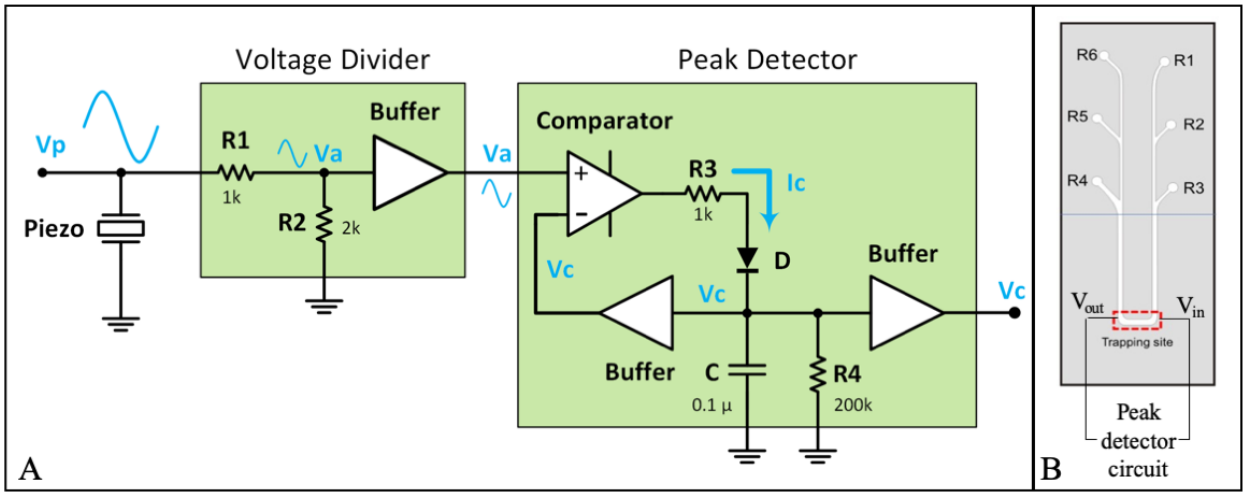


*Figure 4-1. Schematic for measuring voltage output. (A) The circuitry shown measures the voltage across the piezoelectric transducer. This PCB was designed and fabricated by Vahid Farmehini, UVA Electrical Engineering. (B) The voltage monitoring circuit was connected via pogo pins to the piezo on the underside of the microchip.*

transducer [19]. Within the peak detector unit, a fast comparator (Ad8561, Analog Devices, MA) continuously compares the previously held value ($V_c$) with the new input AC voltage ($V_a$). When the new input voltage is higher, the comparator output swings high (+5V) and produces a charging current ($I_c$), which in turn increases the capacitor voltage. If the input voltage is lower than the previously held value, the comparator output drops to 0V and the capacitor voltage is unchanged. The voltage data is plotted using LabView software, which displays the output voltage in real-time

during a test. The operator can then use that information to select a new acoustic frequency during ADE.

### *4.2.2 Hardware and software modifications to the ADE prototype*

The previously described ADE prototype was modified to allow for real-time measurements of the output voltage, and to accommodate manual control of the applied frequency. First, electrical leads were soldered to the brass pogo pins that create electrical contact with the piezoelectric transducer. Those leads connected to the external PCB (**Figure 4-1**) via a Bayonet Neill-Concelman (BNC) connector, providing the voltage data needed for the proposed feedback system. Second, control of the function generator was removed from the ADE software, as the pre-programmed frequency scans were limited in their range, timing, and user manipulation. Instead, the function generator was externally controlled through Hantek DDS-3X25 software, which allowed the user to customize the applied frequency, amplitude, and waveform of the electrical signal. Fluidic control through valves and pumps, as well as the real-time video

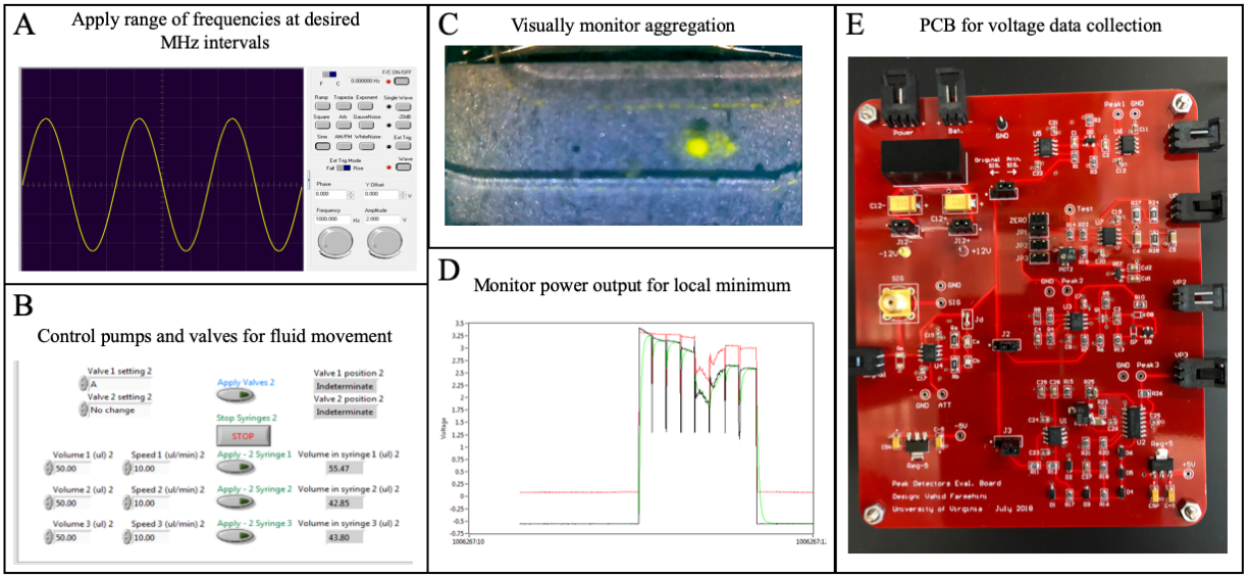


*Figure 4-2. Overall workflow for manual real-time feedback. (A) The operator sets the starting frequency and amplitude of the applied waveform. Once acoustic trapping begins, the frequency can be manually adjusted to any value between 1.0 and 9.9 MHz. (B) The LabView interface allows the operator to control two valves and three syringe pumps, directing fluid between any of 6 fluidic reservoirs. (C) Real-time video shows aggregation of fluorescent beads in the trap site. (D) Voltage data is also collected in real-time, providing the operator with a quantifiable indicator of optimal trapping. (E) The printed circuit board used to measure voltage output from the piezo during ADE.*

monitoring, was left unchanged. With each of these adjustments, the overall workflow could now be represented as shown in **Figure 4-2**. After preparing a sample and loading the microchip, the operator applied a frequency (**Figure 4-2A**) and initiated syringe pumps to move sample through the acoustic trap site (**Figure 4-2B**). Simultaneous video monitoring (**Figure 4-2C**) and voltage measurements (**Figure 4-2D**) were provided during ADE. The voltage data was collected by the PCB shown in **Figure 4-2E**, and was plotted as a function of voltage (y-axis) vs time (x-axis). By analyzing the voltage data and visual aggregation of beads, the user could identify, and then apply, the best trapping frequency in real-time (**Figure 4-2A**), thus retaining the maximum number of particles or cells. This approach would optimize acoustic trapping regardless of the physical characteristics of the sample.

### *4.2.3 Sample composition and experimental workflow*

During evaluation of this real-time feedback system, a wide range of samples were tested. These included solutions of yellow fluorescent beads in water, as well as mock samples containing glycerol, epithelial cell lysate, sperm cells, and human serum. Epithelial cells were collected via buccal swabs, while semen and human serum were collected anonymously under the UVA Institutional Review Board HSR Protocol #12548. Epithelial cells were recovered by manually agitating the swab in 600 μL water for 60 seconds, followed by a spin basket extraction. Epithelial cells and sperm cells were diluted and quantitated via hemocytometry using the green fluorescent nucleic acid stain SYTO-11. When necessary, epithelial cells were lysed using *prep*GEM (ZyGEM NZ Ltd) with incubation at 75°C for 15 min, and 95°C for 5 min.

The previous microfluidic chip design implemented for method development, as described in Chapters 2 and 3, was used for development of this feedback system. The microchip, shown in **Figure 4-3,** contains 6 fluidic reservoirs and an acoustic trapping site. The piezo vibrates against

the glass-PDMS-glass resonator chamber, generating standing acoustic waves, which promote particle aggregation as discussed in Chapters 1 and 2. During testing, the chip was loaded with 10 μL priming solution (5:1:1 ratio of water:ethanol:glycerol), and reservoirs 1, 2, and 3 were loaded with 110 μL of fluorescent bead solution, mock sample, or glycerol dilution.

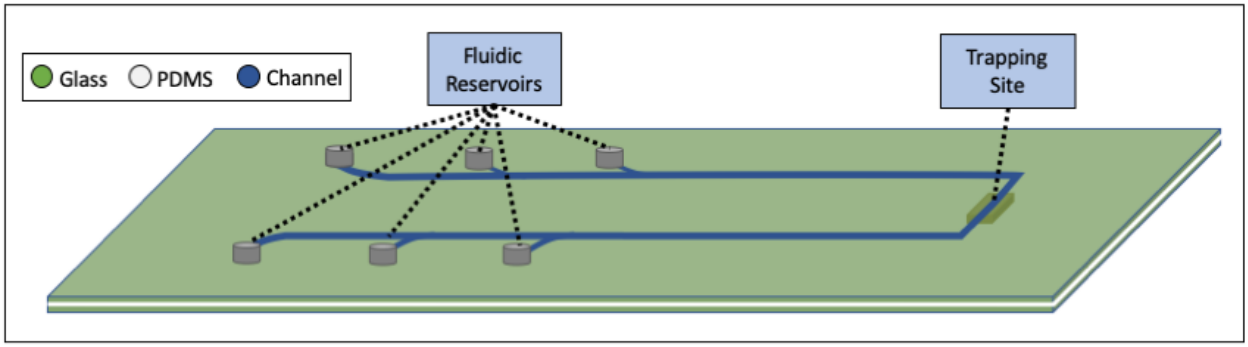


*Figure 4-3. Microchip schematic for acoustic trapping. The multilayer chip composed of glass, polydimethylsiloxane (PDMS), and poly(methyl)methacrylate (PMMA) contains 6 reservoirs and one acoustic trapping site. The "upstream" reservoirs 1, 2, and 3 contain fluorescent beads, sample, and/or wash buffer, dependent upon experimental design. The "downstream" reservoirs 4, 5, and 6 are for collection of the different sample fractions.*

## 4.3 Results and discussion

### *4.3.1 Effect of epithelial cell concentration on optimal trapping frequency*

Based on observations during prototype development and external evaluation of the ADE system, samples containing a high number of epithelial cells showed poor acoustic trapping efficiency at the predicted optimal frequency. In order to test the hypothesis that a high concentration of epithelial cells was responsible for shifting the optimal trapping frequency and causing loss of trapping, samples were prepared with yellow fluorescent beads suspended either in water, lysate from 75,000 cells, lysate from 100,000 cells, or lysate from 150,000 cells. All epithelial cells were collected from the same donor, and lysed as described in section 4.2.3. Each sample was trapped in triplicate using the same microfluidic chip, ensuring that any variance in optimal trapping frequency was due to sample composition. Each sample was exposed to six different applied frequencies, and optimal trapping frequency determined by image analysis of the

single largest aggregate of beads. The results in **Figure 4-4** show video snapshots acquired from the acoustic trapping site during each test, in which clear aggregation is observed. At the same applied frequencies, very different outcomes are observed for each sample. The data shows that the optimal trapping frequency for a solution of beads in water is 7.76 MHz, but this shifts up to 7.78 MHz for a sample containing 75,000 lysed epithelial cells. While there is still some particle

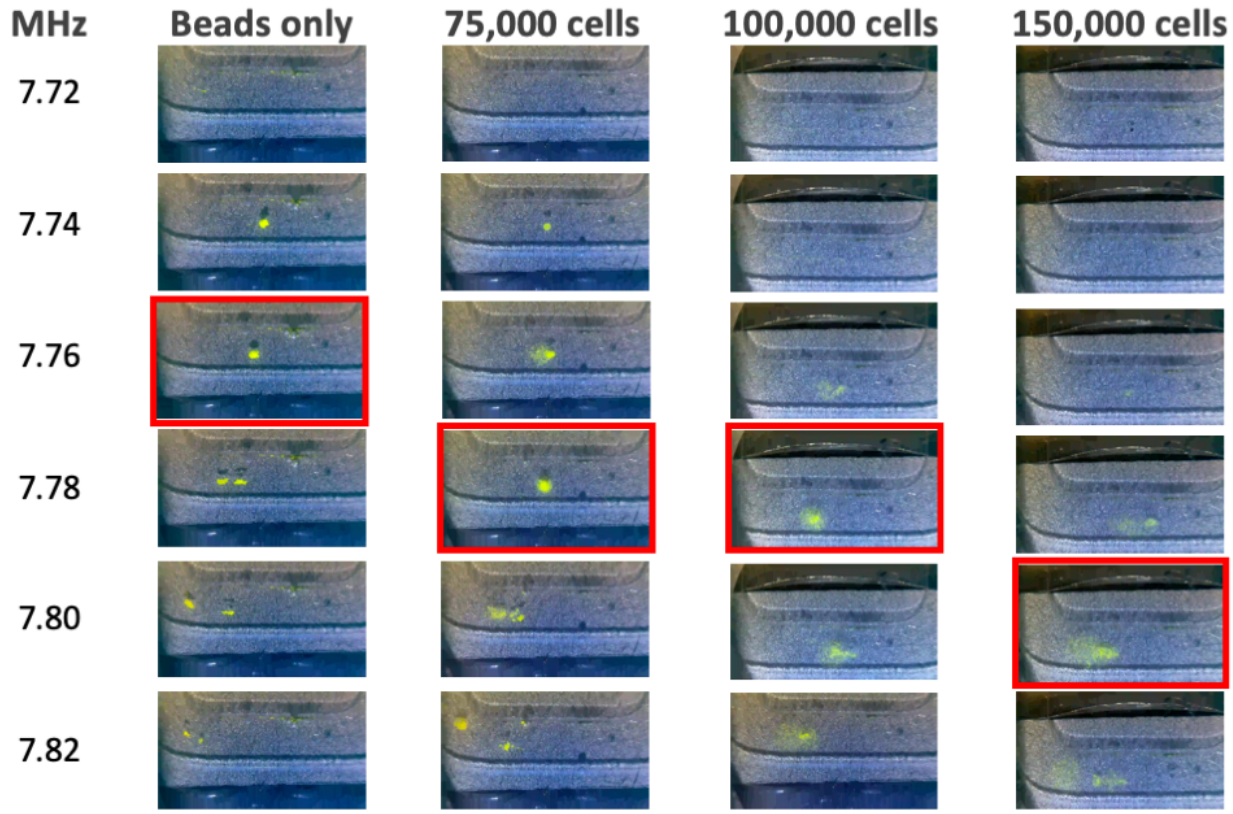


*Figure 4-4. Shift in optimal trapping frequency with increasing epithelial cell concentration. Over a range of 6 applied frequencies (y-axis) different acoustic trapping is achieved, visualized by the aggregation of yellow fluorescent beads. In samples with increasing concentration of lysed epithelial cells (x-axis) there is a clear increase in the optimal trapping frequency.*

aggregation at 7.76 MHz in the 75,000 cell sample, the cluster is smaller and visibly less dense. In the samples containing 100,000 cells and 150,000 cells, the aggregation at 7.76 MHz is further diminished, and the optimal trapping frequency shifts higher. This data clearly shows that epithelial cell concentration has an effect on the optimal trapping frequency, and that increasing the number of epithelial cells shifts the optimal frequency higher. This strengthens the hypothesis generated from observations during external evaluation at the Palm Beach County Sheriff's Office,

in that high epithelial cell samples displayed loss of trapping at a previously predicted optimal frequency. Additional experiments were conducted with samples containing a wider range of epithelial cell concentration, identifying the optimal trapping frequency via bead aggregation. The results in **Figure 4-5** plot the optimal trapping frequency (y-axis) against the number of epithelial cells in the sample (x-axis), and show two trends. With a higher concentration of epithelial cells in the sample, the average optimal trapping frequency shifted higher. Additionally, the average

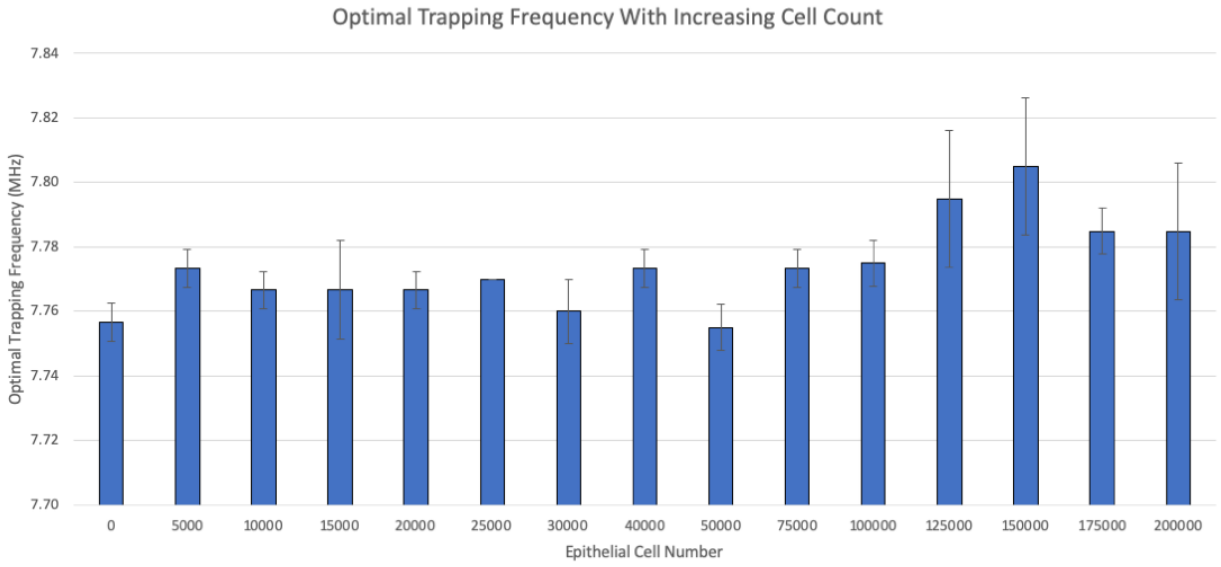


*Figure 4-5. Effect of epithelial cell concentration on optimal trapping frequency. Samples with more epithelial cells display a higher average optimal trapping frequency, and also exhibit larger variance in optimal trapping frequency. Error bars represent ± 1 standard deviation, n = 3 for each data point. The sample with 25,000 cells trapped at the same frequency in all three tests, hence, there is no error bar.*

optimal trapping frequency became more variable at higher epithelial cell concentrations. This variability only adds to the concern that some samples, with a high number of epithelial cells, may not exhibit acoustic trapping as expected based only on channel height.

These findings necessitate analysis of the acoustic trapping phenomenon, and what could impact the standing wave. The resonance condition of an acoustic oscillator is dependent on the sound velocity, frequency, and wavelength, as well as the cavity dimensions. Changes to any of these parameters will impact the resonance condition, which in turn affects the pressure amplitude of the standing wave. The relationship between amplitude and frequency has a narrow range,

where deviation from the resonant frequency will result in drastic loss of acoustic pressure amplitude. That loss manifests as weaker acoustic trapping, and failure to retain particles. Thus, changes in resonance condition due to alteration in fluid compressibility or density, must be addressed by shifting the applied frequency in order to achieve acoustic trapping.

We hypothesize that this distinct shift in optimal trapping frequency is a direct result of changes to the viscosity, density, and compressibility of the liquid. There is an empirical dependence between these properties [20, 21], and upon lysis of hundreds of thousands of epithelial cells, the release of cellular components will drastically impact liquid characteristics [1-4]. Changes in the density and compressibility of the liquid will alter the speed of sound in that medium, as shown by **Equation 1** ($v$ = speed of sound, $K$ = compressibility, $\rho$ = density). In turn, changes to the speed of sound alter the wavelength generated by an applied frequency, as seen in **Equation 2** ($c$ = speed of sound, $\lambda$ = wavelength, $f$ = frequency). Thus, shifts in fluid density or compressibility lead to loss of resonance, and necessitate a corresponding shift in applied frequency to generate a standing acoustic wave.

(1) $$v = (K\rho)^{1/2}$$

(2) $$\lambda = \frac{c}{f}$$

The results from trapping experiments with different epithelial cell samples, shown in **Figure 4-4** and **Figure 4-5**, demonstrate a clear need for an adjustment to ADE in order to handle any type of sample, and hence, our proposed real-time feedback system. This simple experiment showed that, on the same microchip and under the same conditions, acoustic trapping may fail due to unique sample characteristics that are unknown prior to attempting ADE. While our 'frequency scanning' approach can accurately account for *chip-to-chip* differences, a new method is required

to account for *sample-to-sample* differences. The initial scan of frequencies will still be implemented to provide a starting point for acoustic trapping, but when actual sample is introduced into the trap site, a real-time approach that can influence the trapping efficiency right away will be necessary. To achieve this, the previously described voltage measurement approach was implemented during ADE.

### *4.3.2 Correlation of voltage output with resonant frequency*

A proof-of-concept test was conducted to demonstrate the relationship between voltage output of the piezo, and optimal acoustic trapping frequency for a microchip. **Figure 4-6A** shows the voltage data collected while scanning through eight frequencies on an empty microchip, from

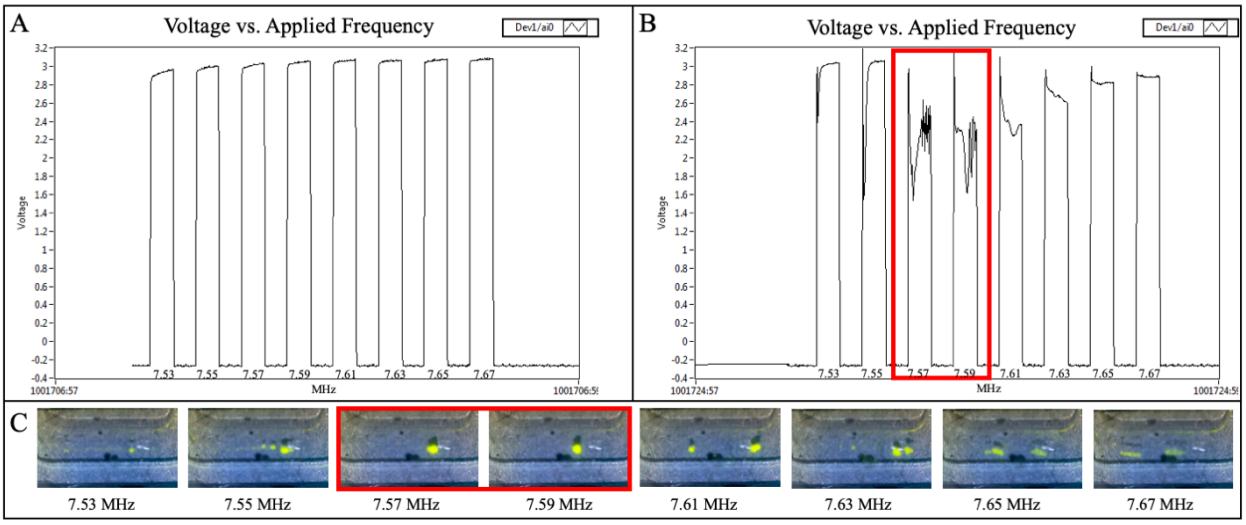


*Figure 4-6. Voltage response to acoustic trapping. (A) An empty ADE microchip was subjected to a scan of 8 applied frequencies. Real-time voltage data shows minimal changes in voltage output across all 8 frequencies. (B) Voltage data from a scan of the same chip, loaded with fluorescent beads in water. There is a minimum in output voltage at 7.57 and 7.59 MHz. (C) Video snapshots collected during frequency scan. The largest single aggregation occurs at the same applied frequencies as the minimum output voltage.*

7.53 MHz to 7.67 MHz. The frequencies were applied for four seconds, the function generator was deactivated, shifted to a higher frequency, and applied again. The voltage data (y-axis) shows almost no change in the output of the piezo, as the microchip was empty and contained no particles to be trapped or liquid to transmit sound waves. The voltage data in **Figure 4-6B** shows the same frequency scan applied when the microchip was loaded with a solution of fluorescent beads in

water. Here, a clear drop in output voltage is observed at both 7.57 MHz and 7.59 MHz, before returning to the initial voltage levels. These two average minimum outputs correspond with the optimal particle trapping observed with fluorescent beads, shown in **Figure 4-6C**. The video snapshots show equivalent trapping at 7.57 MHz and 7.59 MHz, with a single dense aggregate of beads retained under flow. These results demonstrate that monitoring voltage output of the piezo, and specifically locating the minimum in voltage output, can be used to identify optimal trapping frequency. This confirms the hypothesis that voltage output will change in response to shifts in vibration of the piezo, and that lower voltage output correlates with less resistance to vibration, i.e. the optimal trapping frequency.

This experiment was repeated with multiple different microchips and solutions, with additional results shown in **Figure 4-7**. Here the frequency scan was conducted from 7.54 MHz to 7.68 MHz, with a minimum in output voltage occurring at 7.58 MHz. **Figure 4-7B** shows that the strongest aggregation of beads also occurs at 7.58 MHz, confirming that voltage output can be used to determine optimal trapping frequency. One important aspect

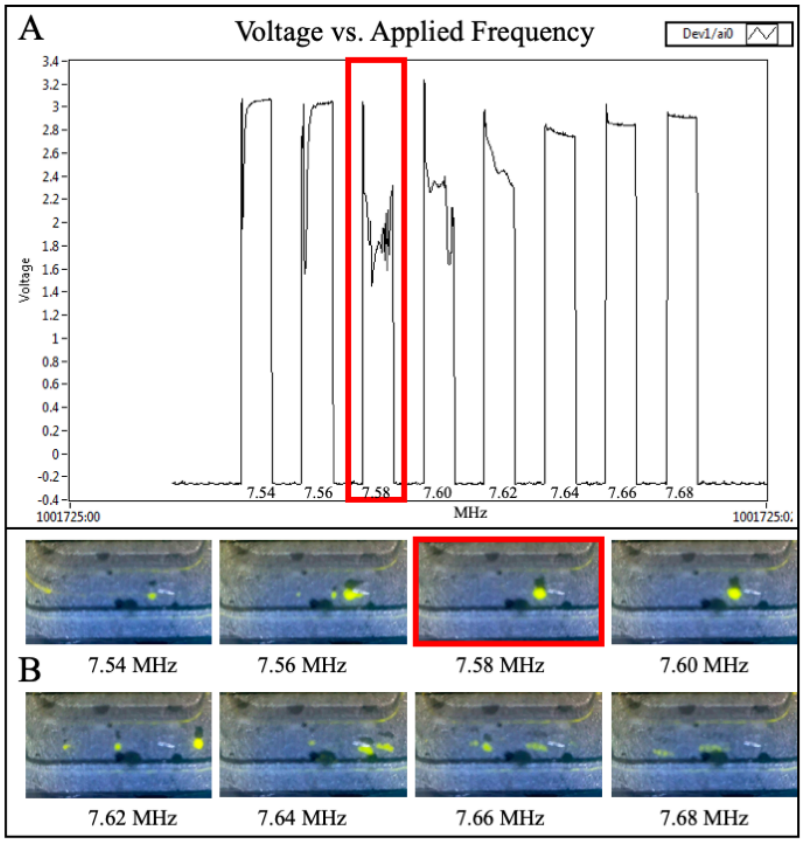


*Figure 4-7. Voltage minimum indicates optimal trapping frequency. (A) During a scan of 8 applied frequencies, output voltage data was collected. The minimum in output voltage across the piezo occurred at 7.58 MHz. (B) Video snapshots from the acoustic trapping test. The largest single aggregate of particles occurs at 7.58 MHz, corresponding with the minimum in voltage output.*

of these results is that measuring the voltage output of the piezo is faster, more objective, and easily automatable than visually determining the strongest aggregation of beads. Therefore, voltage measurements at multiple different frequencies could be preprogrammed, performed on the millisecond timescale, and repeated often throughout sample trapping in order to ensure that the optimal trapping frequency is always applied.

### *4.3.3 Evaluation of voltage measurement circuitry*

The schematic shown in **Figure 4-1** is a general layout for the peak detector circuit, but within the custom PCB built for this project, there were three unique designs included for measuring the output voltage of the piezo. Termed 'Circuit #1, Circuit #2, and Circuit #3,' minute differences were expected to impact the voltage data. Circuit #1 and Circuit #2 shared a similar topology, the classic peak detector, differing only in the orientation of a single diode. This setup captured the peak voltage of the input signal, and held it inside a capacitor until a higher input signal was received. Due to voltage drop across the diodes and some current leakage, the output of the peak detector from Circuits #1 and #2 was expected to be less than the actual value of the peak. Circuit #3 was slightly more complex, using the fast comparator approach described in section 4.2.1. This results in more accurate measurements, with error on the scale of 10 mV as opposed to 500 mV for Circuits #1 and #2.

In order to benchmark the performance of each peak detector circuit, all three were tested by acoustically trapping fluorescent beads in water, across a range of applied frequencies. For Circuit #1, the output voltage data and video snapshots of trapping are shown in **Figure 4-8**. As expected, the minimum output voltage at 7.54 MHz matched the strongest visual trapping of beads. The baseline voltage was approximately -0.5 V, and each new frequency caused an initial spike in voltage, followed by stabilization. This can be compared to Circuit #2, data shown in **Figure 4-9**.

Here the minimum voltage output at 7.65 MHz also corresponds to strong aggregation of beads, and the initial spike in voltage output at each new frequency is also observed. The baseline signal is approximately 0 V, and maximum voltage output is slightly lower than that measured with Circuit #1. The same test was conducted with Circuit #3, the resulting data are shown in **Figure 4-10**. Again the minimum voltage output identified the same optimal trapping frequency as visual monitoring of beads, occurring at 7.59 MHz. The baseline signal for this circuit was approximately 0.1 V, and the initial spike in output voltage was still observed.

Importantly, all three circuit designs showed the same trend from the voltage measurements: a minimum output in voltage from the piezo correlated with the optimal trapping frequency. Directly comparing the data from each of the three circuit designs showed a difference in baseline signal, and potential differences in maximum output voltage (approximately 3.4 V for Circuit #3, approximately 3.2 V for Circuits #1 and #2). The difference in measurement error did not appear to

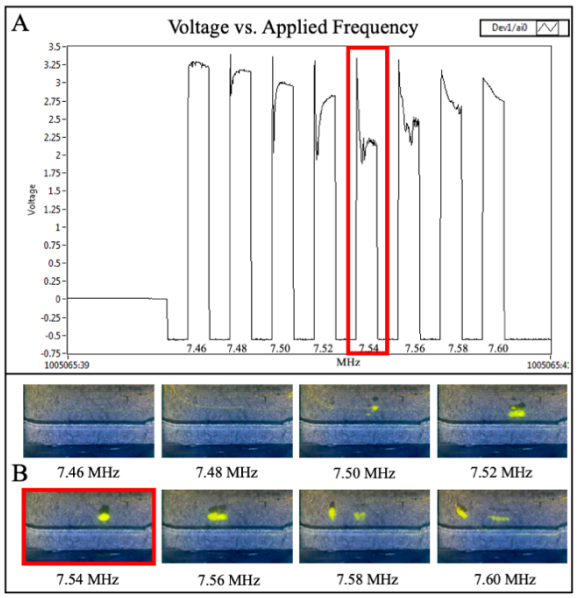


*Figure 4-8. Voltage data from Circuit #1. (A) Voltage data collected from Circuit #1 during a frequency scan. A minimum in output voltage occurred at 7.54 MHz. (B) Video snapshots from the trapping run. The largest single aggregate of particles is seen at 7.54 MHz, matching the frequency identified by output voltage measurements.*

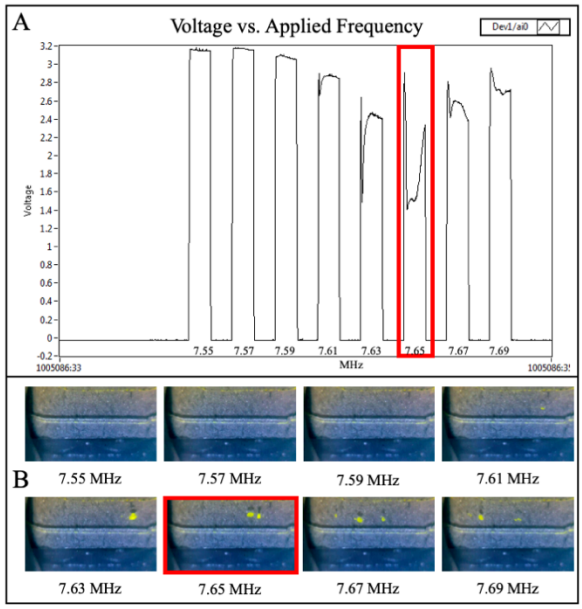


*Figure 4-9. Voltage data from Circuit #2. (A) Voltage data collected from Circuit #2 during a frequency scan. A minimum in output voltage occurred at 7.65 MHz. (B) Video snapshots from the trapping run. The largest single aggregate of particles is seen at 7.65 MHz, matching the frequency identified by output voltage measurements.*

impact the data collection. However, it is important to note that this data was collected from multiple, subsequent tests, and thus any difference in the spectra cannot be solely attributed to the circuit features. For future testing, data acquisition was adjusted to collect data from all three circuits simultaneously.

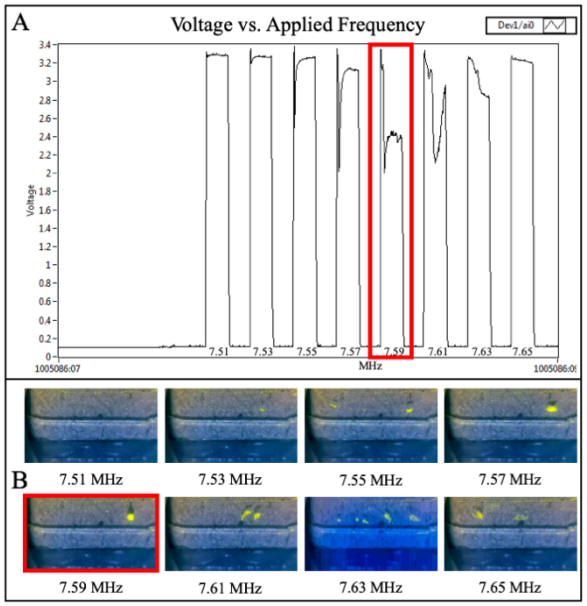


*Figure 4-10. Voltage data from circuit #3. (A) Voltage data collected from circuit #3 during a frequency scan. A minimum in output voltage occurred at 7.59 MHz. (B) Video snapshots from the trapping run. The largest single aggregate of particles is seen at 7.59 MHz, matching the frequency identified by output voltage measurements.*

*4.3.4 Circuit comparison with a continuous scan*

Subsequent testing continued the comparison of Circuits #1, #2, and #3, but also introduced a continuous frequency scan. All previous testing had operated by applying the desired frequency for 4 seconds, deactivating the function generator, shifting to a higher frequency, then reactivating the function generator for another 4 seconds. This on/off stepwise fashion was effective for determining optimal trapping frequency, but would not be suitable for real-time feedback when trapping an actual sample. Deactivating the function generator results in loss of the standing acoustic wave, meaning that during the transition between frequencies, there is no acoustic trapping. If an authentic sample were present, that gap would result in sperm cells lost to the waste reservoir. Instead, a continuous scan is needed, wherein the function generator remains activated, and the frequency is stepped higher without any interruption. As implemented in our manual feedback system, this requires the operator to rapidly delete and enter each frequency value. A comparison of the two methods is shown in **Figure 4-11**. For this data, the black, green, and red traces represent Circuit #1, #2, and #3 respectively. The on/off scan, **4-11A**, results in

voltage minimums at 7.55 and 7.56 MHz, matching the strongest observed trapping (**4-11C**). The voltage data for Circuits #1 and #2 is virtually identical, while Circuit #3 is offset slightly, but

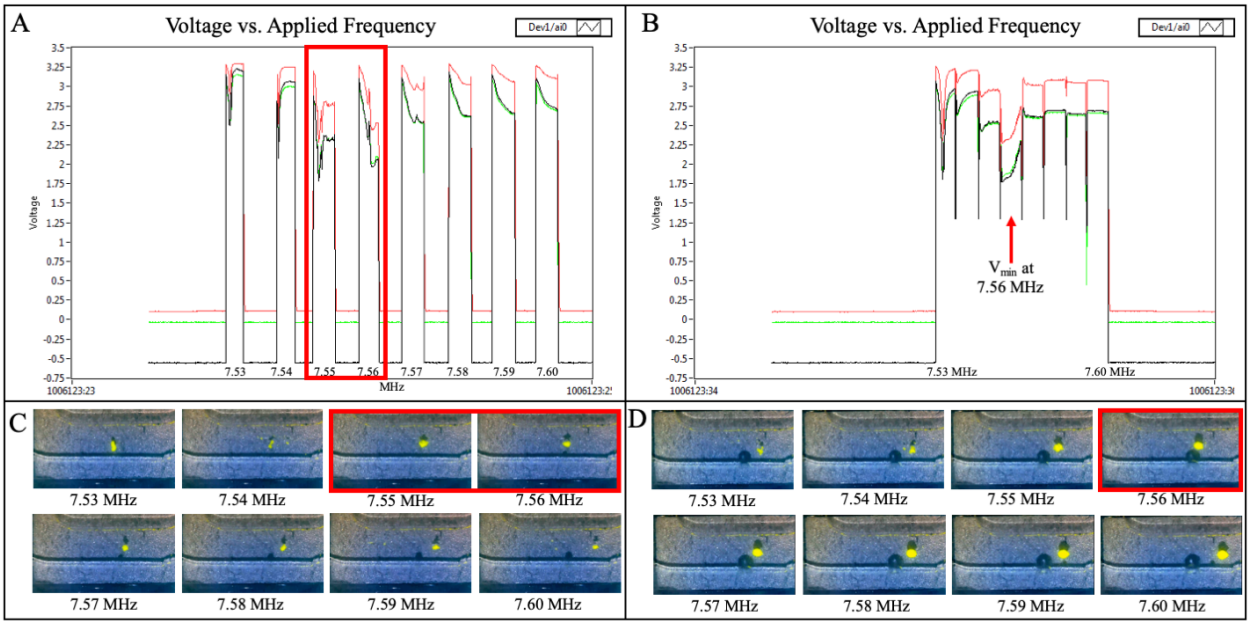


*Figure 4-11. Continuous scan with manual frequency control. The black, green, and red traces represent Circuits #1, #2, and #3, respectively. (A) Voltage data collected during a manual frequency scan. Each frequency was applied for 4 seconds before turning off the function generator, shifting the frequency up by 0.01 MHz, and activating the function generator again. (B) Manual scan conducted by keeping the function generator active throughout, and adjusting the applied frequency every 4 seconds. In both cases, the scan covered 7.53 MHz to 7.60 MHz, and a minimum in output voltage occurred at 7.55 or 7.56 MHz. (C) Video snapshots from fluorescent bead trapping. For both scans, the minimum voltage output corresponds with strong particle aggregation.*

shows the same trend. **Figure 4-11B** shows the voltage data collected during a continuous scan, with the associated video snapshots in **4-11D**. Here a clear minimum in output voltage is identified at 7.56 MHz, which matches the strong trapping observed from the bead aggregation. It can be observed that unlike previous scanning experiments, the aggregate of beads does not drastically diminish in size after the optimal trapping frequency has been reached (i.e. at 7.59 and 7.60 MHz). We hypothesize that this is due to the constant influx of more fluorescent beads, without any pause in the applied frequency. This results in an increasing concentration of beads in the trap site, and the previously trapped aggregate cannot dissipate and flow out of the trap site before the next frequency is applied. This is exactly the desired effect when trapping sexual assault samples, in order to minimize loss of sperm cells. Importantly, however, monitoring the output voltage still

indicates the true optimal trapping frequency, regardless of particle concentration. Furthermore, the continuous scan required half the time of the on/off scan, and by reducing the time each frequency is applied, an entire scan could be conducted in less than two seconds.

The results of this experiment showed that a continuous scan is a viable approach, even with manual entry of each applied frequency. The continuous scan was faster than an on/off scan, resulted in more particles being retained in the trap site, and identified the same optimal trapping frequency as the on/off approach. Moving forward, only a continuous scan was used for testing. Additional analysis of the data showed that the voltage measurements from Circuits #1 and #2 are in fact identical, varying only in their baseline signal amplitude. Circuit #3 values were offset approximately 0.5 V higher, and showed slightly more gradual changes.

*4.3.5 Manual real-time feedback to mock sexual assault samples*

After clearly demonstrating that identifying a minimum in output voltage from the piezo can be used the determine the optimal trapping frequency, mock sexual assault samples were prepared to apply this technique to a relevant sample matrix. One of these samples contained 290,000 total cells, with a ratio of 5:1 female epithelial cells:male sperm cells. The sample underwent a standard differential lysis procedure, as described in Chapter 2 section 2.3.5. The resulting lysate was processed with the manual feedback ADE approach. A rapid scan of eight frequencies was conducted from 7.54 MHz to 7.61 MHz, with 0.01 MHz increments, in order to identify the optimal trapping frequency for this specific microchip. The resulting voltage data is shown in **Figure 4-12Ai**, where a clear minimum in output voltage can be identified at 7.59 MHz. With this starting point of 7.59 MHz, the mock sample was flowed through the trapping site with the piezo activated. The applied frequency was manually increased in 0.01 MHz increments, while the operator monitored the voltage output in real-time. The voltage data is shown in **Figure 4-**

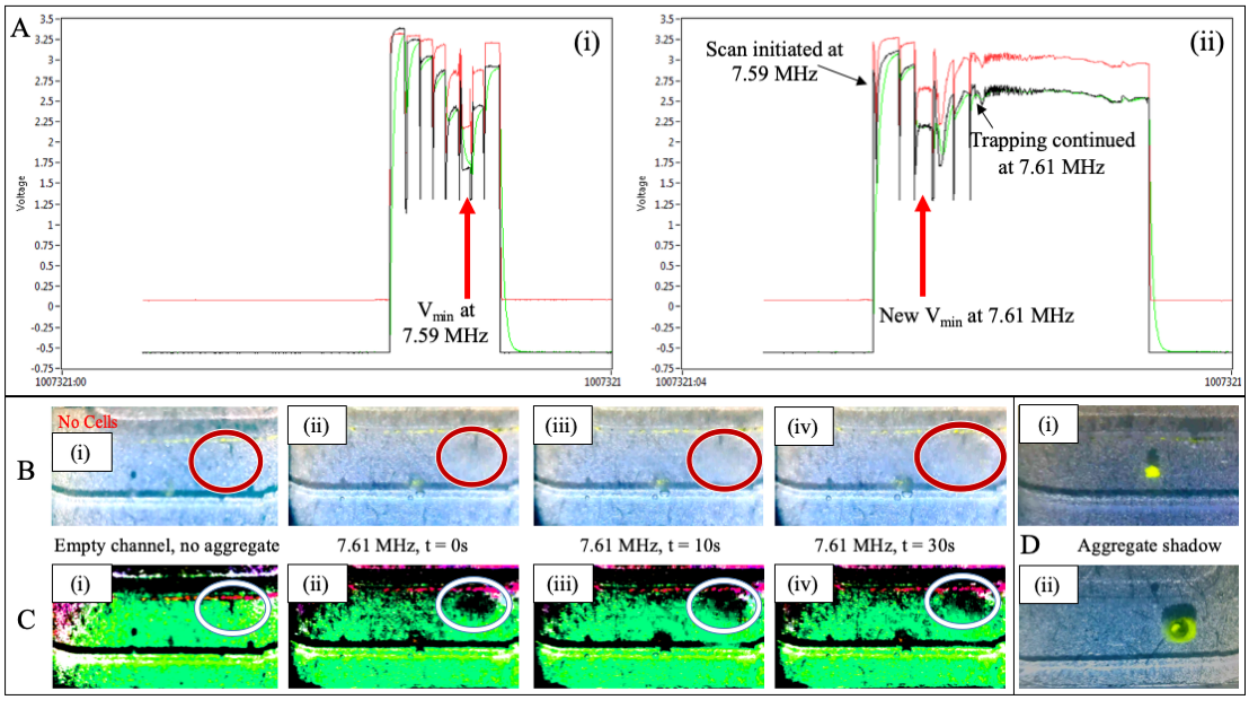


*Figure 4-12. Real-time feedback during mock sample trapping. (Ai) Trapping fluorescent beads in water across 8 frequencies shows a clear voltage minimum at 7.59 MHz. (Aii) While trapping the mock sexual assault sample, the applied frequency is adjusted by 0.01 MHz each step. A local minimum in average voltage is observed at 7.61 MHz, so that frequency is applied for the remainder of the trapping. (Bi-iv) Visual monitoring of the trap site over 30 seconds. At the conclusion of the trapping event, a large aggregate of sperm cells has been captured. (Ci-iv) Color adjusted images from trapping site. Image processing allows for the sperm aggregate to be clearly identified. (D) Images of beads (i) and beads with sperm cells (ii) being trapped. The shadow above and behind the aggregate is clearly visible due to the angle of lighting above the microchip.*

**12Aii**, and during sample trapping a minimum in output voltage was observed at 7.61 MHz, a shift up by 0.02 MHz compared to the frequency scan of beads in water. After two subsequent frequency steps to ensure the minimum had occurred, the frequency was set and held at 7.61 MHz for the remainder of sample trapping. Video snapshots from the sample trapping (**Figure 4-12B**) show that an aggregate of trapped sperm cells grows in size over the 30 second trapping event. In these brightfield images, the region highlighted by the red ellipse in **Bi** shows no cells, while the blurred area encompassed in the red ellipse (**Bii-iv**) is the growing aggregate of cells. While a trained eye can easily discern the cell clumps in Panel B, the aggregation may not be apparent to an untrained observer. The images were also processed with a color adjustment (**Figure 4-12C**) to help visualize the trapped cells. This color adjustment was performed in ImageJ software, utilizing the L*a*b* color space and the 'Color Inspector' plugin, which boosted color contrast by

14X and rotated color -90°. This manipulation of the image provides more intuitive visualization of the shadow associated with the cell aggregate, which grows over time as more cells are acoustically trapped. The shadows can be easily seen in **Cii-iv**, and are highlighted by the white ellipses. To further illustrate this point, **Figure 4-12D** shows brightfield images of beads (**Di**) and beads with sperm cells (**Dii**) during ADE. The shadow on the bottom of the channel is clearly visible behind the aggregates; the color adjustment of images from mock sample trapping allows this to be more easily recognized.

This experiment confirmed that, not only is an initial frequency scan necessary to determine the optimal frequency *for each specific chip*, but also the optimal trapping frequency may change, during a run, dependent on *each specific sample*. Most importantly, it shows that any shift in optimal trapping frequency can be accounted for, in real-time, solely by monitoring the output voltage from the piezo. This kept the piezo at its optimal resonant frequency, resulting in a large aggregate of captured sperm cells. The described feedback method is still 'manual,' requiring user analysis and input during the test. However, this capability now means that samples with excessive amounts of epithelial cells can be processed, maintaining acoustic trapping even under extreme circumstances.

### *4.3.6 Effect of viscosity on optimal trapping frequency*

The core problem with ADE's inability to deal with a broad range of sexual assault samples was the change in viscosity due to cellular lysis. While this specific phenomenon was identified in the context of forensic DNA identification, acoustic trapping of particles is relevant in many other fields. In order to make these findings more applicable for the general microfluidic community, an experiment was conducted using glycerol solutions spiked with fluorescent beads. An ADE microchip was loaded with fluorescent beads in water (reservoir 1), fluorescent beads in

5% glycerol (reservoir 2), and fluorescent beads in 10% glycerol (reservoir 3). A frequency scan from 7.52 MHz to 7.76 MHz, 0.02 MHz increments, was conducted while flowing each solution through the acoustic trap site, with voltage data collected in real-time. The frequency scan with

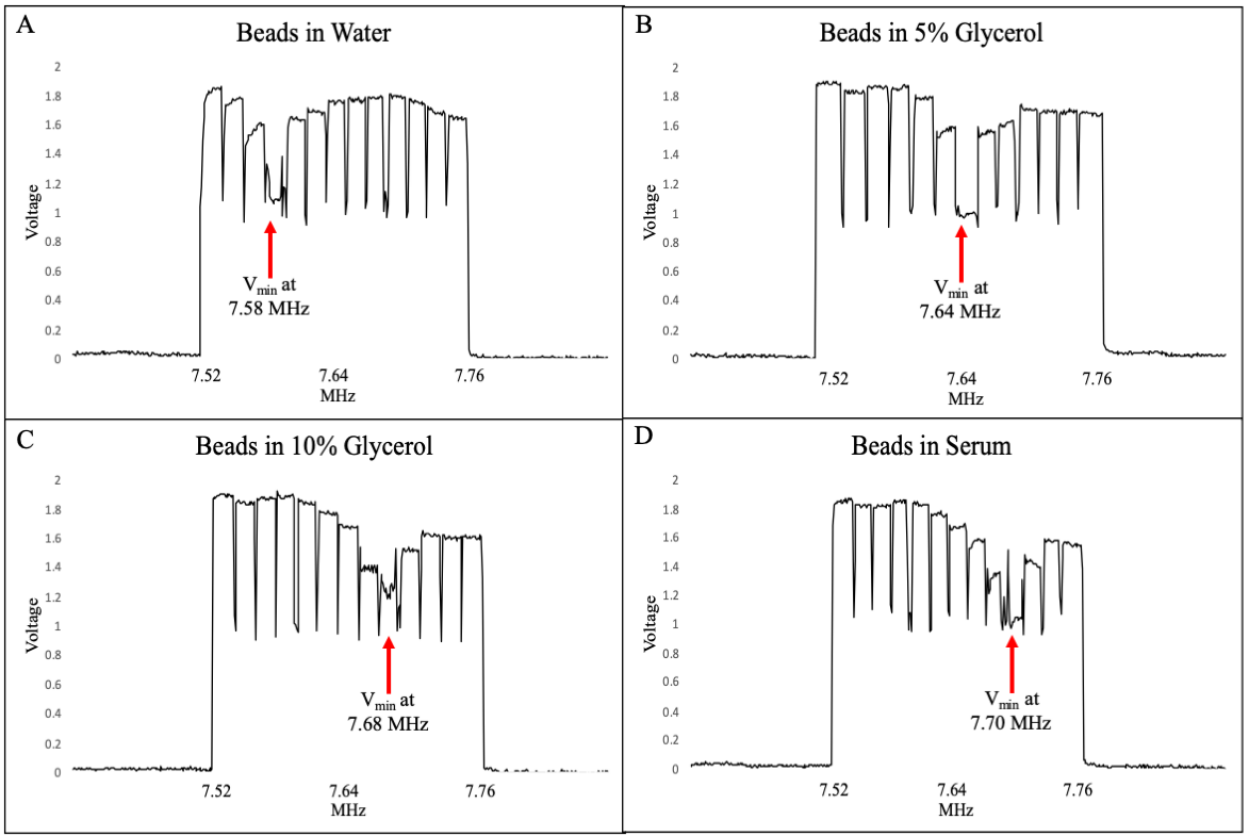


*Figure 4-13. Shift in voltage minimum with changing viscosity. (A) Frequency sweep of fluorescent beads in water. A clear minimum in output voltage is observed at 7.58 MHz, corroborated by visual aggregation of beads. (B) When flow is switched to a solution of 5% glycerol, the optimal trapping frequency shifts up to 7.64 MHz. The new minimum output voltage matches the shift in observed particle trapping. (C) When trapping beads in 10% glycerol solution, the minimum output voltage shifts up to 7.68 MHz. (D) The solution of human serum spiked with fluorescent beads displayed a minimum output voltage at 7.70 MHz.*

fluorescent beads in water showed a clear minimum output voltage at 7.58 MHz (**Figure 4-13A**), indicating the optimal trapping frequency. The subsequent frequency scan was conducted with the 5% glycerol solution, and the minimum output voltage shifted to 7.64 MHz (**Figure 4-13B**). Similarly, when that fluid is replaced by a 10% glycerol solution, the minimum output voltage increased again, to 7.68 MHz (**Figure 4-13C**). This straightforward test demonstrates how the optimal trapping frequency is influenced by viscosity, which will impact acoustic trapping efficiency.

For our applications, any increase in viscosity is due to release of cellular components from lysed epithelial cells. Other, similarly complex sample matrices are prevalent in microfluidic acoustic trapping applications [22, 23], and thus, it was important to establish that this effect is observed in other biofluids. Human serum was selected as a sample matrix because it has modest viscosity (1.4 cP), and is laden with protein (~70 mg/mL). As with glycerol solutions, 100 μL of human serum was spiked with fluorescent beads, and flowed through the ADE chip during a frequency scan, with constant measurement of piezo voltage. **Figure 4-13D** shows the output voltage during the frequency scan, where a clear minimum can be identified at 7.70 MHz. This indicates that human serum is more similar to a 10% glycerol solution (optimal frequency 7.68 MHz), than to water (optimal frequency 7.58 MHz), with regard to liquid properties for acoustic trapping. The dynamic viscosity for serum (1.4 cP) is most similar to 10% glycerol (1.3 cP), as opposed to 5% glycerol (1.1 cP) or water (0.9 cP), and the shift in optimal trapping frequency reflects those relative values. It noteworthy that a sample of serum diluted 5X in water was tested, resulting in an optimal trapping frequency of 7.60 MHz. This is indicative of the reduced viscosity, causing the fluid to behave more like water and experience acoustic trapping at a similar frequency. This serum experiment also supports the hypothesis that viscosity is the driving force behind the observed shift in optimal trapping frequency, that is to say, there is not an additional factor unique to cell lysate or serum that shifts the optimal frequency independent of viscosity.

### *4.3.7 Current measurements for optimal frequency determination*

The previous results have clearly shown that real-time, electronic measurements of an acoustic trapping system can be used to identify the optimal trapping frequency on a sample-to-sample basis. However, they are not limited to measuring the output voltage from the piezoelectric transducer. A new custom PCB was designed, which measured the DC current from the function

generator entering the amplifier. The theory behind this design was that in the electrical circuit, there is some variable resistance due to changes in vibration of the piezo at different applied frequencies. That variable resistance should result in different amounts of current drawn through the circuit, which can be easily measured. The main benefit to this approach is that an external peak detector circuit is not necessary, as the output voltage from the piezo would not need to be monitored. An additional feature of this new PCB was the ability to program frequency scans for duration, step size, and range, allowing for much faster and more precise frequency changes as compared to the manual feedback approach.

A demonstration of this principle is shown in **Figure 4-14**, as beads in water were acoustically trapped during a frequency scan from 7.50 MHz to 7.60 MHz. In each plot, the green trace indicates a change in applied frequency (shifting up 0.01 MHz), the red trace is the output voltage from the piezo, and the black trace is the measured current into the amplifier. The plot in **Figure 4-14A** was generated from a scan with a four second hold at each frequency. Both a minimum in output voltage (red) and a maximum in input current (black) were observed at the penultimate frequency, 7.59 MHz, indicating the optimal trapping frequency. This showed that

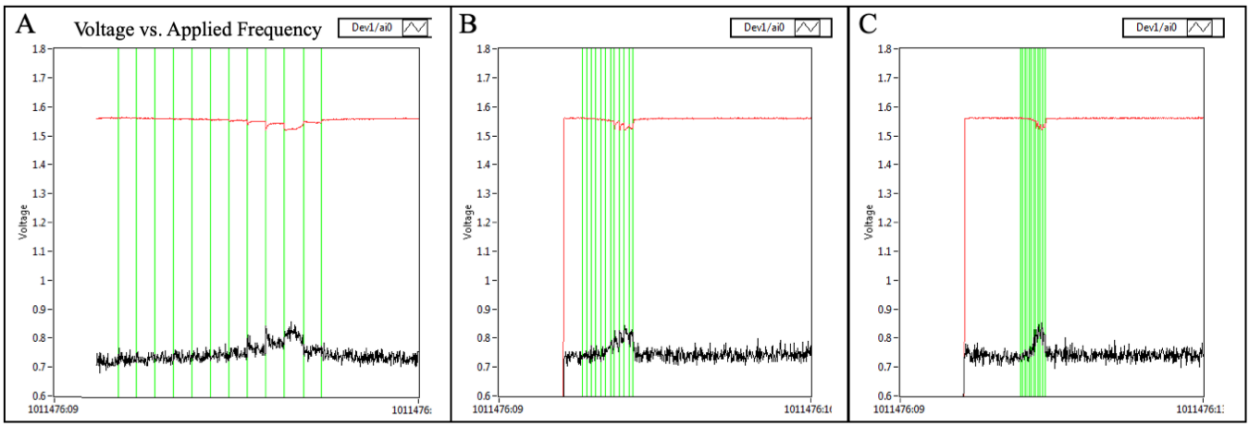


*Figure 4-14. Current and voltage measurements during automated scan. (A) A frequency scan was conducted from 7.50 MHz to 7.60 MHz, shifting up 0.01 MHz every 4 seconds. The green trace indicates a change in applied frequency, while the red trace is the voltage output from the piezo, and the black trace is the current into the amplifier. The minimum output voltage corresponds with the maximum input current, indicating that current measurements can also be used to identify the optimal trapping frequency. (B) The same scan was conducted with a 1 second scan time, and the same trend is observed. (C) A 500 ms scan time generates the same results, a maximum input current corresponding with minimum output voltage.*

monitoring the input current will generate the same results as measuring the output voltage from the piezo, but require less complex hardware. **Figure 4-14B and C** were generated from frequency scans at 1.0 and 0.5 second frequency steps, respectively, moving closer to the timescale desired for implementation during automated feedback for ADE. In both of those scans, the same trend was observed, with a minimum output voltage and maximum input current occurring at 7.59 MHz, identifying the optimal trapping frequency.

This more automated, DC measurement approach was also tested using with epithelial cell lysate samples. An ADE microchip was loaded with a solution of beads in water, as well as a mock sample containing lysate from 160,000 epithelial cells, and subjected to acoustic trapping. With the ability to preprogram rapid frequency scans, two back-to-back scans covering 7.52 MHz to 7.64 MHz were conducted with each solution. The data for a solution of beads in water, **Figure 4-15**, plotted the input current at each applied frequency. The black trace is raw data, and the red trace has been smoothed with a moving average. In both scans, the maximum current was identified at 7.58 MHz, indicating the optimal trapping frequency. When the mock sample of epithelial cell lysate was flowed through the trap site, the frequency scan results indicated a new optimal trapping frequency at 7.61 MHz (**Figure 4-16**). Again, both frequency scans showed the same

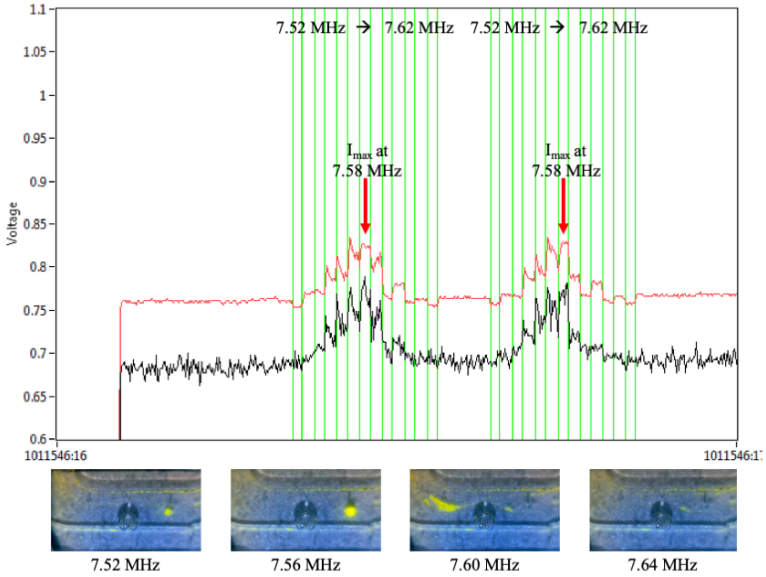


*Figure 4-15. Input current data during frequency scan. A frequency scan from 7.52 MHz to 7.64 MHz, 0.01 MHz increments, was conducted with fluorescent beads in water. Based on maximum in input current signal, the optimal trapping frequency occurs at approximately 7.58 MHz in both tests. Note: the y-axis unit is volts, and is equal to 5 X the current in amperes. The black trace is the raw current data, while the red trace has been smoothed. They are offset for visibility.*

maximum input current, demonstrating that this method is sufficient for rapidly identifying the optimal trapping frequency during a run. These results indicate that DC current, measured independently of the piezo, can quickly and accurately identify shifts in the optimal trapping frequency due to changes in liquid properties.

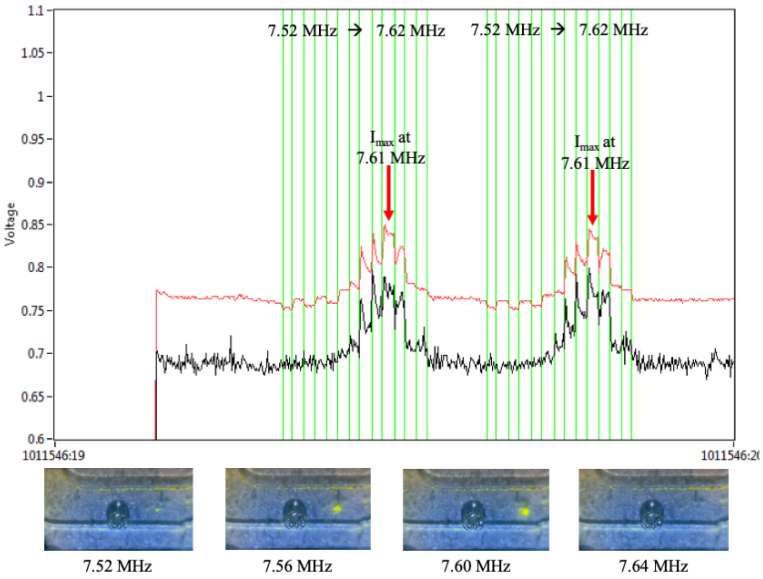


*Figure 4-16. Frequency scan with epithelial cell lysate. Fluorescent beads in epithelial cell mock sample were trapped during a frequency scan from 7.52 MHz to 7.64 MHz, 0.01 MHz increments. The maximum input current with an epithelial cell lysate solution is shifted up by 0.03 MHz as compared to trapping in water.*

## 4.4 Summary

In solutions with an increasing number of lysed epithelial cells, a corresponding shift to a higher resonant acoustic frequency was observed. When more than 100,000 epithelial cells were present in solution, the resulting lysate displayed a higher average optimal trapping frequency than a solution of water, also with higher variability. The observed frequency shift can be attributed to changes in viscosity, density, and compressibility of the liquid, which alters the speed of sound through the medium. Consequently, the wavelength generated by an applied frequency will be shifted: a denser fluid possess a higher speed of sound, which results in a longer wavelength from the same frequency of sound as compared to water. The connection between sample cell concentration and shifting resonant conditions was a breakthrough that helped launch the next stage of ADE research. The described phenomenon, combined with observations made during evaluation of the ADE technology with non-probative sexual assault samples, led to the conclusion

that sample-to-sample variability caused acoustic trapping failure with some non-probative samples tested at forensic laboratories. Those specific sample-to-sample differences cannot be accurately predicted prior to ADE, and they directly impact the necessary frequency to achieve resonance.

A distinct relationship was shown between the output voltage of a piezoelectric transducer, and the optimal frequency for a resonant acoustic wave. Through straightforward experiments that combined visual aggregation monitoring and real-time voltage measurements, the minimum output voltage was shown to reproducibly correlate with the optimal trapping frequency. Furthermore, it was demonstrated that when the resonant frequency is affected by solution viscosity, monitoring the output voltage from the piezo is sufficient for detecting this change and identifying the new optimal trapping frequency. This principle has not been described elsewhere in the literature, as no groups have reported directly on the effect of viscosity on resonant trapping frequency. This real-time feedback system allowed for multiple, rapid scans of different frequencies during ADE. Determining the shift in optimal frequency during a run allowed for a new frequency to be selected during the sample trapping stage, resulting in successful sperm cell capture. Finally, it was demonstrated that measuring the DC current entering amplifier, as opposed to voltage out of the piezo, is equally viable for identifying the optimal trapping frequency. Due to the greater simplicity in measuring DC, and less invasive hardware modifications, this approach will be explored for future prototypes.

The future directions of this research will seek to combine the established ADE protocol with real-time feedback, providing the bandwidth to process any sexual assault sample. The immediate steps that must be taken are to automate the optimal frequency identification, either through voltage or current measurements, and program a feedback loop that will update the applied

frequency independent of any operator. In theory, this approach will first conduct a scan of multiple frequencies, and select the frequency that generated a voltage minimum or current maximum. From that point, the applied frequency will be shifted up or down by 0.01 MHz, the new voltage or current value compared to the previous data point, and dependent on an increase or decrease in signal, the frequency will either remain the same, or be adjusted to the new optimal trapping frequency. This will occur in approximately 100 ms, and be repeated throughout the trapping process, in order to account for any changes in sample viscosity due to temperature, or other factors, during ADE. The described approach for maintaining the optimal trapping frequency is essentially 'cruise control' for ADE. The data and findings from this chapter will allow for accurate, rapid frequency identification to occur in real-time, and when implemented into an ADE prototype, lead to faster processing of all sexual assault samples.

## 4.5 Acknowledgements

I would like to thank Vahid Farmehini and Dr. Nathan Swami for their contributions to this research. Without their expertise in design and fabrication of the necessary electronics, this work would not have been possible.

## 4.6 References

1. J. Newton, D. Schofield, J. Vlahopoulou, Y. Zhao, *American Institute of Chemical Engineers Journal*, 2016, 1069-76.
2. G. Dhillon, S. Brar, S. Kaur, M. Verma, *Food and Bioprocess Technology*, 2013, **6**, 1240-50.
3. C. Perley, J. Swartz, C. Cooney, *Biotechnology and Bioengineering*, 1979, **21**, 519-23.

4. B. Shimmons, W. Svrcek, J. Zajic, *Biotechnology and Bioengineering*, 1976, **18**, 1793-1805.
5. T. Laurell, F. Petersson, A. Nilsson, *Chemical Society Review*, 2006, **36**, 492-506.
6. H. Bruus, *Lecture notes for the advanced CISM school, Technical University of Denmark*, 2010.
7. A. Doinikov, *Recent Research Developments in Acoustics,* 2003, **1**, 39-67.
8. W. Konig, *Annals of Physics*, 1891, **42**, 353.
9. S. Woodside, B. Bowen, J. Piret, *American Institute of Chemical Engineers Journal*, 1997, **43**, 1727-36.
10. P. Dayton, K. Morgan, A. Klibanov, G. Brandenburger, K. Nightingale, K. Ferrara, *IEEE Transactions on Ultrasonics, Ferroelectrics, and Frequency Control*, 1997, **44**, 1264-77.
11. S. Sepehrirahnama, F. Chau, K. Lim, *Physical Review*, 2016, **93**, 023307.
12. Palm Beach County Sheriff's Office, *FB Semen and Epithelial Cell Microscopy*, 2018, 1-3.
13. B. Hammarström, M. Evander, J. Wahlstrom, J. Nilsson, *Lab on a Chip*, 2014, **14**, 1005-13.
14. J Dual, P. Hahn, I. Leibacher, D. Moller, T. Schwarz, *Lab on a Chip*, 2012, **12**, 852-62.
15. J. Hawkes, W. Coakley, *Enzyme and Microbial Technology*, 1996, **19**, 57-62.
16. K. Uchino, *Ultrasonic Transducers*, 2012, 70-116.
17. R. Millikan, M Grover, *Automotive Ignition Systems*, 1917, 54.
18. K. Aroom, M. Harting, C. Cox, R. Radharkrishnan, C. Smith, B. Gill, *Journal of Surgical Research*, 2009, **153**, 23-30.
19. J. McLucas, *EDN Design Ideas*, 2007, 74-76.

20. Y. Atanov, A. Berdenikov, *Plenum Publishing Corporation*, 1983, 878-79.

21. G. Elert, *The Physics Hypertextbook*, 1998.

22. C.M. Cousins, P. Holownia, J.J. Hawkes, M.S. Limaye, C.P. Price, P.J. Keay, and W.T. Coakley, *Ultrasound in Medicine and Biology*, 2000, **25**, 881-888.

23. P. Li, Z. Mao, Z. Peng, L. Zhou, Y. Chen, P. Huang, C. Truica, J. Drabick, W. El-Deiry, M. Dao, S. Suresh, T. Huang, *PNAS*, 2015, **112**, 4970-5.

# Chapter 5: Microchip separations of explosive compounds on native polymeric substrate

## 5.1 Introduction

### *5.1.1 Detection of military-grade explosives*

Military installations, munitions manufacturing sites, and other government facilities are at high risk for inadvertent contamination of soil and groundwater with toxic explosive compounds [1]. These sites can leach nitrated explosives into the surrounding environment, requiring regular monitoring for human health, as well as plant and animal life [2, 3]. The often remote, inconvenient location of these installations, as well as the labor-intensive protocols required for sample testing, pose significant challenges to this task. The only Environmental Protection Agency (EPA) approved method for detecting explosive compounds in soil and groundwater is not field-portable [4], and few commercial alternatives exist to meet this need. This chapter describes a new project that seeks to provide rapid, on-site detection of multiple explosive compounds for environmental and forensic applications.

One of the most common classes of military explosives are organic, nitro-containing compounds. These molecules are typically neutral, contain one or more nitro groups, and have been used extensively throughout history [5]. The majority of these compounds were implemented as explosives, propellants, or chemical intermediates during munitions manufacturing. Though many are no longer used by the U.S. military, stockpiles of these explosives and their degradation products remain throughout the country, and pose a risk to human health and environmental safety. The current gold standard for detecting these compounds uses high performance liquid chromatography (HPLC), but micellar electrokinetic chromatography (MEKC) is an attractive

alternative for several reasons. Like HPLC, MEKC can rapidly separate neutral compounds, yet does not require a packed column or external pressure source. MEKC has also been implemented as a portable microchip technology [6], which remains a major hurdle for HPLC. Several research groups have investigated the separation of explosive compounds through MEKC, with promising results. Bailey et al. [7] and Kennedy et al. [8] applied MEKC to detect a panel of 14 explosive compounds. These approaches used indirect laser-induced fluorescence (ILIF), the same detection scheme employed herein, to resolve all 14 explosives in less than 15 minutes. While their separations were performed on a commercial benchtop capillary electrophoresis instrument, the aim of this research is to adapt the rapid MEKC approach to a microfluidic platform that is amenable for portability.

### *5.1.2 Cyclic olefin copolymer for microchip separations*

In order to scale this technology to the micro realm, we performed electrophoresis on a thermoplastic polymer microdevice. Glass microchips are typically preferred for electrophoresis based on their optical transparency and chemical stability, but their fragility, high cost, and difficult fabrication are detrimental for on-site analyses [9]. One research group has demonstrated separation of several explosive compounds on a glass microchip [10], but neither the hardware nor microchip were portable or rugged enough for practical use. In contrast, cyclic olefin copolymer (COC) microchips were employed for the research presented herein. This polymer substrate was chosen for its similar optical properties to glass, but with an increased resistance to scratching or breaking, making COC a durable, low-cost alternative. One drawback of COC, however, is its lack of formal surface charge. For this reason, most research groups who perform electrokinetic driven separations on COC implement a surface treatment, which provides charge and adds functionalization to the channel walls, promoting a larger zeta potential [11,12]. Zeta potential

describes the electric potential between the bulk solution and the channel wall, and is an important representation of ion distribution in the dispersed medium. Application of surface treatments to thermoplastic microdevices is one approach for fabricating devices with a higher zeta potential, and ultimately, a stronger electric double layer. However, such surface modifications are seldom straightforward, and can result in single-use-only microchips [13]. For our purposes, a native COC device was selected, as it could be purchased commercially, stored indefinitely with no surface modifications, and resist deformation or breaking during portable use. Despite its lack of functionalized groups, literature has suggested that adsorption of anions to neutral surfaces can impart charge to materials that would otherwise lack the requirements for performing electrokinetic separations [14, 15]. For this reason, COC was considered a suitable potential substrate.

This chapter describes free-solution, electrokinetic driven separations on a native COC device, identifying explosive compounds for environmental and forensic samples. Previous research in this area has relied on microdevices using either glass substrates, surface modifications, or benchtop instruments to achieve explosive compound detection in a timely manner. Our goal was to demonstrate a path toward on-site explosives detection, using a low-cost, durable, native thermoplastic-based microfluidic platform.

## 5.2 Materials and methods

### *5.2.1 Selection of explosive compounds*

With advice from collaborators at the Naval Research Laboratories, eleven explosive compounds were selected for testing. These compounds were chosen for their relevance in environmental and forensic science, their inclusion in the EPA method, as well as their amenability to separation via MEKC. **Table 5-1** lists the explosives chosen, as well as their toxic effects in

| Compound | Toxic effects | Main exposure source |
|---|---|---|
| TNT | Anemia, abnormal liver function | Explosives manufacturing |
| DNT | Vomiting, cyanosis | Explosives manufacturing |
| Tetryl | Vomiting, skin rashes | Military installations |
| 2-nitrophenol | Skin irritation, aquatic toxicity | Industrial manufacturing |
| 4-nitrophenol | Inhibited DNA repair | Water contamination |
| 2,4-dinitrophenol | Cataracts | Industrial manufacturing |
| 3,5-dinitroaniline | Skin and eye irritation | Explosive blasting |
| NTO | Muscular atrophy | Munitions storage |
| Picric acid | Skin disease, poisoning | Explosives manufacturing |
| Nitroguanidine | Skin and eye irritation | Environmental exposure |
| Nitroglycerin | Low blood pressure, nausea | Explosives manufacturing |

*Table 5-1. Explosive compounds of interest. These eleven explosives are all hazardous to humans, plants, and animals. Exposure may occur through many avenues, often via environmental contamination near military storage or munitions manufacturing sites.*

humans, and the most common route of exposure [16-23]. Many of these compounds are also hazardous to plant and animal life, often through contamination of soil and groundwater. Analytical standards were acquired from Cerilliant (TX, USA) and Accustandard (CT, USA). Each standard was purchased in dilute form (0.1-5 mg/mL), dissolved in either methanol or acetonitrile. Prior to testing, each explosive standard was further diluted, and in some cases, combined to form mixtures of compounds.

### *5.2.2 Microchip separation conditions*

COC microchips were purchased from Microfluidic ChipShop (Germany), and were fabricated from injection molded Topas® polymer. Two microchip designs were selected, each with a 50 x 50 µm separation channel: one standard cross-T injection, and one staggered cross-T. The four reservoirs (sample, sample waste, buffer, outlet) each held up to 20 µL of liquid, and were connected via 50 x 50 µm channels. Separations were performed using a high voltage power supply (0-2000 V) with platinum electrodes. Indirect laser-induced fluorescence (ILIF) detection

was implemented, with rhodamine B as the background fluorophore. ILIF measures the baseline signal of a fluorescing species in the background electrolyte (BGE), and detects analytes when they displace the fluorophore, causing a drop in signal. This detection scheme has been widely reported for a variety of analytes [24, 25], and was shown to be more sensitive than indirect UV absorbance, a similar detection technique [26]. In our system, rhodamine B is displaced by the explosive compounds of interest, which themselves do not fluoresce, causing a drop in signal. Laser excitation was achieved using a 488 nm sapphire laser, with fluorescence data collected via photomultiplier tube.

Separations were performed in a sodium tetraborate buffer system, at pH 9.2. Unless otherwise specified, all experiments were performed with 10 mM sodium tetraborate in both the BGE and sample matrix (SM). The surfactant present in the BGE was sodium dodecyl sulfate (SDS), at a concentration of 80 mM unless otherwise stated. Rhodamine B was added to all BGE at 200 nM. The BGE also contained 2,000,000 $M_v$ polyethylene oxide (PEO) at 0.5% by weight. PEO was included to increase the viscosity of the BGE, which limits diffusion of analytes, resulting in higher resolution of peaks. Injection voltages were applied between 300 V and 750 V, over the course of 20 to 240 seconds. Separation voltages ranged from 1000 V to 1800 V, for up to 400 seconds. The separation channel was 5.8 cm in length, and separation currents were held below 60 μA at all times, to minimize Joule heating effects. For data analysis, resolution was calculated using **Equation 1**, where $t$ = retention time (for peak $a$ or $b$), and $w_{1/2}$ = peak width at half height (for peak $a$ or $b$).

$$R = 1.18\left(\frac{t_a - t_b}{w_{1/2(a)} + w_{1/2(b)}}\right) \quad (1)$$

## 5.3 Results and discussion

### *5.3.1 Adapting MEKC to native COC microchip*

The COC microchip employed for these separations was untreated, with no surface modifications to enhance formation of the electric double layer. It was hypothesized that this would not be a detriment, however, as literature has shown that under elevated pH (>8), native COC will exhibit a zeta potential similar to that of borosilicate glass [27], indicative of electric double layer formation. By using solutions at high pH and generating a large negative zeta potential, ions in solution should still partition at the channel-fluid interface as they would with a charged glass surface. If this is the case, then sufficient electroosmotic flow (EOF) could still be generated without any surface treatment of the COC. This was tested by loading the microchip (**Figure 5-1A and B**) with a BGE of sodium tetraborate at pH 9.2, and filling the sample wells with BGE containing rhodamine B fluorescent dye. When monitored via fluorescence microscopy, the staggered cross-T injection site of the microchip can be seen in **Figure 5-1C**, exhibiting no visible fluorescence. However, when 1500 V are applied from the sample to sample waste reservoirs, the injection site is filled with the fluorescent rhodamine B solution. (**Figure 5-**

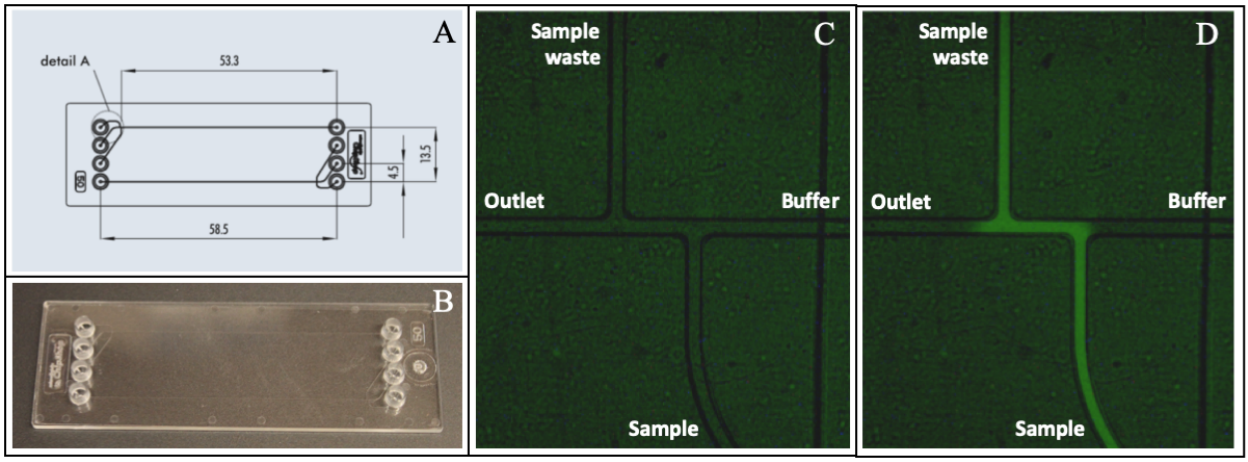


*Figure 5-1. Demonstration of electroosmotic flow on native COC microchip. (A) Microchip schematic from ChipShop (Germany). 50 micron diameter channels with both a standard and staggered cross-T injection. (B) Image of the COC microchip used for experimentation. (C) Microscopic view of staggered injection channel, prior to sample loading. (D) Injection site after electrokinetic loading of rhodamine B sample by applying 1500 V.*

**1D**). After voltage was applied from the buffer to outlet reservoirs, a sample plug was electrokinetically driven towards the detector. This simple experiment demonstrated the ability to generate rapid, reproducible electroosmotic flow on a native COC microchip, under appropriate conditions.

This same experiment was conducted with laser excitation at 488 nm and fluorescence detection (as described in section 5.2.2), with the results shown in **Figure 5-2**. When rhodamine B was injected, **Figure 5-2A**, the y-axis (relative fluorescence units) shows a steady baseline signal before a rapid rise in fluorescence at 190 seconds. When the trailing end of the plug passes the detector, signal returns to baseline. The drop in signal is not as abrupt as the rise, indicating that diffusion may lead to band broadening during actual separations. **Figure 5-2B** shows the results from the inverse experiment: the separation channel initially filled with rhodamine B solution, and a plug of non-fluorescent SM was injected. Here the baseline signal is high, and when the fluorescent solution is displaced by the SM, a sharp drop in signal is observed. Both of these tests show that concise plug of sample can be injected, electrokinetically driven down the channel, and detected using measured changes in fluorescence.

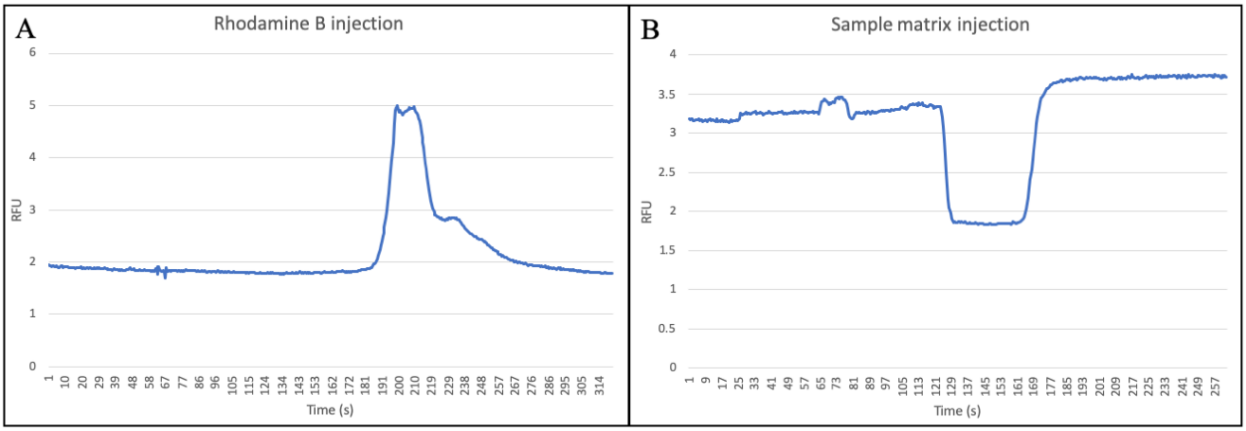


*Figure 5-2. Injections of rhodamine B and sample matrix. (A) With the microchip filled with buffer, a plug of rhodamine B solution was injected and electrokinetically driven past the detector. Increase in fluorescent signal indicates the plug of dye moving through the channel. (B) In a channel filled with rhodamine B solution, a plug of the sample matrix (buffer) was electrokinetically driven past the detector. The drop in fluorescence indicates the plug.*

### *5.3.2 Microchip detection of nitroaromatics*

A panel of eleven explosives was acquired, based on their relevance for military and environmental concerns, as well as their neutral character (**Table 5-1**). Each explosive was analyzed individually, at final SM concentrations ranging from 0.02 mg/mL to 0.1 mg/mL, and detecting via ILIF following a MEKC-based separation as described in section 5.2.2. The first explosive detected was TNT, shown in **Figure 5-3**. Initial baseline signal is low, as the fluorophore rhodamine B can be thermally quenched due to elevated temperature during prolonged laser exposure [28]. Once voltage was applied from the buffer to outlet reservoirs, fresh BGE was driven past the detector, causing an immediate rise in signal due to the introduction of unquenched fluorophore. The EOF indicator, methanol, is observed after 80 seconds, indicating the fastest possible elution time, as methanol has no micelle permeability and will migrate with the bulk EOF. After 150 seconds, a sharp drop in fluorescence indicates the band of TNT passing the detector, displacing the rhodamine B from the background electrolyte in the detection zone. This proof-of-principle result showed that using low-cost, non-surface modified COC microchips, a rapid, electrokinetically driven separation can detect a neutral explosive compound.

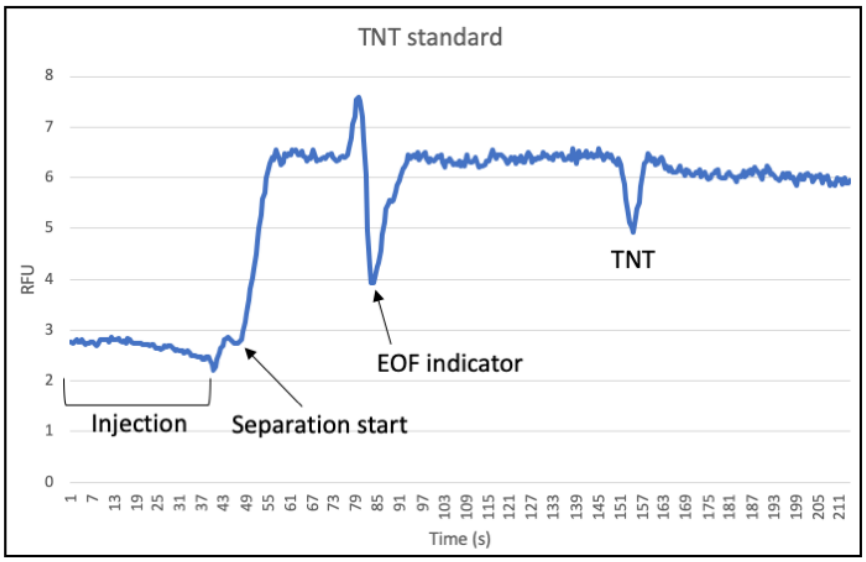


*Figure 5-3. Detection of TNT. The signal disturbance at 80 seconds is due to methanol passing the detector, displacing the rhodamine B and indicating the speed of bulk EOF. A drop in fluorescent signal at 155 seconds is due to a band of TNT passing the detector.*

Two additional nitroaromatic compounds, DNT and tetryl, were detected under these conditions. **Figures 5-4 and 5-5** show the spectra for DNT and tetryl, respectively, which were each detected within 150 seconds. Due to the higher micelle permeability of DNT relative to TNT or tetryl, a higher methanol concentration was implemented in the BGE. Increasing methanol reduced micelle-analyte interactions, leading to a faster migration time and more rapid detection. These three nitroaromatic compounds in particular, TNT, DNT, and tetryl, pose a significant challenge, as they differ only by the number of nitro groups on the aromatic ring. This causes them to interact similarly with micelles, leading to comparable migration times, increasing the difficulty of resolving these compounds in a mixture. This is especially relevant as tetryl, a common military grade explosive, will degrade over time first into TNT, then DNT, with the sequential loss of nitro groups [29]. Detecting the presence of some, or all of these nitroaromatics, and the ratio of each, would provide information about the age and degradation state of a sample.

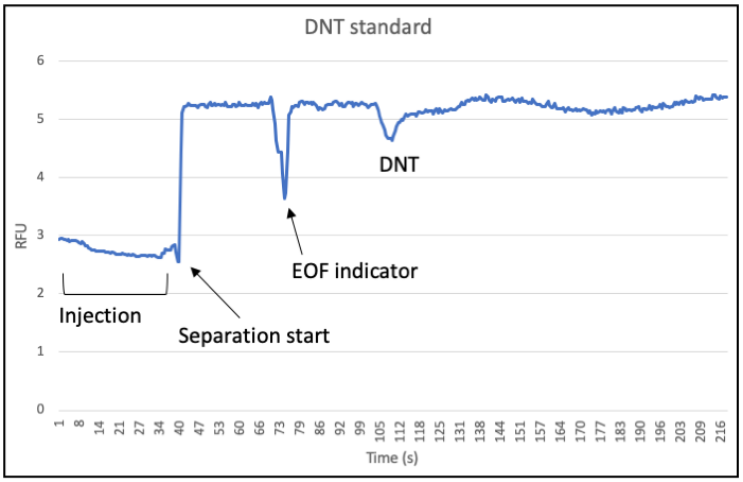


*Figure 5-4. Detection of DNT. DNT is detected at 110 seconds due to a drop in fluorescent signal. This separation is faster than that observed for TNT due to higher applied voltages, as well as lower concentration of polymer.*

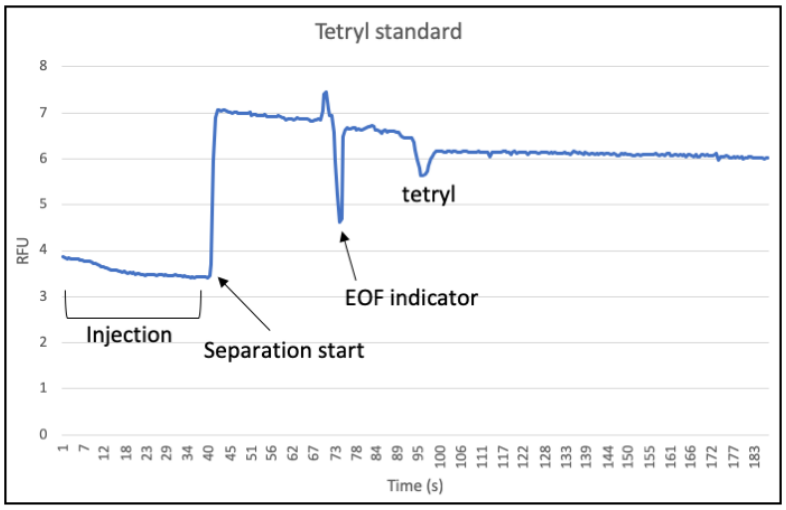


*Figure 5-5. Detection of tetryl. Clear drop in fluorescence is observed at 95 seconds, indicating the band of tetryl passing the detector.*

### *5.3.3 Microchip detection of nitrophenols*

Four compounds from the nitrophenol family were identified using the described method. Diluted standards of 2-nitrophenol (**Figure 5-6**), 4-nitrophenol (**Figure 5-7**), and 2,4-dinitrophenol (**Figure 5-8**) were all detected within 200 seconds, with similar migration times observed for each compound. These nitrophenols are the major components of Shellite, a military grade explosive, and all have high acute toxicity for humans [30]. The other component of Shellite is 2,4,6-trinitrophenol, also known as picric acid, which was detected via the described MEKC method. That electropherogram, shown in **Figure 5-9**, resulted in two distinct drops in fluorescent signal at approximately 165 and 180 seconds. This result was unexpected, as the picric acid standard was high purity (98%) and should not contain detectable contaminants. It is our hypothesis that picric acid had partially degraded over time, resulting in both 2,4,6-trinitrophenol and 2,4-dinitrophenol in solution. There are multiple competing theories regarding the breakdown of picric acid [31, 32], which result in various degradation products. If the standard of picric acid had partially degraded, then the presence of another nitrophenol compound in solution would migrate differently, and cause a second drop in fluorescence. It is not known which degradation product

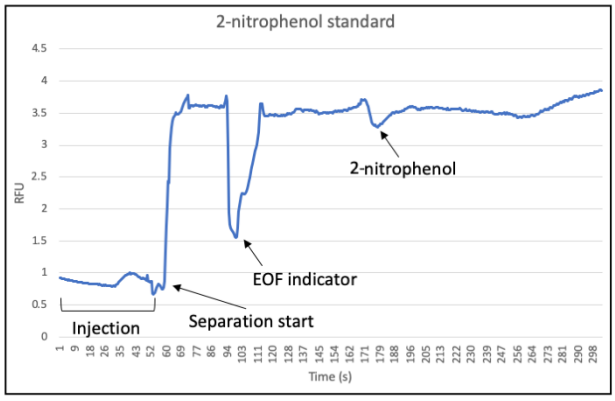


*Figure 5-6. Detection of 2-nitrophenol. 2-nitrophenol is detected at 175 seconds after injection, with some fronting observed.*

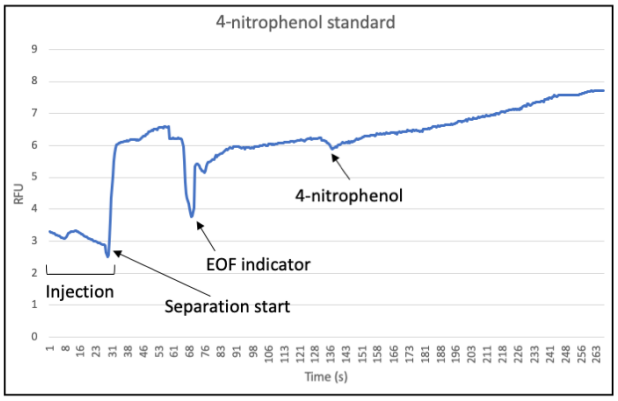


*Figure 5-7. Detection of 4-nitrophenol. A slight drop in fluorescence is indicative of the 4-nitrophenol band displacing rhodamine B as it passes the detector.*

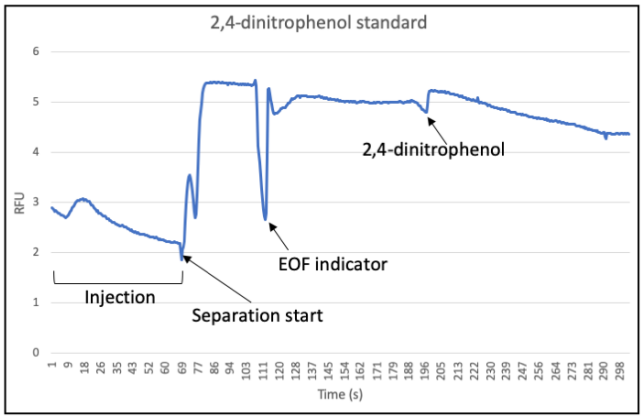


*Figure 5-8. Detection of 2,4-dinitrophenol. 2,4-dinitrophenol displays a slower migration time than either 2- or 4-nitrophenol, passing the detector at 200 seconds.*

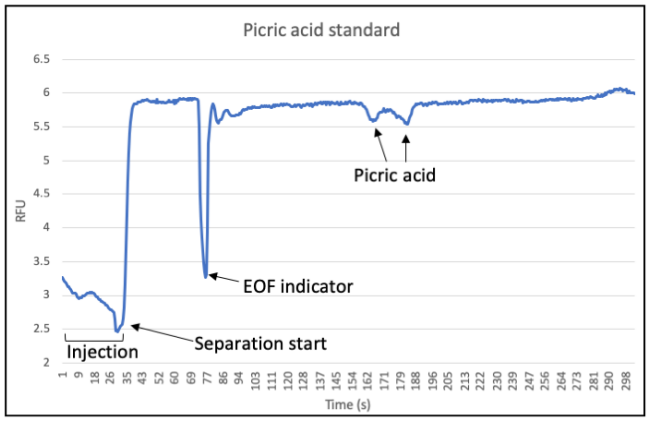


*Figure 5-9. Detection of picric acid. Each test for picric acid displayed two rhodamine B displacement events. Based on this data, picric acid has separated into two distinct bands.*

may have been in solution with picric acid, but the distinctive double displacement event was observed with each test of this compound.

### *5.3.4 Detection of additional explosive compounds*

Another explosive compound tested was 3-nitro-1,2,4-triazol-5-one (NTO), an army-grade munition from the early 1900's. Like picric acid, this analyte displayed two distinct drops in fluorescence during the separation, indicative of multiple compounds displacing rhodamine B from the detection site. The spectrum shown in **Figure 5-10** shows the two distinct peaks, with the earlier eluting molecule generating a larger drop in fluorescence. However, unlike the picric acid anomaly, for this compound we hypothesize that NTO isomerized to one of its many known conformations [33], resulting in the detection of two conformers, each migrating at a different rate..

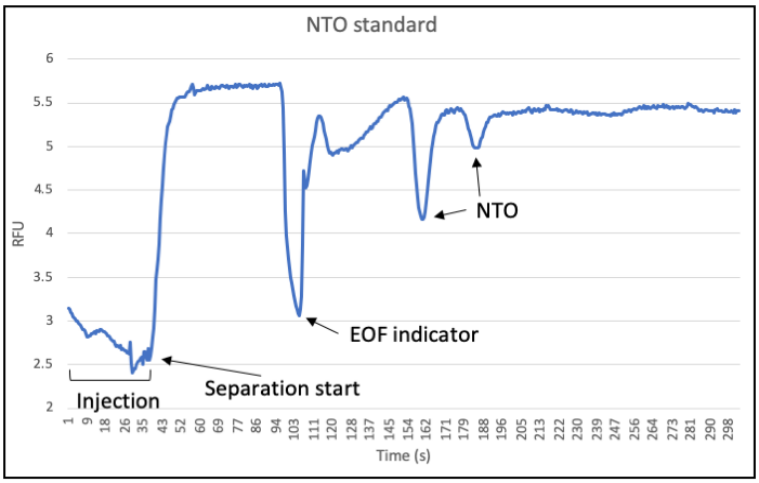


*Figure 5-10. Detection of 3-nitro-1,2,4-triazol-5-one (NTO). The electropherogram for NTO displays two distinct negative troughs, which were also observed in replicates of this test. Rhodamine B displacement at 160 and 190 seconds are indicative of NTO passing the detector.*

The final three compounds detected were 3,5-dinitroaniline, nitroguanidine, and nitroglycerin. **Figure 5-11** shows the electropherogram for 3,5-dinitroaniline, which was clearly identified by the drop in fluorescence at 220 seconds. The sharp band shape observed with 3,5-dinitroaniline was not present for nitroguanidine (**Figure 5-12**) or nitroglycerin (**Figure 5-13**), which were each identified by broad depressions in the spectra. This significant band broadening may be attributed to the length of the separations, each exceeding 400 seconds, which allows for diffusion and Joule heating to exert a larger impact on peak width.

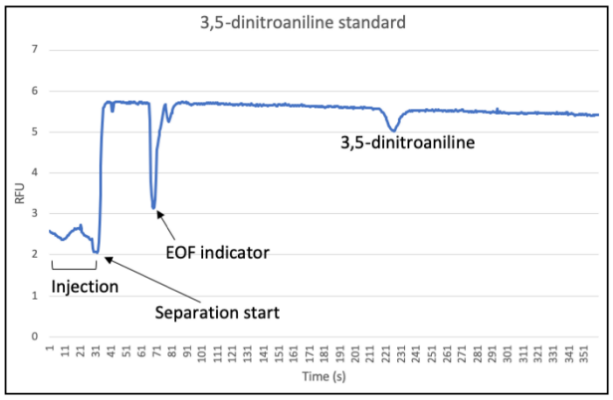


*Figure 5-11. Detection of 3,5-dinitroaniline. Displacement of rhodamine B by 3,5-dinitroaniline is observed at 220 seconds.*

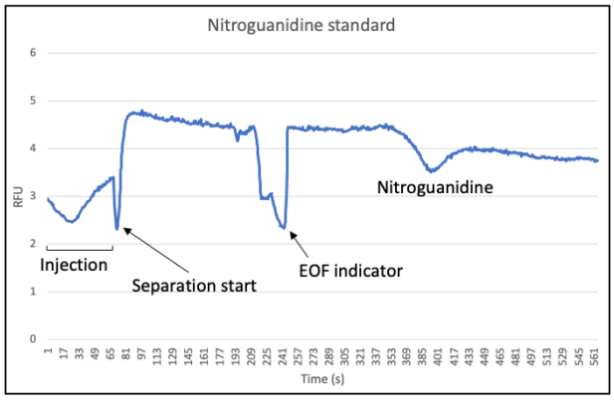


*Figure 5-12. Detection of nitroguanidine. A single, broad depression is observed for nitroguanidine, passing the detector at 385 seconds.*

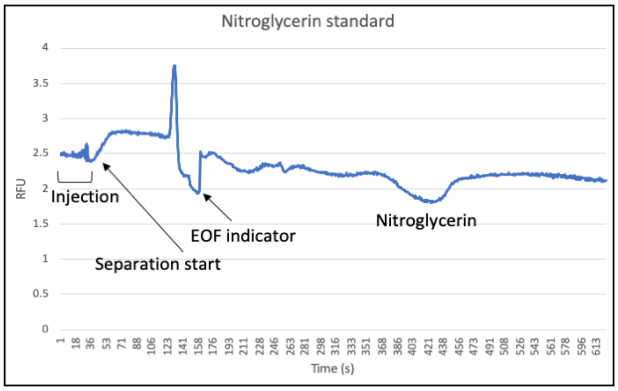


*Figure 5-13. Detection of nitroglycerin. Nitroglycerin is detected as a broad depression at 420 seconds.*

### *5.3.5 Separation of explosive mixtures*

Having detected all eleven compounds individually, several relevant mixtures were tested using our microchip MEKC separation and ILIF detection strategies. To start, TNT and 3,5-dinitroaniline were added to the SM at 0.05 mg/mL and 0.02 mg/mL, respectively, and separated using the same previously described conditions. These compounds were chosen due to their large difference in micelle permeability, and therefore, migration time, which should allow for sufficient

separation. The results (**Figure 5-14**) show that TNT, with less micelle interaction, passed the detector first at 140 seconds, causing a distinct drop in fluorescence. The analyte band for 3,5-dinitroaniline, which interacts more extensively with the micelle, is observed at 170 seconds. While this result shows adequate separation of the compounds, there was concern over failure to return to baseline fluorescent signal after detection of TNT. This effect was not observed in every test, but it is hypothesized that lack of pull-back on the injection arms resulted in leaking of SM into the separation chamber. This diluted the overall concentration of rhodamine B in solution, leading to a lower background signal once the sample matrix reached the detector.

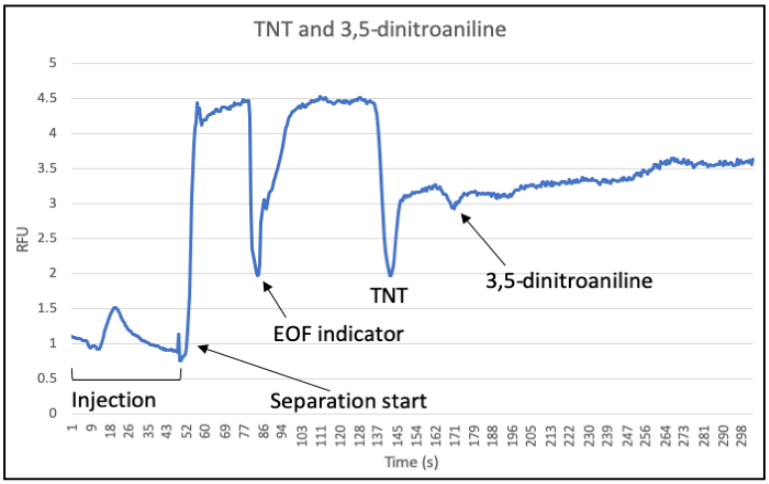


*Figure 5-14. Separation of TNT and 3,5-dinitroaniline. Two distinct rhodamine B displacement events are observed. The first at 140 seconds is attributed to TNT, the second at 170 seconds is due to 3,5-dinitroaniline.*

Another combination of interest was a solution of mixed nitrophenols, which may be common in samples that have partially degraded from the parent compounds of 2,4,6-trinitrophenol or 2,4-dinitrophenol. **Figure 5-15** shows the electropherogram from a sample containing 2,4-dinitrophenol and 4-nitrophenol, each at 0.25 mg/mL in solution.

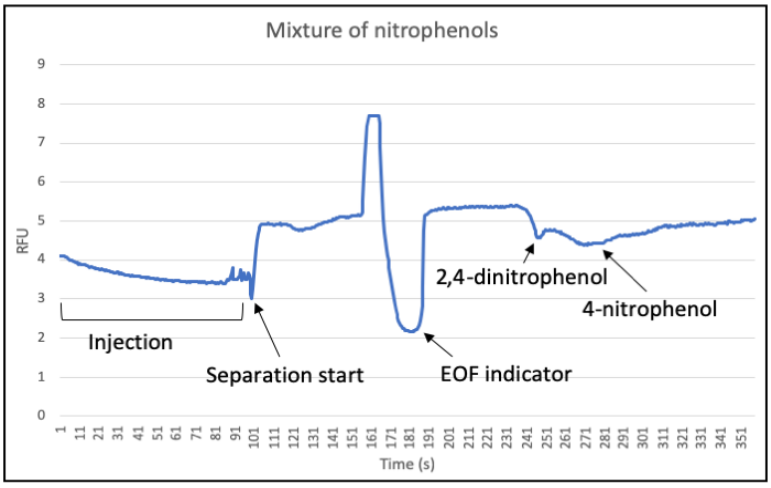


*Figure 5-15. Separation of 2,4-dinitrophenol and 4-nitrophenol. A clear trough is observed for 2,4-dinitrophenol at 245 seconds. Immediately following that appears a broad depression, possibly due to 4-nitrophenol passing the detector.*

The first analyte to pass the detector, 2,4-dinitrophenol, can be easily identified by the drop in fluorescence at 245 seconds. However there is poor separation from the second compound, 4-nitrophenol, which appears as a broad band immediately following 2,4-dinitrophenol. Subsequent tests were unable to improve the resolution, indicating that in its current state, this technique may not be able to distinguish between different members of the nitrophenol family of explosives.

The nitroaromatic family was also investigated as a mixture, with TNT, DNT, and tetryl each added to the sample matrix at 0.05 mg/mL. Each of these analytes is independently relevant, but may also be present in environmental samples as a mixture, due to degradation over time. However, due to their similar micelle permeability and observed similarity in migration time, full resolution of all three molecules was not achieved. **Figure 5-16** shows an initial attempt to resolve

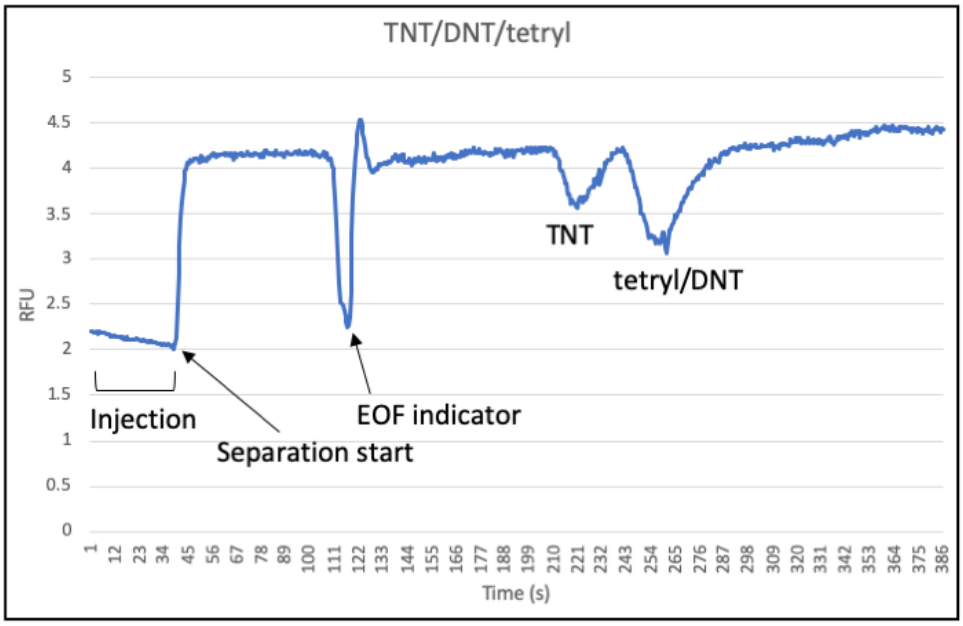


*Figure 5-16. Separation of TNT, DNT, and tetryl. Two broad troughs are observed at 220 seconds and 255 seconds. The first is due to TNT passing the detector, while the second can be assigned to both tetryl and DNT, which were not resolved.*

the three nitroaromatics, with clear identification of TNT at 220 seconds. A second, broader drop in fluorescence is observed at 255 seconds, which can be attributed to tetryl and DNT comigrating, simultaneously passing the detector and displacing rhodamine B. To address this issue, subsequent testing was performed with a higher concentration of SDS (175 mM), which increased the number

of micelles in solution, and in theory, increased analyte-micelle interactions. By increasing those interactions, even small differences in micelle permeability should lead to larger differences in migration time, therefore improving resolution between DNT and tetryl. The results are shown in **Figure 5-17**, in which all three compounds can be identified by drops in the fluorescent signal. However, baseline resolution is not achieved for tetryl and DNT, and the background fluorescent signal does not return to baseline after the DNT band. These results could not be improved further

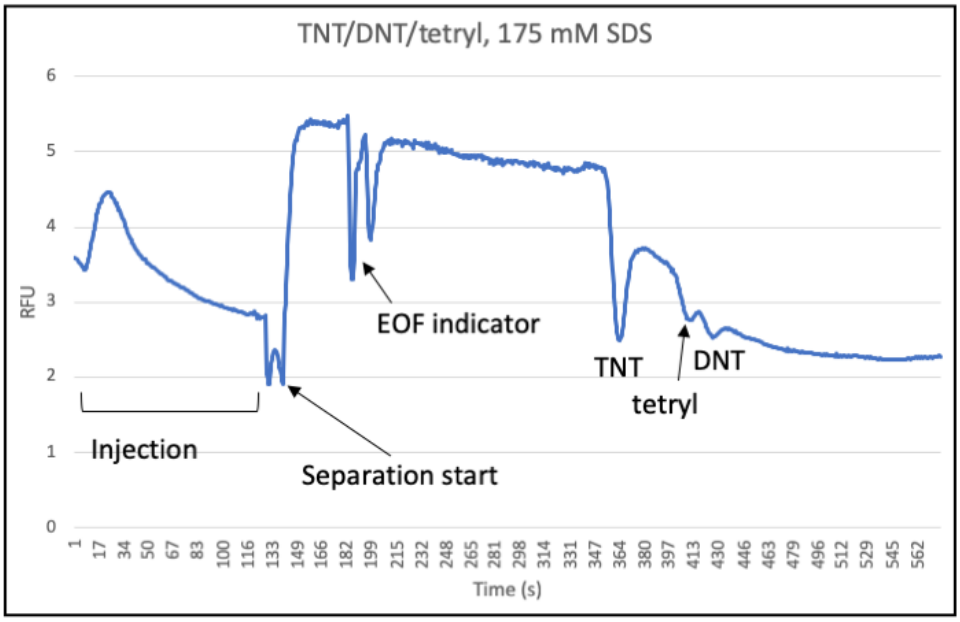


*Figure 5-17. Separation of TNT, DNT, and tetryl, elevated SDS. A separation employing a higher concentration of SDS was able to resolve all three analytes. TNT, tetryl, and DNT are detected at 360, 410, and 425 seconds, respectively.*

by solely adjusting the surfactant concentration.

### *5.3.6 Field-amplified stacking*

With the goal of improving separation conditions for better resolution of multi-component mixtures, TNT and DNT were selected as a test matrix for tuning a variety of parameters. Of particular interest was the implementation of field-amplified stacking, or analyte preconcentration, which takes advantage of differences in ionic strength between the BGE and SM to generate regions of varying conductivity [34]. This principle, when applied to MEKC, results in an increased concentration of micelles at the boundaries between the BGE and SM, due to difference

in migration speed of the two solutions [35, 36]. This boundary stacking of micelles then increases the analyte-micelle interactions in a narrow region, causing tighter migration of analytes, and diminished band broadening during separation. The effect of this field-enhanced stacking can be observed by comparing **Figures 5-18 and 5-19**, both separations of TNT and DNT, performed with and without stacking. For **Figure 5-18**, a mixed sample of TNT and DNT was separated under the same conditions used for individual compound detection in section 5.3.2. The analytes are clearly separated, with a calculated resolution of 1.30. However, when the borate concentration in the SM is decreased five-fold, the separation improves dramatically. **Figure 5-19** shows the electropherogram from a field-enhanced stacking separation of TNT and DNT, with sharper, better resolved drops in fluorescence observed for each analyte. The calculated resolution between TNT and DNT was 2.27, a pronounced improvement relative to the success of separation without stacking.

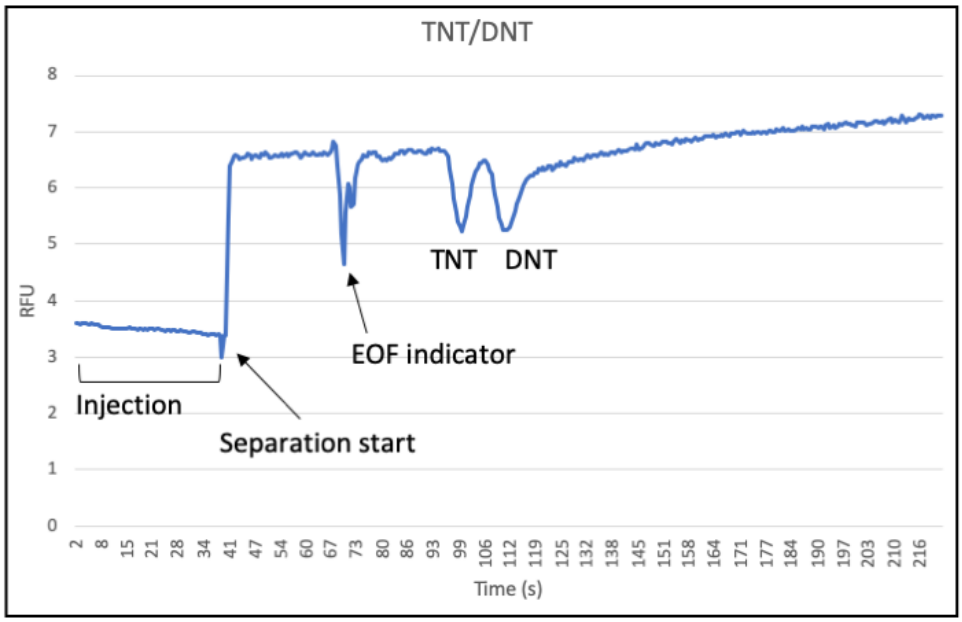


*Figure 5-18. Separation of TNT and DNT. TNT and DNT are detected at 100 and 115 seconds, respectively. Baseline resolution was achieved, with clear separation of analytes. Resolution was calculated at 1.30.*

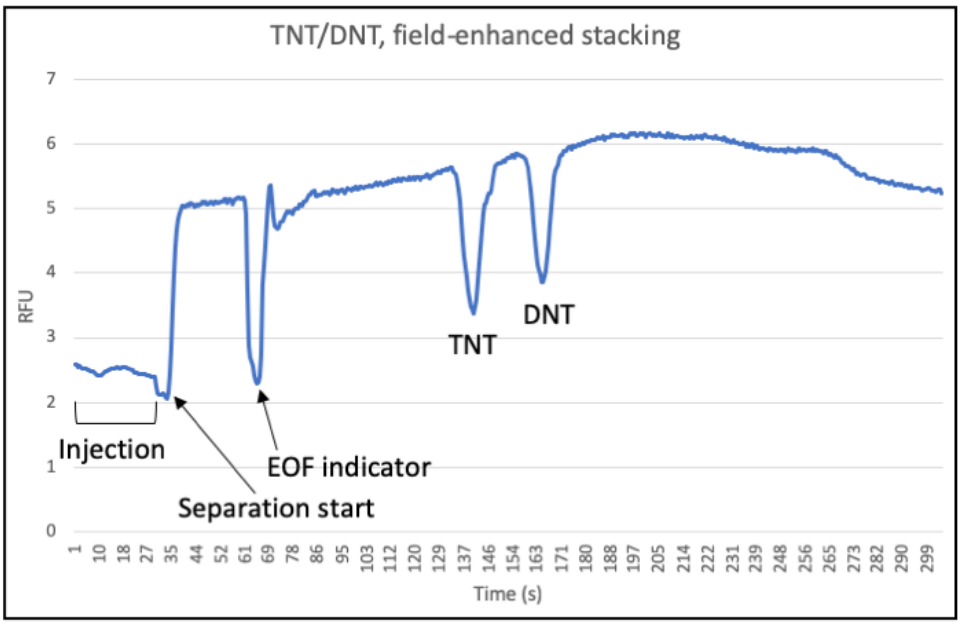


*Figure 5-19. Separation of TNT and DNT, field amplified stacking. A separation with stacking, or analyte preconcentration, resulted in improved resolution (2.27) as compared to prior TNT and DNT experiments.*

### *5.3.7 Addition of β-cyclodextrin*

To further improve separation of multiple explosives and promote enhanced resolution, β-cyclodextrin was added to the BGE. Often used as a chiral selector in capillary electrophoresis [37], β-cyclodextrin forms complexes with molecules in a similar fashion to micelles, dependent upon their inclusion into the hydrophobic cavity. In the context of MEKC, β-cyclodextrin adds a secondary method of resolving similar compounds, as they will partition in and out of the hydrophobic centers. This effectively establishes a second 'pseudo stationary' phase for the separation, as analytes can either be incorporated into the micelles or the cyclodextrin molecules. While also employing field-amplified stacking, β-cyclodextrin was added to the BGE at 40 mM for a separation of TNT and DNT. The resulting spectrum, **Figure 5-20**, shows baseline resolved bands for each analyte, with a calculated resolution of 2.41, exceeding the previous best separation conditions. A direct comparison of the effect of β-cyclodextrin is shown in **Figure 5-21**, which

overlays three separations with different conditions. The top trace (gray) shows TNT and DNT separated with no stacking or additives, with a resolution of 1.80. When field-enhanced stacking

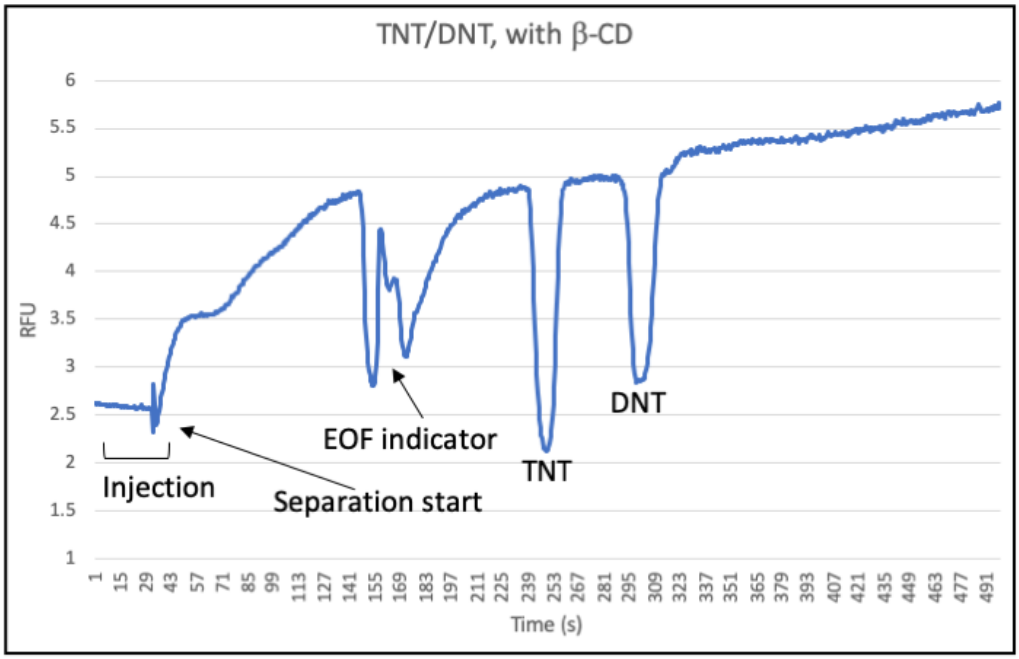


*Figure 5-20. Separation of TNT and DNT, β-cyclodextrin. Addition of β-cyclodextrin results in improved resolution (2.41) for this separation. A second drop in fluorescence is observed for the EOF indicator, cause unknown.*

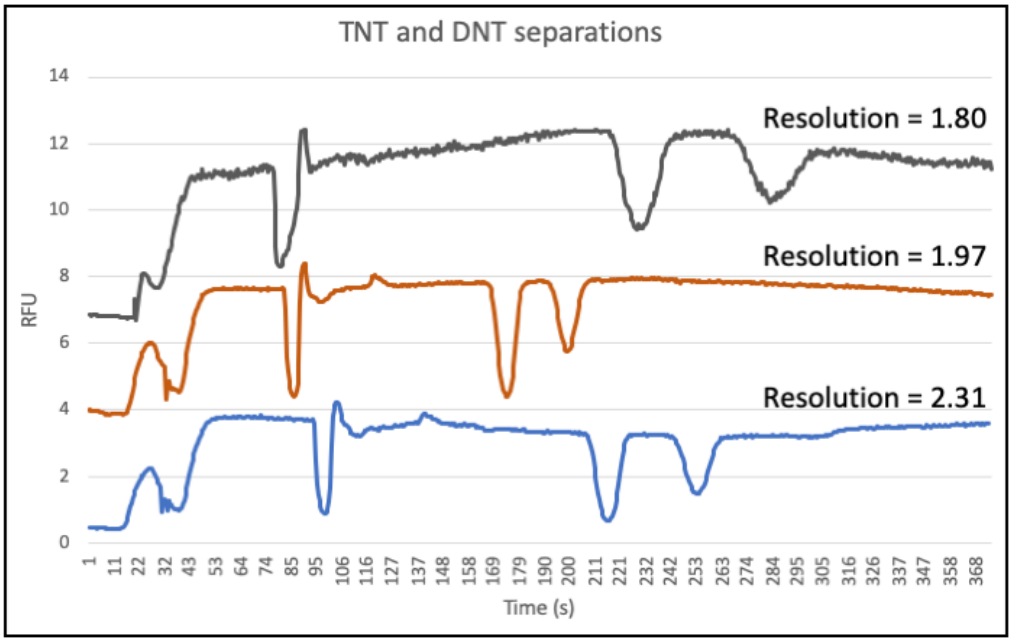


*Figure 5-21. Separation of TNT and DNT under different conditions. (A) Upper trace displays a separation with equal buffer concentration in SM and BGE, no additives. Resolution = 1.80. (B) Middle trace has analyte stacking (10X buffer concentration in BGE) and β-cyclodextrin (20 mM) added. Resolution = 1.97. (C) Lower trace with analyte stacking (10X buffer concentration in BGE) and β-cyclodextrin (40 mM) additive. Resolution is 2.31. Note: y-axis has been offset for visibility of each spectrum.*

was implemented, and 20 mM β-cyclodextrin added (orange trace), the bands become sharper, and resolution improves to 1.97. By increasing the β-cyclodextrin concentration to 40 mM (blue trace) the resolution is further improved to 2.31, still completing the separation within 5 minutes. This combination of field-enhanced stacking and β-cyclodextrin shows that exceptional resolution of similar nitroaromatic compounds is achievable on our microchip MEKC system, and that improved mixture separations may be feasible.

Using these improved parameters, as well as other adjusted conditions including polymer, organic modifier, and surfactant concentrations, improved resolution of tetryl and DNT was sought. In previous tests, a single broad band caused by comigration of tetryl and DNT was observed in mixed samples, resulting in a failure to resolve either analyte (**Figure 5-16**). **Figure 5-22** shows that there are distinct local minima in the fluorescent signal for tetryl and DNT, but baseline resolution is not achieved. Further adjustments to the ionic strength, applied voltages, and other separation conditions were unsuccessful in improving these results, indicating that other

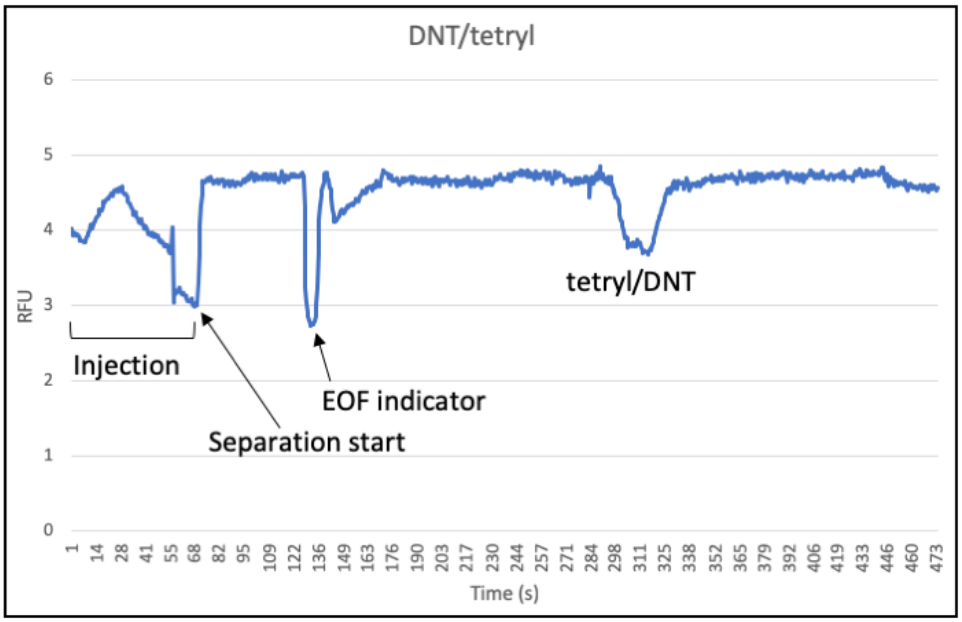


*Figure 5-22. Separation of tetryl and DNT. Using field-enhanced stacking and 40 mM β-cyclodextrin, some resolution of tetryl and DNT is achieved.*

approaches may be necessary for complete separation of the nitroaromatic family of explosive compounds.

### *5.3.8 Alternative surfactant molecules*

A drastic change was explored to improve resolution of difficult compounds, by replacing the surfactant molecule and generating different micelles. SDS remains one of the most common surfactants in separations chemistry, but literature reports on several other successful candidates including sodium cholate [38], Triton X-100 [39], Tween 20 [40], and various others. Differences in the micelle size, charge dispersion, and hydrophobic cavity can all contribute to variable analyte retention with these alternative surfactant molecules. It was hypothesized that a new surfactant system may result different partitioning of the explosive analytes into the micelle, either by replacing SDS in the BGE entirely, or combining it with a nonionic surfactant to form a mixed micelle.

A complete replacement of SDS was tested with sodium cholate at 80 mM, all other BGE conditions remaining the same. The initial results (**Figure 5-23A**) showed analyte peaks immediately following the EOF indicator, with significantly less micelle retention than had been previously observed. When a lower voltage was applied, the bands became distinct and more

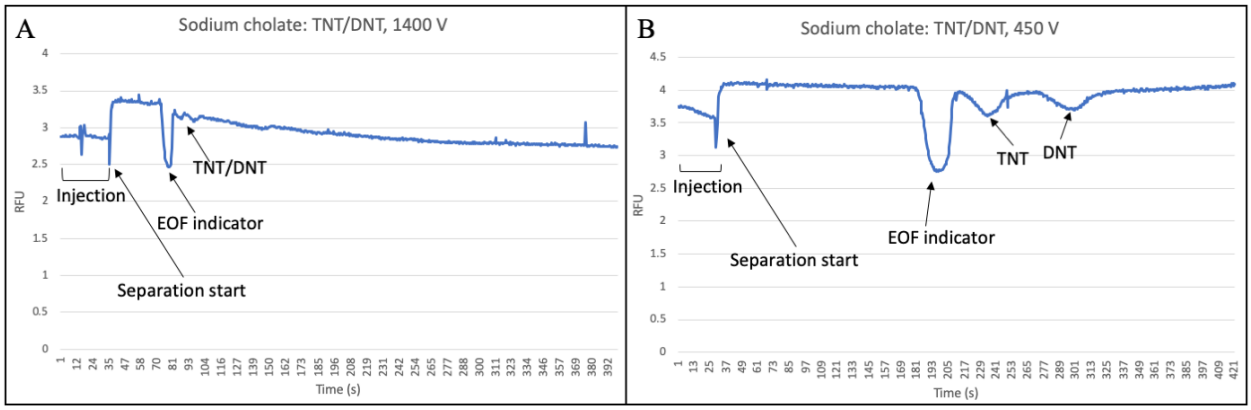


*Figure 5-23. Separation of TNT and DNT with sodium cholate micelle. (A) The electropherogram for a 1400 V separation shows possible analyte troughs immediately following the EOF marker. (B) When separation voltage is reduced to 450 V (CHECK THIS), distinct troughs are observed for TNT and DNT.*

visible, yet still migrated at almost the same speed as the EOF indicator (**Figure 5-23B**). Although TNT and DNT were successfully separated, they were not as well resolved as previous experiments using SDS. In addition, their migration so close to the EOF marker implies that there is very little micelle interaction during the separation, and that addition of other explosive compounds would result in a single broad band that could not be resolved into individual analytes. We hypothesized that this was due to fundamental differences in micelle structure and formation between sodium cholate and SDS. With a lower aggregation number than SDS (n = 59), sodium cholate (n = 14) generates smaller micelles. The sodium cholate micelles in fact form a flat, pancake-like shape, rather than a sphere [41, 42]. This, in turn, leaves hydrophobic analytes more exposed during interaction with the micelle, causing faster diffusion out of the hydrophobic core. Overall, this would lead to less retention of explosive compounds in the micelle, and faster migration times during separation.

Mixed micelles were investigated using combinations of SDS with either Triton X-100 or Tween 20, which have been exploited successfully for other applications in MEKC [43, 44]. Using a combination of ionic and nonionic surfactants can provide enhanced selectivity in the separation, but the mixed micelle will also have lower electrophoretic mobility due to its decreased charge/size

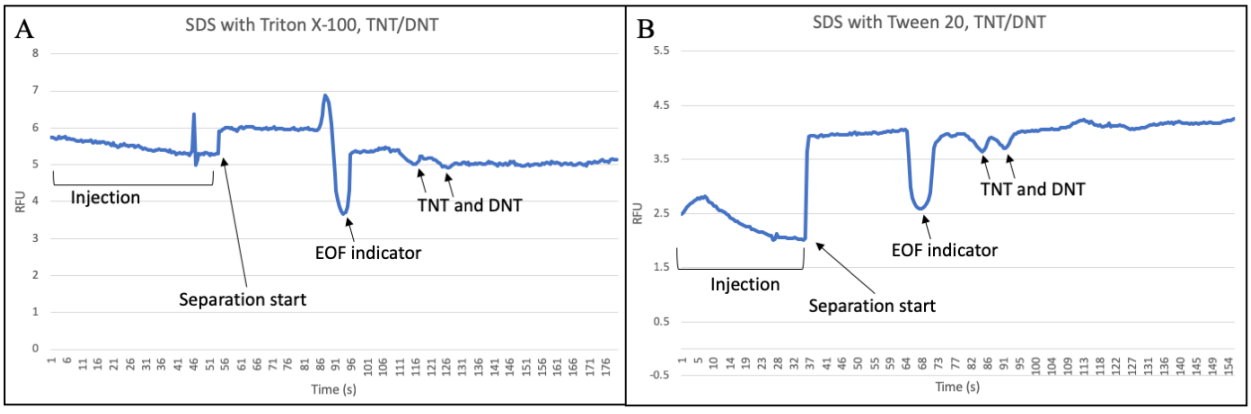


*Figure 5-24. Separation of TNT and DNT with a mixed micelle system. (A) Electropherogram from a separation using 30 mM SDS and 30 mM Triton X-100 in the BGE. Slight depressions are observed for TNT and DNT. (B) Separation of TNT and DNT using 50 mM SDS and 10 mM Tween 20. Clear troughs are observed for each analyte.*

ratio [45]. The nonionic surfactants were incorporated at different concentrations relative to SDS, with most promising results generated from mixtures of 30 mM SDS with 30 mM Triton X-100, and from 50 mM SDS with 10 mM Tween 20. The spectra in **Figure 5-24A and B** show successful separation of TNT and DNT, each identified by drops in fluorescence soon after the EOF indicator. However, the poor resolution and lack of significant difference in migration times indicate that neither of these mixed micelle systems are superior to SDS for our application of separating nitroaromatic explosive compounds via microchip MEKC.

## 5.4 Summary

Using microchip MEKC with ILIF detection, eleven explosive compounds were identified on native COC devices without any surface modification. Each explosive was detected in less than five minutes, by observing a distinct drop in fluorescent signal due to displacement of the background fluorophore. This work is the first reported free-solution, MEKC separation of explosives on a native COC substrate, and shows high resolution separation of the nitroaromatic molecules TNT and DNT. Separations were improved through the implementation of field-enhanced stacking, as well as the addition of β-cyclodextrin. Attempts to improve resolution using mixed micelles and alternate surfactants were unsuccessful, though future work may incorporate different micelle-forming species. These separations were conducted on hardware that is fully amenable for portable, on-site usage. The high voltage power supply, laser excitation source, and data collection optics have all been compressed to a shoebox-size prototype for a related project [46], and would be field deployable if necessary. The research presented herein has shown impactful results in a relevant timeframe. We expect further improvements to be made with continued research, and anticipate continued meaningful collaboration with our government partners.

One of the most significant remaining challenges for this project is to optimize separation parameters for full resolution of complex mixtures. To date, several two-compound mixtures have been separated, with partial success in samples containing three explosives. However, samples collected near military installations may contain varying levels of many explosives, and poor resolution would confound the results from an authentic sample. The previously discussed EPA 8330 method, as well as leading research groups, have shown identification of up to 14 compounds in a single sample [4, 7, 8]. However, none of these approaches are fully portable for field use, and thus more development is required. Achieving a rapid, high-resolution separation of explosives on a rugged, portable microfluidic platform would meet a distinct need in the forensic science community. This project has made strides towards achieving that goal, and demonstrated new advances in separations chemistry.

## 5.5 References


1. K. Panz, K. Miksch, T. Sojka, *Bulletin of Environmental Contamination and Toxicology*, 2013, **91**, 555-9.
2. R. Garg, D. Grasso, G. Hoag, *Hazardous Waste Hazardous Materials*, 1991, **8**, 319-40.
3. J. Goodpaster, V. McGuffin, *Analytical Chemistry*, 2001, **73**, 2004-11.
4. Environmental Protection Agency, *Method 8330a*, 2007.
5. D. Bodeau, *Occupational health: The soldier and the industrial base*, 1993, 305-57.
6. L. Jang, M. Razu, E. Jensen, H. Jiao, J. Kim, *Lab on a Chip*, 2016, **16**, 3558-64.
7. C. Bailey, S. Wallenborg, *Electrophoresis*, 2000, **21**, 3081-7.
8. S. Kennedy, B. Caddy, J. Douse, *Journal of Chromatography A*, **1996**, 211-22.
9. M. Rashid, *Micro and Nanosystems*, 2010, **2**, 108-36.

10. S. Wallenborg, C. Bailey, *Analytical Chemistry*, 2000, **72**, 1872-8.

11. K. Faure, *Electrophoresis*, 2010, **31**, 2499-2538.

12. S. Roy, T. Das, C. Yue, *Applied Materials and Interfaces*, 2013, **5**, 5683-9.

13. Y. Ladner, G. Cretier, K. Faure, *Journal of Chromatography A*, 2010, 8001-8.

14. C.Tian, Y. Shen, *PNAS*, 2009, **106**, 15148-53.

15. K. Lukacs, J. Jorgenson, *J. of High Res. Chrom. & Chrom. Comm.* 1985, 407-11.

16. P. Richter-Torres, A. Dorsey, C. Hodes, *U.S. Department of Health and Human Services*, 1995.

17. P. Tchounwou, C. Newsome, K. Glass, J. Centeno, J. Leszczynski, J. Bryant, J. Okoh, A. Ishaque, M. Brower, *Reviews on Environmental Health*, 2003, **18**, 203-29.

18. Agency for Toxic Substances and Disease Registry, *Toxicological profile for tetryl*, 1995.

19. Agency for Toxic Substances and Disease Registry, *Toxicological profile for nitrophenols*, 1992.

20. New Jersey Department of Health and Senior Services, *Hazardous substance fact sheet, dinitroanilines*, 1999.

21. L. Crouse, E. Lent, G. Leach, *International Journal of Toxicology*, 2015, **34**, 55-66.

22. Centers for Disease Control and Prevention, *International chemical safety cards*, 2012.

23. J. Arena, R. Drew, *Poisoning-toxicology, symptoms, treatments*, 1986, 596.

24. X. Yang, X. Wang, X. Zhang, *Journal of Separation Science*, 2006, **29**, 677-83.

25. D. Boudko, *Journal of Chromatography B*, 2007, **851**, 186-210.

26. J. Melanson, C. Boulet, C. Lucy, *Analytical Chemistry*, 2001, **73**, 1809-13.

27. P. Mela, A. van den Berg, Y. Fintschenko, E. Cummings, B. Simmons, B. Kirby, *Electrophoresis*, 2005, **26**, 1792-1799.

28. G. Arnaoutakis, D. Nather, *Edinburgh Instruments*, 2016, **1**, 1-2.

29. D. Khue, T. Lam, N. Chat, V. Bach, D. Minh, V. Loi, N. Anh, *Journal of Industrial and Engineering Chemistry*, 2014, **20**, 1468-75.

30. J. Grundlingh, P. Dargan, M. El-Zanfaly, D. Wood, *Journal of Medical Toxicology*, 2011, **7**, 205-12.

31. J. Oxley, *Theoretical and Computational Chemistry*, 2003, **12**, 5-48.

32. Y. Tan, G. Davidson, C. See, D. Dunbar, J. O'Haver, S. Rice, D. Harrelson, M Zakikhani, *Water, Air, and Soil Pollution*, 2006, **177**, 169-81.

33. L. Turker, T. Atalar, *Journal of Hazardous Materials*, 2006, 1333-44.

34. B. Giordano, D. Newman, P. Federowicz, G. Collins, D. Burgi, *Analytical Chemistry*, 2007, **79**, 6287-94.

35. J. Quirino, S. Terabe, *Journal of Chromatography A*, 2000, **902**, 119-35.

36. Z. Liu, P. Sam, S. Sirimanne, P. McClure, J. Grainger, D. Patterson, *Journal of Chromatography A,* 1994, **673**, 125-32.

37. M. Rogan, K. Altria, D. Goodall, *Chirality*, 1994, **6**, 25-40.

38. C. Hebling, L. Thompson, K. Eckenroad, G. Manley, R. Fry, K. Mueller, T. Strein, D. Rovnyak, *Langmuir*, 2008, **24**, 13866-74.

39. X. Wang, Y. Hu, F. Qu, R. Khan, *Journal of Chromatography A*, 2017, **1501**, 161-6.

40. L. Liu, B. Wu, K. Liu, C. Li, X. Zhou, P. Li, H. Yang, *Journal of Pharmaceutical and Biomedical Analysis*, 2016, **126**, 1-8.

41. D. Jobe, *Langmuir*, 1995, **11**, 2476-9.

42. L. Hao, R. Lu, D. Leaist, P. Poulin, *Journal of Solution Chemistry*, 1997, **26**, 113-25.

43. M. Bhattacharya, S. Dixit, *International Journal of Chemical Studies*, 2015, **3**, 22-5.

44. Y. Esaka, K. Tanaka, B. Uno, M. Goto, *Analytical Chemistry*, 1997, **69**, 1332-8.

45. G. Hancu, B. Simon, A. Rusu, E. Mircia, A. Gyeresi. *Advanced Pharmaceutical Bulletin*, 2013, **3**, 1-8.

46. D. Nelson, B. Thompson, A. Tsuei, C. Birch, J. Duvall, D. Le Roux, J. Li, D. Mills, A. Khim, M. Startseva, D. Cook, A. McGhee, S. Panesar, C. Clark, J. Ferrance, B. Root, J. Landers, *PNAS*, in prep.

# Chapter 6. Final remarks

## 6.1 Conclusions

This dissertation has described advances made in microfluidic applications to forensic science, specifically with regard to human identification in sexual assault investigations and on-site explosive detection. Each of these areas has been the target of commercial product development, as well as dedicated academic research, but to date, no technologies have been introduced that can adequately address the current analytical shortcomings. For processing sexual assault samples, the existing differential extraction (DE) protocol is laborious, time-consuming, and has resulted in hundreds of thousands of backlogged sexual assault samples. The need for on-site explosive detection from contaminated soil and groundwater sources poses its own challenges in achieving efficient, informative chemical analysis at the point-of-need. Microfluidic approaches are enticing for both of these capacities, and the research presented herein describes acoustic and electrophoretic separation techniques developed to address the stated forensic and environmental needs.

**Chapter 2** detailed the development of an acoustic differential extraction (ADE) prototype instrument, capable of isolating sperm cells from sexual assault samples in a rapid, automated fashion. The reported technique applied a standing acoustic wave within a glass and polymer microchip, creating a resonant chamber for particle capture. This acoustic trapping approach has been previously applied to a range of biomedical and physical separations, and was attractive for this project due to the ability to separate particles based on size, density, and compressibility. The unique dimensions, chemical composition, and physical properties of sperm cells make them unique within forensic biological samples, and thus, they were the ideal target for acoustic

separations. It was demonstrated that ADE could isolate and purify sperm cells from mock sexual assault samples, sequestering fractions of sperm and non-sperm particles within a microfluidic chip. The mock samples were composed of female epithelial cells, sperm cells, and other exogenous biomaterials. The presence of contaminating materials such as blood and yeast cells were shown to have no negative impact on acoustic trapping of sperm. The presence of E. coli, however, did demonstrate inhibition of acoustic trapping, when foreign cells exceeded 20% of the total epithelial cell concentration. Further experimentation showed that through optimization of liquid flow rate, sample preparation, and polymerase chain reaction (PCR) amplification chemistry, purified sperm fractions could be generated from samples containing lower sperm concentration and higher mass of female DNA than had been previously achieved. This was verified using short tandem repeat (STR) analysis, which generated DNA profiles for comparison to cell donors. STR analysis confirmed that ADE succeeded in isolating sperm cells in samples containing up to 40-fold more epithelial cells than sperm, producing clean male STR profiles from samples containing 500 and 1000 total sperm cells. Finally, ADE was applied to an extreme mock sample, containing 100-fold more epithelial cells than sperm cells in solution. Acoustic capture drastically improved the female to male cell ratio in these samples, a valuable improvement, but did not fully remove all female DNA contributions.

The work presented in **Chapter 3** described an external evaluation of the ADE prototype instrument and microchip, which was conducted with three goals in mind. First, to evaluate ADE as a replacement for DE by testing authentic, non-probative sexual assault samples. Second, to train professional forensic analysts in ADE protocols, and obtain their expert feedback with regard to the feasibility of ADE establishing a foothold in forensic workflows. The third goal was to identify shortcomings of ADE, by exposing the method to a wider range of samples and conditions

than were available during research and development at UVA. Each of these goals was met, as ADE was rigorously evaluated over the course of several months at multiple locations. The Palm Beach County Sheriff's Office (PBSO) in Florida and the Mesa Police Department in Arizona each hosted a validation test phase, and provided samples for analysis. At PBSO, dozens of non-probative samples were tested, ranging from 'ideal' samples, containing hundreds of sperm cells with few female cells present, to more 'challenging' samples, some of which showed no visible sperm cells during the screening process. With ideal samples, ADE was shown to replicate the results of conventional DE, generating full male STR profiles which matched the known attacker. With some of the more challenging samples, when conventional DE failed to produce a clean separation, ADE could not improve upon that result, also generating a partial STR profile. Importantly, once chemical modifications were made to the post-ADE workflow, DNA amplification was improved, and some re-tested challenging samples showed successful sperm cell capture. On the whole, the evaluation demonstrated that ADE rivals the performance of conventional DE in some situations, but falls short with a subset of more challenging samples. Importantly, it was demonstrated that acoustic trapping performance was not uniform across all samples, which led to unexpected failure to capture sperm cells. This observation was made by analyzing video of acoustic trapping, which showed loss of particle aggregation during the transition from frequency scanning to sample trapping. This indicated that not only does each microchip possess its own unique trapping frequency, but that the optimal resonant condition may change based on each sample. When testing samples with extremely high numbers of epithelial cells, the previously applied optimal acoustic frequency was not sufficient for sperm cell capture. We discovered that sample-to-sample differences played an important role achieving optimal

acoustic trapping, and hypothesized that specific changes to the liquid's viscosity, density, and compressibility resulted in variable resonant conditions.

Those sample-to-sample differences were addressed by the research presented in **Chapter 4**. It was hypothesized that changes in sample viscosity, due to cellular lysis, altered the density and compressibility of the liquid on a sample-to-sample basis. Those changes directly impacted the speed of sound through that medium, altering the resonant condition. This change in speed of sound generated different wavelengths when the same frequency was applied through each sample. Essentially, the piezoelectric transducer was vibrating at the same frequency during the frequency scanning and sample trapping stages. However, when a different liquid entered the acoustic trap site, that vibrational frequency no longer generated the same wavelength of sound, as it was now being transmitted through a more viscous medium. This changed the resonance condition on a sample-to-sample basis, which could not be accurately predicted based solely on sample screening information. This effect was illustrated via acoustic trapping of fluorescent beads, in which solutions of varying epithelial cell lysate concentration demonstrated a shift in the optimal trapping frequency. This simple demonstration was the first direct observation of this acoustic effect in biological samples, shedding light on an important factor in acoustic separations. To address this challenge as it pertains to sexual assault samples, a real-time feedback system was developed for ADE. This 'cruise control' approach employed real-time measurements of voltage from the piezo, and used that data to improve acoustic trapping performance during sperm cell capture. It was demonstrated that when resonance is achieved in the acoustic chamber, the voltage output of the piezo reaches a local minimum. This phenomenon was demonstrated using fluorescent bead solutions, combining visual aggregation measurement with voltage data collection to show a direct relationship. It was shown that performing a constant frequency scan, as opposed to the on/off

scan required for bead aggregation, was a faster and equally accurate method for determining optimal trapping frequency. Furthermore, this constant scan could be applied during sample trapping, providing feedback on changing liquid conditions without losing the already-capture sperm cells. This real-time feedback was demonstrated with mock sexual assault samples, and identified shifts in optimal frequency during trapping that resulted in successful sperm cell capture. The frequency shift phenomenon has an impact well beyond the ADE technology, and thus, more general quantitation of the effect was conducted. Diluted glycerol solutions were spiked with fluorescent beads, along with a human serum solution, and subjected to a voltage-monitored frequency scan. It was shown that, in addition to other factors, optimal trapping frequency is directly dependent on solution viscosity. The description of this effect, as well as the resulting real-time feedback system, are the future of a more robust ADE technology that can process samples containing any number of epithelial cells, and adapt to changing liquid environments.

In **Chapter 5**, microchip micellar electrokinetic chromatography (MEKC) was demonstrated as a viable approach for detecting explosive compounds on a native, thermoplastic polymer for portable use. This project sought to fill the unmet need for on-site, sensitive detection of explosives in environmental and forensic samples. Using an untreated cyclic olefin copolymer (COC) microchip, 11 explosive compounds were detected at sub-0.05 mg/mL levels. Despite the lack of charged surface groups on COC, electroosmotic flow (EOF) was generated at elevated pH, due to preferential adsorption of ions to the polymer surface. Multiple mixtures of explosive compounds were separated, including nitroaromatics, nitrophenols, various combinations found in military explosives. To enhance resolution and achieve higher quality separations, field-enhanced stacking was applied. A 5-fold difference in ionic strength between the background electrotype (BGE) and sample matrix (SM) resulted in dramatic improvement in separation of nitroaromatic

molecules TNT and DNT. This was further improved through the addition of β-cyclodextrin, which provided a second pseudo stationary phase for analytes to interact with during the separation. Adding β-cyclodextrin at 20 and 40 mM resulted in the best resolution achieved for TNT and DNT mixtures, exceeding 2.40 for these compounds. Alternative surfactant molecules were investigated, but showed no improvement over sodium dodecyl sulfate (SDS) when tested individually or as mixed micelle systems. The work in **Chapter 5** is the first reported free-solution MEKC separation of explosives on a COC device, which is attractive for its ruggedness, optical properties, and potential for field use.

## 6.2 Future work

The ADE project presented in this dissertation resulted in a fully functional prototype instrument, but there are still many improvements that can be made and research paths worth investigating. In its current state, the real-time feedback system for ADE is largely manual, requiring operator input for each applied frequency, as the user must monitor voltage data and determine when the minimum output occurs. In future iterations of this technology, the feedback system must be automated to become truly paradigm-shifting for the forensic community. Specifically, voltage data collection must be linked directly to the function generator, with software to identify the minimum voltage point and apply that frequency automatically. The feedback system will constantly update trapping parameters, even after determining the optimal trapping frequency for each unique sample. Sperm cell trapping requires 45-60 seconds per sample, during which, liquid properties may change as the scanning solution is fully replaced by the sample. Over that time, constant adjustments to the frequency can be made, comparing new voltage output to the previous data point. If a new minimum in voltage is identified at any point during the test, it will indicate a new optimal trapping frequency. Without deactivating the piezo,

and without any user input, the function generator will shift to that newly identified frequency, which becomes starting point for future measurements.

An additional direction for future work is to redesign the ADE microchip, adding multiplex capabilities for processing samples in parallel. Sexual assault samples typically contain a minimum of four evidentiary swabs, and yet, neither conventional DE nor ADE can process more than a single sample at one time. This multiplexing will be achieved by fabricating a glass and polymer microchip, similar to the design described in Chapters 2 and 3, but with four parallel acoustic trapping domains. A proposed schematic is shown in **Figure 6-1**. Each trap site will be connected to a different sample reservoir, actuated by its own piezoelectric transducer, and operate with independent frequency application from the other regions. The fluorescent bead (Be) and buffer solutions (Bu) will be connected to all four domains, for microchip quality control and pellet washing, respectively. The independent acoustic trapping sites will allow for optimized, unique trapping parameters to be applied for each sample, employing the cruise control feature described previously. Implementing the ability to process four samples at once will ease a major bottleneck in forensic workflows, as sexual assault kits are typically submitted with four evidentiary swabs (vaginal, vaginal-cervical, perianal, and external genitalia). With a 4-plex microchip, a single ADE procedure will be required to capture sperm cells from all four swabs simultaneously, expediting investigations.

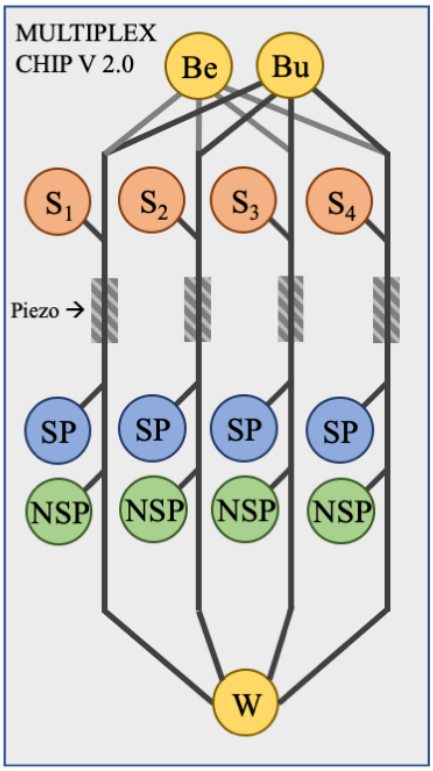


*Figure 6-1. Multiplex chip for parallel ADE. Sperm cells from 4 samples can be simultaneously captured and purified by acoustic trapping, generating distinct sperm (SP) and non-sperm (NSP) fractions.*

These proposed changes to the feedback system and microchip will necessitate updates to the ADE hardware. Currently encompassed in the prototype instrument are a function generator, amplifier, Raspberry Pi camera, solenoid valves, and syringe pumps. However, all electronic components can be combined onto a printed circuit board (PCB), with similar fabrication to the voltage peak detector circuit. That PCB contains a function generator and amplifier, capable of replacing the external components of the current ADE instrument. By also integrating the Raspberry Pi system, and eliminating the laptop currently used for user input, the overall footprint of the instrument will shrink from desktop computer size, to roughly shoebox size. In addition, the programming and operational requirements will be significantly reduced.

Multiple future directions are envisioned for the explosives detection project employing microchip MEKC. Alternate polymeric substrates may be investigated, including poly(methyl)methacrylate (PMMA) and other formulations of cyclic olefin copolymer (COC) such as Zeonor. Changes to the surface chemistry of the microchip may result in less adsorption of analytes to the channel walls, which could have contributed to the band broadening observed during separations. Alternative substrates may also demonstrate stronger electroosmotic flow (EOF), which could reduce the time of each separation and lower the required voltage to generate EOF, which would in turn generate less heat. Minimizing heating during a separation is always a priority, as the reduction of band broadening due to diffusion leads to higher resolution separations. Future studies will also implement mock sample testing, to uncover any challenges with sample matrices that may be encountered. It is predicted that salinity, the presence of solid particles, and other properties of groundwater samples will need to be accounted for during microchip separations.

## 6.3 Summary

Microfluidic separations offer solutions for complex problems, both forensic and environmental, and can fill multiple unmet needs in the scientific community. Growing DNA evidence backlogs require novel approaches for processing sexual assault samples, and environmental concerns over the spread of toxic explosives need to be monitored in an efficient, portable manner. The methods described in this thesis offer solutions to each of these issues, applying acoustic trapping to sperm cell capture, and microchip MEKC to explosive compound detection. Each of these projects is driven by a clear forensic need, and continued development will result in competitive alternatives to existing technologies.